Title
FORMALDEHYDE PHOTODISSOCIATION: MOLECULAR BEAM, PRODUCT APPEARANCE RATE, AND CARBON-14 ISOTOPIC ENRICHMENT STUDIES

Author
Ho, P.

Publication Date
1981-12-01

LBL-13869

Lawrence Berkeley Laboratory
UNIVERSITY OF CALIFORNIA

Materials & Molecular Research Division

FORMALDEHYDE PHOTODISSOCIATION: MOLECULAR BEAM, PRODUCT APPEARANCE RATE, AND CARBON-14 ISOTOPIC ENRICHMENT STUDIES

Pauline Ho
(Ph.D. thesis)

December 1981

Prepared for the U.S. Department of Energy under Contract W-7405-ENG-48

DISCLAIMER

FORMALDEHYDE PHOTODISSOCIATION:
MOLECULAR BEAM, PRODUCT APPEARANCE RATE, AND CARBON-14
ISOTOPIC ENRICHMENT STUDIES

Pauline Ho

Ph.D. Thesis

December 1981

Materials and Molecular Research Division
Lawrence Berkeley Laboratory
University of California
Berkeley, CA 94720

This work was supported by the Assistant Secretary for Nuclear Energy, Office of Advanced Systems and Nuclear Projects, Advanced Isotope Separation Division of the U.S. Department of Energy under Contract Number W-7405-ENG-48.

FORMALDEHYDE PHOTODISSOCIATION:
MOLECULAR BEAM, PRODUCT APPEARANCE RATE, AND CARBON-14 ISOTOPIC ENRICHMENT STUDIES

Pauline Ho

ABSTRACT

Several aspects of the formaldehyde photopredissociation mechanism were studied. The technique of crossed laser and molecular beams was used to study the system under collisionless conditions. Detection of the molecular product CO after excitation of H_2CO near the S_1 origin gives strong support to the sequential decay model for fast nonradiative decay of S_1 states. For H_2CO excitation at 283.9 nm, formation of the radical product HCO dominates dissociation to molecular products by an order of magnitude.

CO appearance rates for H_2CO excitation at 354.7, 317.0, 298.5 and 283.9 nm were measured by time-resolved absorption of a CO laser, and were the same within ~20%. These measurements could be complicated by rotational relaxation; an impulse approximation calculation using the CO translational energy distribution from the molecular beam experiment suggests that CO should be formed in high J states. The evidence for an intermediate in H_2CO photodissociation may thus be compromised.

Simultaneous high resolution spectra of $H_2{}^{14}CO$ and $H_2{}^{12}CO$ between 290 and 345 nm were measured. About 30 lines with spectra selectivities $C \gtrsim 50$ were found. Photolyses on one such line at 326.9 nm of a dilute mixture of $H_2{}^{14}CO$ in natural H_2CO gave one-step enrichment factors of up to 150. Since a factor of 150 in ^{14}C concentration corresponds to

~7.2 half-lives, or 41,000 years, laser enrichment of archaeological samples could greatly improve the range of radiocarbon dating.

C. Bradley Moore

Dedicated to

my parents and my sisters

ACKNOWLEDGMENTS

One of the best aspects of my years in Berkeley was being part of a friendly and cooperative research group. I consider myself fortunate to have worked for Brad Moore and thank him for his help, guidance, and patience. Dr. Nicholas Nogar first initiated me into the world of lasers and formaldehyde; Dr. Robert Hedges introduced me to carbon-14 and isotope separation, and did the spectroscopy part of that project. Rick Buss and Professor Y. T. Lee provided expertise on molecular beams for the collisionless photofragmentation project; Doug Bamford also worked on that project and contributed his experience with dye lasers and fluorescence lifetime measurements. Rick is also thanked for helping with last minute drawings, filing this thesis, and generally being helpful and supportive. Chi-ke Cheng did a great deal of work on the CO appearance rates, and her enthusiasm and friendliness made those long nights of data taking much more bearable. Linda Young, my long term roommate and office mate is thanked for many things, not the least of which was making sure I got up for quantum mechanics class; Joan Frisoli also shared apartment and office, though not for as long. Mike Berman and Hai-lung Dai are thanked for many rides home; Alison Abbate is thanked for last minute ir filter spectra. Jim Weisshaar and Andy Langford were fellow "formaldehyders"; Wes Natzle was around for many a helpful discussion. Dr. Andy Kung is thanked for his assistance with laser problems and for the use of his PET. Jackie Denney was very helpful when it came to knowing who to talk to about whatever, and her organization of group parties is muchly appreciated. Vera Mainz, Greg Girolami, Henry Luftman and Geri Richmond also get mentioned. I would

also like to thank the University of California for a Regents Fellowship, the Environmental Health and Safety Department for the loan of their radiation monitor, and the National Science Foundation, via the San Francisco Laser Center and a Grant for Chemical Instrumentation, for some of the lasers used in this work.

This work was supported by the Assistant Secretary for Nuclear Energy, Office of Advanced Systems and Nuclear Projects, Advanced Isotope Separation, Division of the U.S. Department of Energy under Contract Number W-7405-ENG-48.

TABLE OF CONTENTS

Chapter List of Figures Page

Chapter List of Figures (continued) Page

Chapter List of Tables Page

CHAPTER I. INTRODUCTION

In the last decade, formaldehyde has been the subject of a great deal of experimental and theoretical work aimed at elucidating the details of its photopredissociation mechanism. Gelbart, et al.[1] have recently reviewed much of this work. The reasons for this interest range from a fundamental interest in understanding the dynamics of photodissociative processes to the modeling of polluted atmospheres[2] and applications to laser isotope separation[3] and combustion.[4] Formaldehyde is a conveniently sized molecule. It is large enough to have interestingly complex photochemistry; a detailed understanding of this molecule could prove useful as a prototype for the photochemistry of small polyatomics. But formaldehyde is small enough for ab initio calculations and can therefore serve as a testing ground for theoretical investigations. In particular, its small size permits a priori calculation of radiationless transition rates for comparison to quantum-state resolved experiments.

The overall photodissociation process of interest is

$$\begin{aligned} H_2CO + h\nu\ (280 - 355\ \text{nm}) &\rightarrow H_2CO\ (S_1, v) \\ H_2CO\ (S_1, v) &\rightarrow H_2 + CO \\ &\rightarrow H + HCO, \end{aligned}$$

but this simple representation belies the complexity of the dynamics.

The absorption spectrum of the formaldehyde $\tilde{A}\ {}^1A_2 \leftarrow \tilde{X}\ {}^1A_1$ transition is well understood; individual rotational lines can be resolved and assigned for many vibrational bands.[5] S_1 does not correlate with the ground state products of either channel (Fig. I-1), so dissociation at the energies of interest can only occur via a radiationless transition to S_0 or T_1. Although ground state H_2CO is almost isoenergetic with the molecular products H_2 + CO, recent ab initio calculations of the S_0 surfaces[6-8] indicate that the top of the barrier between the two is within a few kcal/mole of the S_1 origin. Photochemical quantum yield studies[9] also indicate a barrier in this range. The threshold for radical formation is well established: photochemical[9-11] and thermochemical[12] determinations agree, and ab initio calculations[6,13] show no barrier in the exit channel for radical dissociation on the S_0 surface. The spectrum of T_1 near its origin is also well studied.[5] Several discrete, diatomic-like S_1-T_1 perturbations have been observed and assigned in higher vibronic bands.[14] T_1 can dissociate to ground state radicals over a barrier.[13]

The S_1 and T_1 origins, the threshold for radical formation, the top of the barrier for dissociation to molecules on the S_0 surface and possibly that for dissociation to radicals on the T_1 surface are all close in energy, as shown in Fig. I-1. Thus the number of available pathways can complicate the photodissociation mechanism.

There have been several generations of $H_2CO(S_1)$ fluorescence lifetime measurements[15-17] with ever-decreasing laser linewidths and H_2CO pressures. The most recent involve the excitation of individual rotational lines at sub-mTorr pressures and in molecular beams. Collision-free decay rates of single rovibronic levels near the S_1 origin were found to vary over two orders of magnitude with no systematic

Fig. I-1. Energy level diagram for formaldehyde. The dashed lines show the correlations between bound states and continua. Approximate barrier heights shown are from *ab initio* calculations.

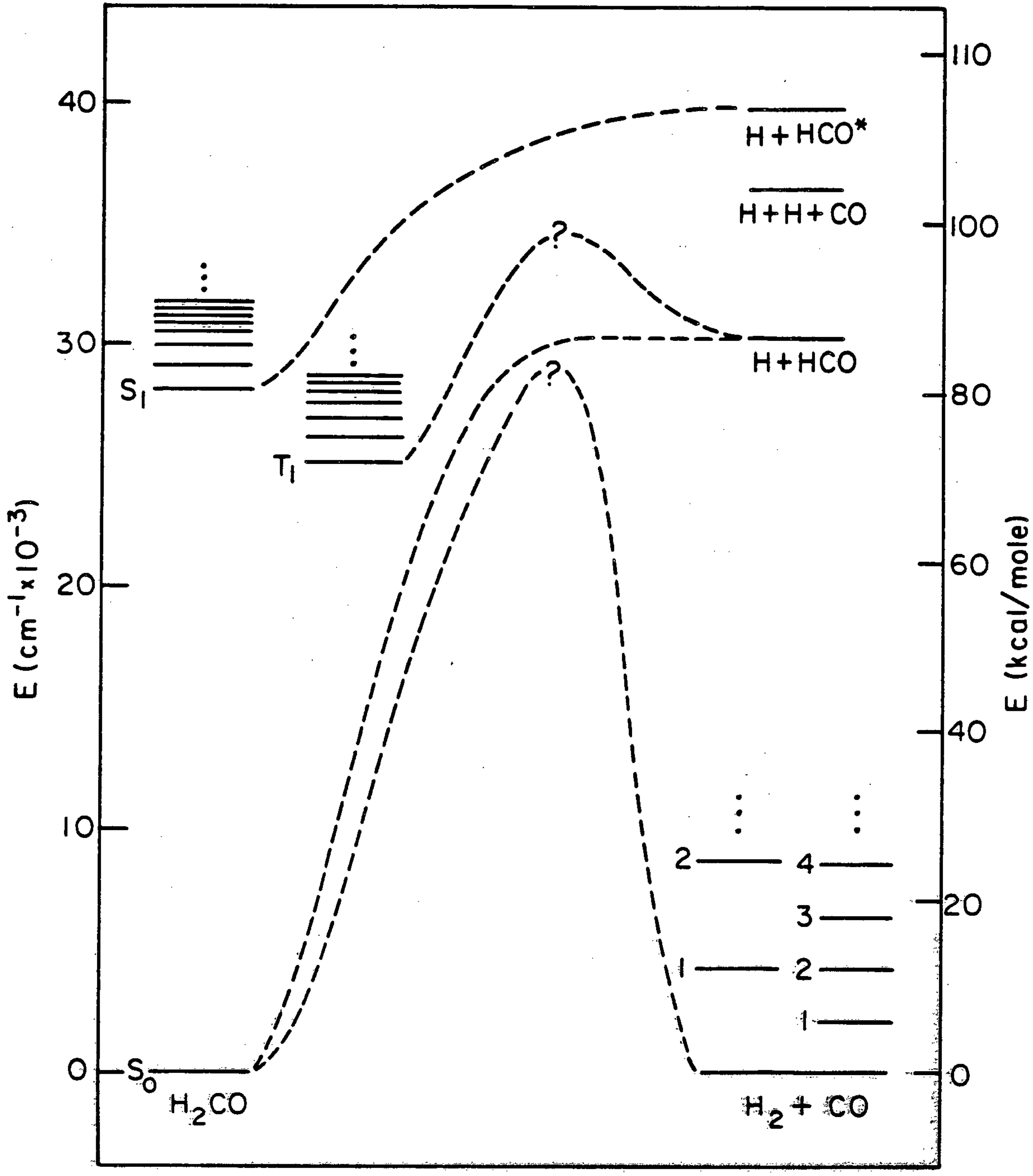

XBL 818-11415

Fig. I-1.

dependence on rotational quantum numbers.[16,17] A model has been proposed[16b] in which S_1 levels decay via a "lumpy continuum" comprised of S_0 levels broadened by dissociation to H_2 + CO. $H_2CO(S_0)$ cannot provide the dissipative continuum required to explain the fast irreversible decays--it is estimated to have only ~10 vibrational states per cm^{-1} at these energies. Thus, the fast collision-free nonradiative decays observed require the dissociative continuum as the final state. The energies involved may be less than the barrier to dissociation on the S_0 surface,[6] but calculated tunneling rates through such a barrier provide a reasonable magnitude of S_0 level broadening.[18] Tunneling would also provide a rationale for the higher photochemical threshold observed for D_2CO.[9] The sequential decay model is supported by the dramatic changes in decay rate observed as energy resonances are tuned with a Stark field[16c] but no experimental observation of collision-free dissociation has previously been made.

Photochemical product studies have been done under conditions where collisions are involved in the decay of S_1. Photochemical quantum yields for the molecular and radical channels have been measured at pressures $\geq$5 Torr.[9-11] At longer wavelengths (340-360 nm), the molecular dissociation channel dominates, occurring with a quantum yield of 0.7-1.0. Between 330 and 340 nm, the radical channel becomes energetically allowed and the quantum yield for radical formation rises from 0 to ~0.5, with the molecular channel decreasing accordingly. There is some inconsistency in the data for the radical/molecule branching ratio at higher energies--this is discussed further in Chapter III.

The kinetics of CO formation after H_2CO photolysis at 337 nm have been studied by the time-resolved absorption of individual rotational lines from a CO laser.[19] CO ($J \cong 10$) was produced slowly (~1.7 μs^{-1} $Torr^{-1}$) compared to the S_1 decay, and at a rate proportional to pressure for 0.1-5 Torr. Extrapolation of the data to zero pressure gave a CO appearance rate of 0.0 ± 0.26 μs^{-1}, which indicated that collisions were required for product formation. CO risetimes after H_2CO photolysis at 354.7 nm have also been measured by infrared chemiluminescence.[20] These experiments also showed a delayed appearance for CO of ~1.7 μs^{-1} $Torr^{-1}$, even though the molecules have 1300 cm^{-1} less energy. CO appearance rates have also been measured as a function of foreign gas pressure (He, Ar, Xe, NO) and for CO production from D_2CO.[19,20]

The delayed appearance of CO was interpreted in terms of an intermediate state I, which is formed as $H_2CO(S_1)$ decays and requires a collision to dissociate to H_2 and CO

$$H_2CO(S_1) \rightarrow I$$

$$I + M \rightarrow H_2 + CO + M.$$

T_1, high vibrational states of S_0, and the isomer trans-HCOH have all been suggested as candidates for the long-lived intermediate;[19] it has also been suggested that the intermediate may actually be several intermediate states.[16d,e] All of these candidates for I have their advantages and disadvantages--Weisshaar[16] has discussed these in detail, but none of them can be proven or disproven at present. The CO risetime results appear to be in direct conflict with the prompt H_2CO dissociation required by the theory for collision-free non-radiative decay.

These two interpretations can be reconciled by postulating that between the m Torr pressures used for the lifetime measurements and the lowest pressure used in the appearance rate measurements (0.1 Torr), collisional quenching of $H_2CO(S_1)$ to a non-fluorescing state (which requires a further collision to dissociate) becomes competitive with the collisionless decay mechanism.

The work in this thesis addresses two of the major remaining questions in the formaldehyde photodissociation mechanism. In the absence of collisions, the direct observation of dissociation products is clearly the crucial test for the sequential decay model. Chapter II describes an experiment that provides this test using the technique of crossed laser and molecular beams. Dissociation does indeed occur without collisions; angular and translational energy distributions are given for products of the molecular and radical dissociation channels. In the presence of collisions, the major unknown is the identity of the intermediate. The work presented in Chapter III attempts to identify the intermediate by studying its behavior at different photolysis energies, but antithetically results in a questioning of its existence. Chapter IV reports the 150-fold enrichment of ^{14}C by selective laser photolysis of formaldehyde and its possible application to radiocarbon dating.

REFERENCES

1. W. M. Gelbart, M. L. Elert, and D. F. Heller, Chem. Rev. 80, 403 (1980), and references therein.
2. J. G. Calvert, J. A. Kerr, K. L. Demerjian, and R. D. McQuigg, Science 175, 751 (1972).
3. J. H. Clark, Y. Haas, P. L. Houston, and C. B. Moore, Chem. Phys. Lett. 35, 82 (1975); J. Marling, J. Chem. Phys. 66, 4200 (1977); L. Mannik, G. M. Keyser, and K. B. Woodall, Chem. Phys. Lett. 65, 231 (1979).
4. A. G. Gaydon, The Spectroscopy of Flames, 2nd Ed., (Chapman & Hall, London, and Wiley & Sons, New York, 1974).
5. D. C. Moule and A. D. Walsh, Chem. Rev. 75, 67 (1975).
6. a) J. D. Goddard and H. F. Schaefer, J. Chem.Phys. 70, 5117 (1979); b) J. D. Goddard, Y. Yamaguchi, and H. F. Schaefer, J. Chem. Phys. 75, 3459 (1981).
7. M. J. Frisch, R. Krishnan, and J. A. Pople, J. Phys. Chem. 85, 1467 (1981); L. B. Harding, H. B. Schlegel, R. Krishnan, and J. A. Pople, J. Phys. Chem. 84, 3394 (1980).
8. G. F. Adams, G. D. Bent, R. J. Bartlett, and G. D. Purvis, J. Chem. Phys. 75, 834 (1981).
9. J. H. Clark, C. B. Moore, and N. S. Nogar, J. Chem. Phys. 68, 1264 (1978).
10. K. Y. Tang, P. W. Fairchild, and E. K. C. Lee, J. Phys. Chem. 83, 569 (1979).
11. A. Horowitz and J. G. Calvert, Int. J. Chem. Kinet. 10, 805 (1978).

12. R. Walsh and S. W. Benson, J. Am. Chem. Soc. 88, 4570 (1966); P. Warneck, Z. Naturforsch., Teil A26, 2047 (1971); 29, 350 (1974).

13. D. M. Hayes and K. Morokuma, Chem. Phys. Lett. 12, 539 (1972).

14. J. C. D. Brand and C. G. Stevens, J. Chem. Phys. 58, 3331 (1973); R. E. Linder, G. Barth, E. Bunnenberg, C. Djerassi, L. Seamans, and A. Moscowitz, Chem. Phys. Lett. 28, 490 (1974); F. W. Birss, D. A. Ramsay, and S. M. Till, Chem. Phys. Lett. 53, 14 (1978).

15. E. S. Yeung and C. B. Moore, J. Chem. Phys. 58, 3988 (1973).

16. a) J. C. Weisshaar, A. P. Baronavski, A. Cabello, and C. B. Moore, J. Chem. Phys. 69, 4720 (1978); b) J. C. Weisshaar and C. B. Moore, J. Chem. Phys. 70, 5135 (1979); c) 72, 5415 (1980); d) J. C. Weisshaar, D. J. Bamford, E. Specht, and C. B. Moore, J. Chem. Phys. 74, 226 (1981); e) J. C. Weisshaar, Ph.D. Thesis, University of California, Berkeley, 1979; f) H. L. Selzle and E. W. Schlag, Chem. Phys. 43, 111 (1979).

17. a) K. Shibuya, R. A. Harger, and E. K. C. Lee, J. Chem. Phys. 69, 751 (1978); b) K. Shibuya and E. K. C. Lee, J. Chem. Phys. 69, 5558 (1978); c) K. Shibuya, P. W. Fairchild, and E. K. C. Lee, J. Chem. Phys. 75, 3397 (1981); d) P. W. Fairchild, K. Shibuya, and E. K. C. Lee, J. Chem. Phys. 75, 3407 (1981).

18. W. H. Miller, J. Am. Chem. Soc. 101, 6810 (1979); S. K. Gray, W. H. Miller, Y. Yamaguchi, and H. F. Schaefer, J. Am. Chem. Soc. 103, 1900 (1981).

19. P. L. Houston and C. B. Moore, J. Chem. Phys. 65, 757 (1976).

20. M. B. Zughul, Ph.D. Thesis, University of California, Berkeley, 1978.

CHAPTER II. PHOTODISSOCIATION OF FORMALDEHYDE IN A MOLECULAR BEAM

A. INTRODUCTION

The sequential coupling model proposed by Weisshaar[1] is the culmination of a great deal of work on H_2CO fluorescence decay times. In this model, collisionless non-radiative decay of S_1 occurs via coupling of S_1 to a sparse manifold of high vibrational levels of $H_2CO(S_0)$, which in turn is coupled to the H_2 + CO product continuum. The S_1-S_0 coupling is best viewed in terms of a state-mixing picture; the S_0-continuum coupling is provided by quantum-mechanical tunneling through the barrier on the S_0 surface. The large variation observed in the lifetimes of individual rotational states near the origin of the S_1 absorption is primarily due to resonances between specific rovibrational levels in the S_1 and S_0 states. Although this model is supported by changes in the S_1 decay rate in the presence of a Stark field, a crucial test of the model is clearly the direct observation of product formation under collisionless conditions. The work described in this chapter uses the technique of crossed laser and molecular beams to provide this test.

B. EXPERIMENTAL

The molecular beam apparatus used for the photofragmentation studies has been described in detail elsewhere.[2] The laser and molecular beams crossed at 90 degrees, and dissociation fragments were detected by an electron bombardment quadrupole mass spectrometer which could be rotated in the plane of the beams.

A Quanta-Ray YAG-pumped dye laser and wavelength extension system were used in these experiments. For studies of the molecular channel of formaldehyde photodissociation, ~1 mJ of tunable uv between 338 and 353 nm was obtained by summing the visible output from Coumarin 500 (Exciton) with 1.06 μm YAG fundamental in a KDP cyrstal. Etalons were used in both the YAG and dye lasers, and the uv linewidth was ≤ 0.25 cm^{-1} as estimated from the width of the narrowest lines in a gas phase fluorescence excitation spectrum of H_2CO (Doppler width = 0.06 cm^{-1} at 300 K). Fluorescence from an external gas cell containing ~1 Torr of H_2CO was used as a wavelength reference, as described by Weisshaar.[1a] Individual rotational lines were easily assigned using high resolution spectral data from Ramsay.[3] For studies of the radical channel of H_2CO dissociation, ~3 mJ of 284 nm light with a linewidth of ~2 cm^{-1} (no etalons) were obtained by frequency doubling the output from Rh 6G (Exciton). In this wavelength range the H_2CO spectrum is not well understood, precluding detailed rotational assignments. The laser entered and exited the molecular beam apparatus via quartz Brewster angle windows. For the molecular channel studies the laser beam (3 mm diameter) was double passed through the formaldehyde beam. At the shorter wavelength, experiments done with the laser unfocused (10 mm diameter, 2 passes) and focused on the interaction region (1 mm diameter, 1 pass) gave qualitatively identical results. The focused configuration was generally used because of somewhat better signal. The laser repetition rate was 10 Hz, and the uv pulse length was ~4 ns.

The formaldehyde beam was made by heating paraformaldehyde powder (Matheson) in an oil bath to ~90 C with helium flowing over it. A fritted glass disk was usually used to trap any particles being carried in the gas stream, and a dry-ice/isopropanol bath trapped any water or trioxane formed during the depolymerization. Two hundred Torr of the mixture of 10% H_2CO in helium were expanded through a 0.23 mm diameter glass nozzle. A 0.76 mm diameter skimmer was located 7.5 mm from the nozzle. Mass spectrometric analysis of the resulting beam was done by chopping the beam, measuring the signal level with the beam on and off, and taking the difference. No evidence was seen for the presence of dimer (< 0.1%) or trimer (< 1.0%) in the beam (the limits given represent the statistical noise), nor for impurities in the beam in the mass range 37 to 59 amu. The velocity distribution of the beam was obtained by the time-of-flight (TOF) method. The average beam speed was 1.27×10^5 cm/s and the full-width-half-maximum (FWHM) velocity spread was ~10%. Three stages of differential pumping, two skimmers and a final defining slit gave sufficient spatial definition to the beam to allow CO product detection 8° from the H_2CO beam. The distance from the nozzle to the interaction region was 8 cm, and the pressure in the main chamber was $\sim 3 \times 10^{-7}$ Torr with the beam on. With the resolution of the quadrupole set at FWHM = 1 amu and with the detector at 10°, the mass 28 background was ~7.5 x 10^5 counts/s with the beam on, and 6.0 x 10^5 counts/s with the beam off, giving 30 background counts during the 50 μs time interval for signal acquisition after each laser pulse. Velocity spectra of the product at a given detector angle were obtained from analysis of the flight time of the product from the interaction region to the ionizer located 21 cm away.

The signal from the detector was amplified, processed by a pulse-height discriminator, then sent to a 256 channel scaler used for TOF measurements. A photodiode provided a trigger pulse for the multichannel scaler, and an LSI-11 computer handled data acquisition and signal averaging.

The rotational temperature of the beam was estimated from the relative peak heights in the fluorescence excitation spectrum of the formaldehyde in the beam. The relative fluorescence intensity observed following excitation of a particular rovibrational line,

$$I_{fl} \alpha \phi_{fl} \sigma A l I_l g e^{-E_r/kT}.$$

σ is the absorption cross section averaged over all molecules, and is the same for all rotational lines of a vibronic band. A is the rotational line strength factor for an asymmetric rotor, I_l is the incident laser intensity, g = 2J+1 is the degeneracy of the initial state, and E_r is the rotational energy thereof. ϕ_{fl} is the fluorescence quantum yield and is equal to the ratio of the observed fluorescence decay time and the radiative lifetime, i.e. τ_{fl}/τ_{rad}. When E_r is plotted against ln $[\tau_{fl} Ag/(I_{fl}/I_l)]$, the slope of the line is kT_r. Table II-1 shows data for the $rR_1(4)0$ – $rR_1(7)0$ lines[4] in the 4^1 absorption band and the analysis yielding T_r, which was between ~25 and 50 K. The uncertainty in T_r is caused by irreproducibility of the relative fluorescence peak heights, and disguises any possible variation of T_r with beam conditions.

Table II-1. Rotational temperature determination for the H_2CO molecular beam.

					Spectrum 1[a]		Spectrum 2[a]		Spectrum 3[b]		Spectrum 4[c]	
Line[d]	$E_r(\mathrm{cm}^{-1})$[e]	$g = 2J+1$[f]	$\tau_{f1}(\mathrm{ns})$[g]	A[h]	I_{f1}/I_1[i]	x[j]	I_{f1}/I_1[i]	x[j]	I_{f1}/I_1[i]	x[j]	I_{f1}/I_1[i]	x[j]
$rR_1(4)0$	32.2	9	292	2.10	116	3.86	49	4.72	51	4.68	24	5.44
$rR_1(5)0$	44.2	11	104	2.33	23.5	4.73	16	5.12	15	5.18	4	6.50
$rR_1(6)0$	58.6	13	254	2.57	46	5.22	36.5	5.45	31	5.61	10	6.74
$rR_1(7)0$	75.4	15	142	2.81	10	6.39	12.5	6.17	9	6.50	2	8.00
slope[k]					17.51		30.12		24.00		17.27	
r^2[l]					0.98		0.98		0.99		0.95	
T_r[m]					25.2		43.3		34.5		24.9	

a) Molecular beam of 20 Torr H_2CO + 180 Torr He.
b) Molecular beam of 20 Torr H_2CO + 80 Torr He.
c) Molecular beam of 20 Torr H_2CO + 268 Torr He.
d) Rotational line excited in the 4^1 vibronic band of H_2CO.
e) Rotational energy of initial state.
f) Rotational degeneracy of initial state.
g) Measured fluorescence decay time--Ref. 5.
h) Rotational line strength factors for an asymmetric rotor.
i) Fluorescence intensity normalized by laser intensity. Arbitrary units.
j) $x = \ln\,[\tau_{f1}Ag/(I_{f1}/I_1)]$.
k) Linear least-squares fit for E_r vs x. Slope = kT_r.
l) Goodness-of-fit parameter for least-squares fit.
m) Rotational temperature of the H_2CO in the beam.

C. RESULTS AND ANALYSIS

1. Molecular Dissociation near the S_1 Origin

The photodissociation of formaldehyde to H_2 + CO was studied for individual rotational states in the $2^1 4^1$ (where this notation indicates molecules in S_1 with 1 quanta of excitation each in ν_2 and ν_4) and the 4^1 vibrational bands (339 and 353 nm, respectively). Figure II-1 shows time-of-flight (TOF) measurements of the product angular distribution for excitation of the $rQ_1(3)E$ and $rQ_1(4)0^4$ rotational lines in the $2^1 4^1$ band of H_2CO (29515.2 cm^{-1}), which overlap within the bandwidth of the laser. The measured lifetime for these states was short (48 ns),[5] so dissociation is expected to be the major decay channel. The $2^1 4^1$ band was used for the angular distribution data because the signal intensity was twice that of the 4^1 band. There was no signal in the mass 28 TOF spectrum when the laser was tuned out of resonance with a formaldehyde absorption line (Fig. II-2), nor when either the laser or the molecular beam was blocked. No TOF signal for masses 29 or 30 was observed, and TOF spectra for the 4^1 and $2^1 4^1$ bands were superimposable within the experimental error. After two hours of counting at each angle, the integrated signal intensities at the different laboratory angles (10°-35°) were the same to within 11%. Since the recoil velocity of CO is comparable to the H_2CO velocity (see Fig. II-3), this suggests that the center-of-mass (CM) product angular distribution is also near isotropic. This was confirmed when an excellent fit to the data was obtained using an isotropic CM angular distribution. The data shown in Fig. II-1 are the results of 2 hours of counting at 10, 15 and 25°, and 8 hours at 35°.

Fig. II-1. Angular distribution of CO produced by H_2CO dissociation at 339 nm. $rQ_1(3)E$ and $rQ_1(4)0$ in the $2^1 4^1$ vibronic band were excited. The solid curves are computer fits to the data for the P(E) shown in Fig. II-4.

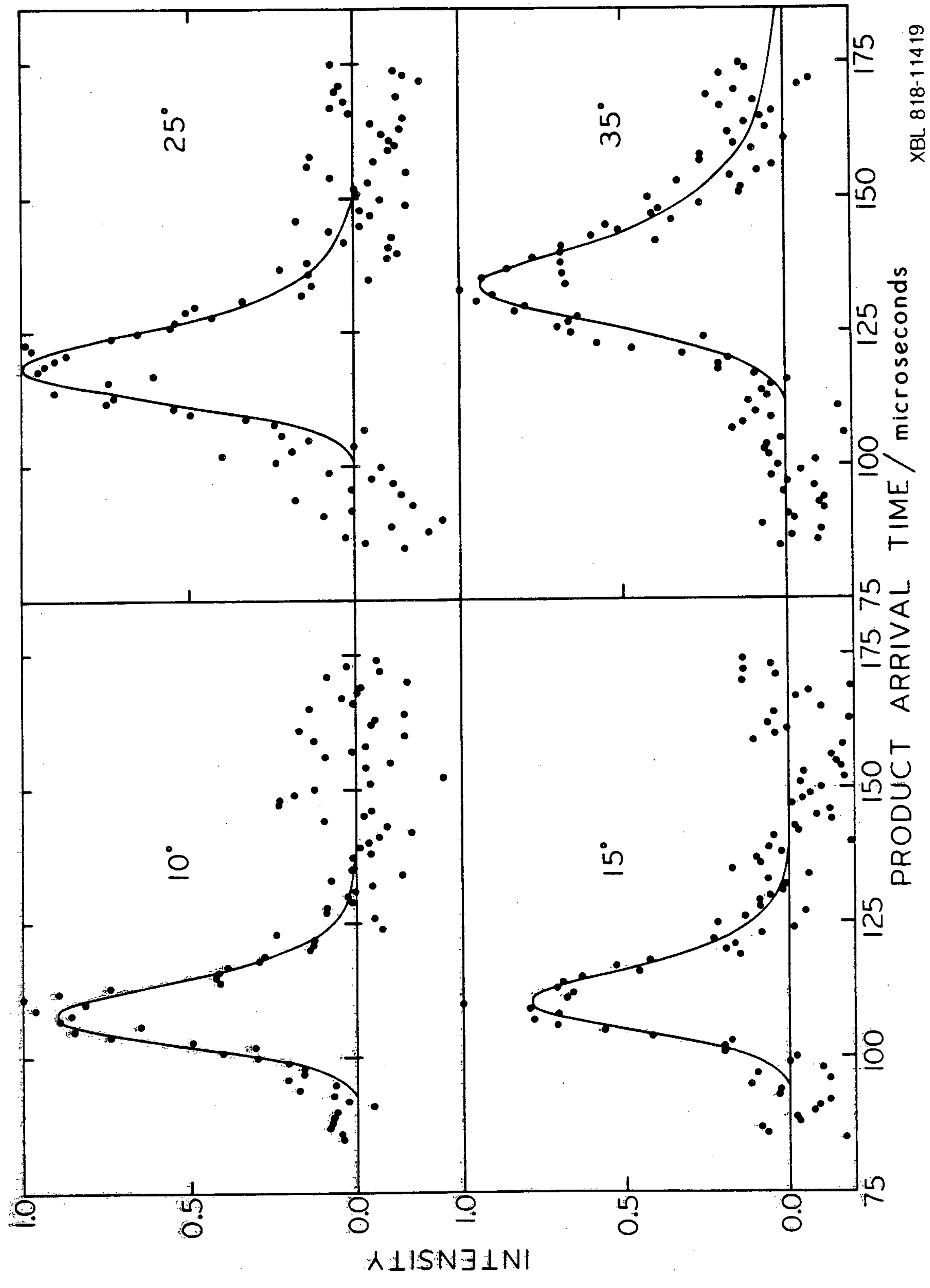

XBL 818-11419

Fig. II-1

Fig. II-2. The top half shows the M28 TOF signal with the laser tuned to $rQ_1(3)E + rQ_1(4)0$ in the $2^1 4^1$ absorption band of H_2CO. The lower half shows an identical TOF spectrum with the laser tuned off resonance.

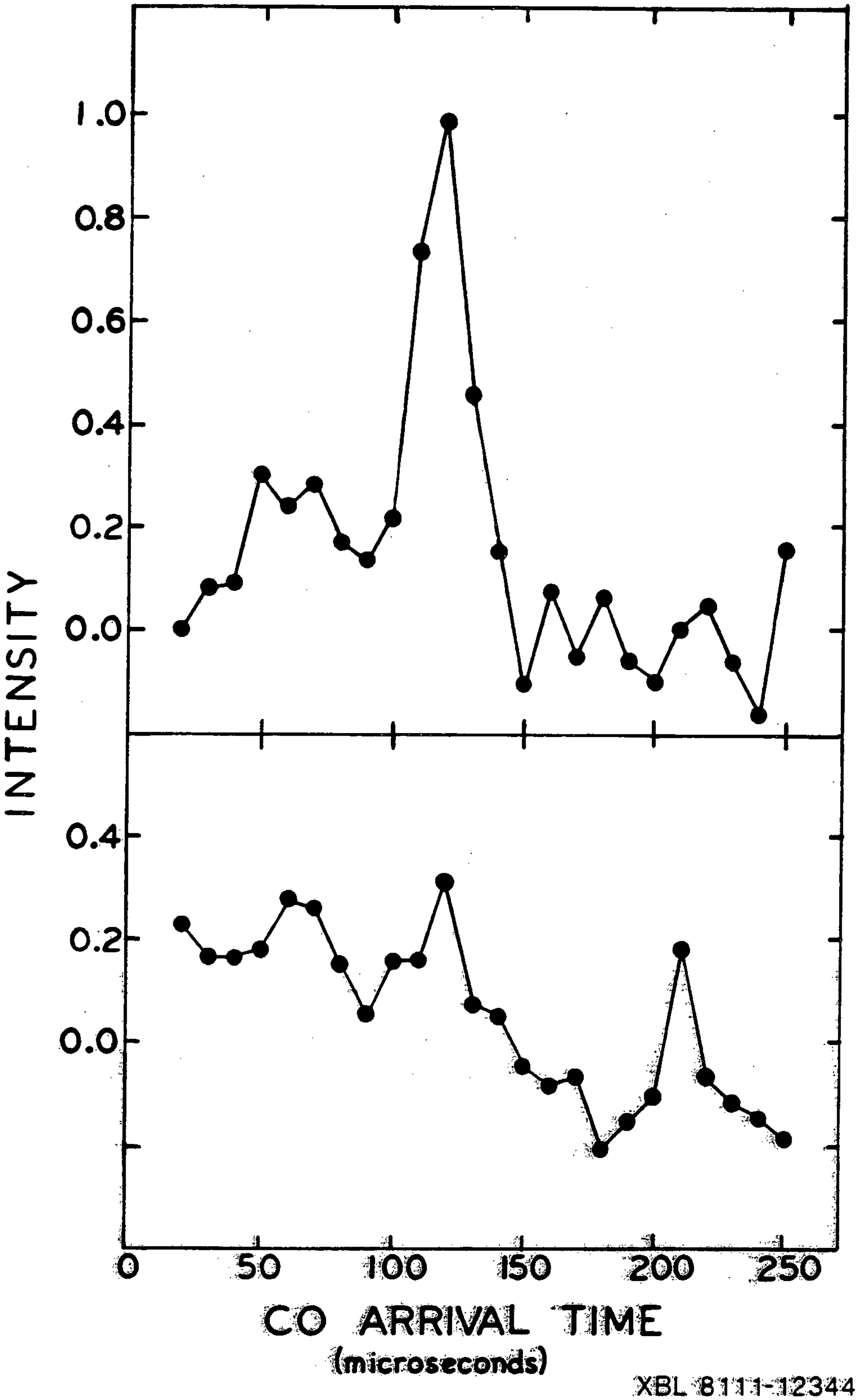

INTENSITY
1.0
0.8
0.6
0.4
0.2
0.0
0.4
0.2
0.0
0
50
100
150
200
250
CO ARRIVAL TIME
(microseconds)
XBL 8111-12344

Fig. II-2.

Fig. II-3. Newton diagram for formaldehyde dissociation. Solid line indicates product velocity in LAB frame of reference, dashed line indicates product velocity in CM frame. Angles shown are in the LAB frame. (a) Indicates CM velocity for CO produced at 339 nm if all excess energy goes into product translation. (b) Indicates CM velocity for HCO produced at 283.9 nm if all excess energy goes into product translation. (c) Indicates HCO CM velocity for dissociation to radicals with 4 kcal/mole translational energy. Shaded area indicates the velocity range of CO products observed at 339 nm and corresponds to the 10% height limits of the P(E) in Fig. II-4.

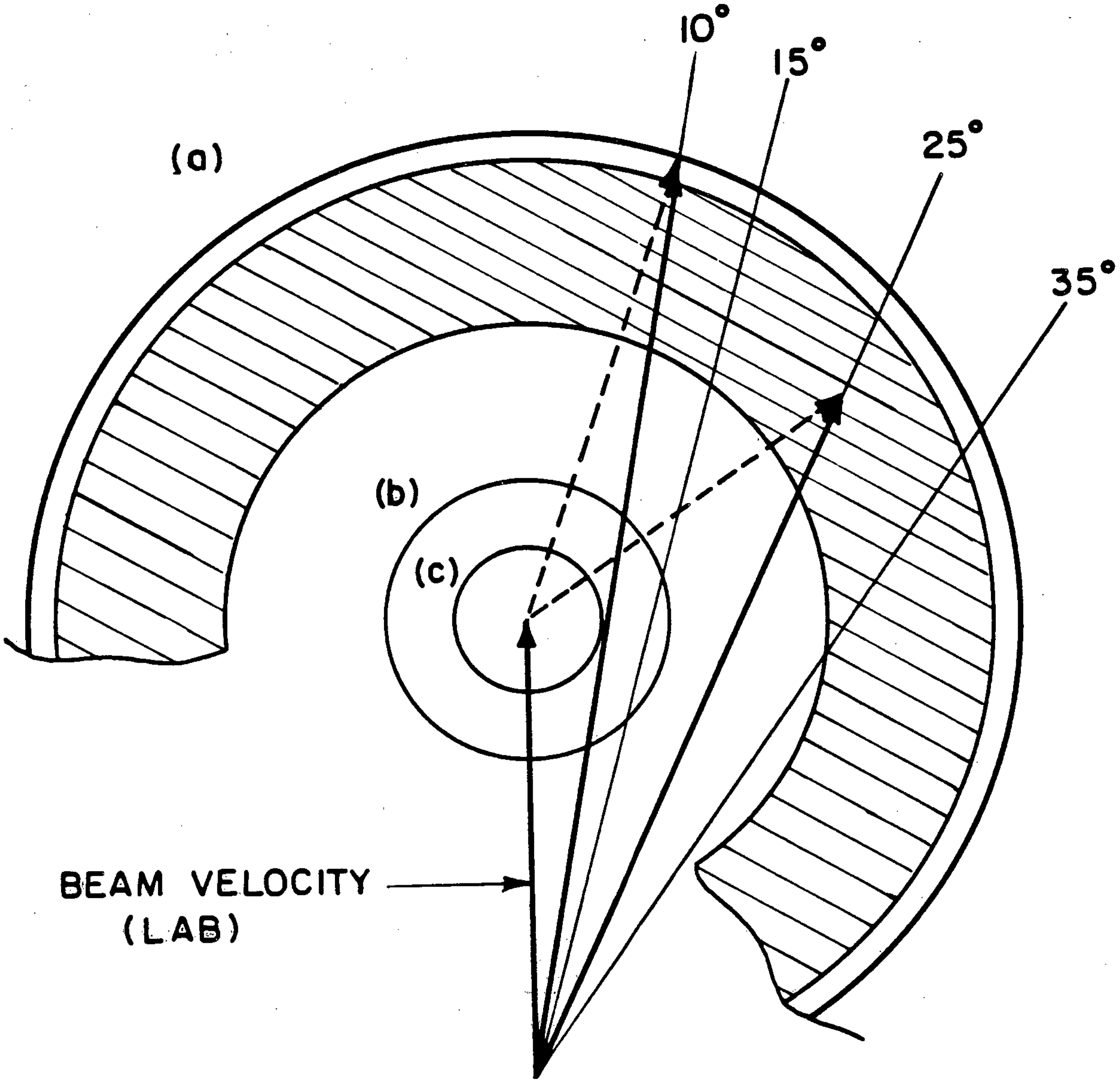

XBL 818-11414

Fig. II-3.

A product translational energy distribution, P(E), is obtained from the experimental time-of-flight data by calculating TOF spectra for various postulated P(E)'s, then refining the P(E)'s until a good fit to the experimental data is obtained. The computer programs used for this analysis have been described elsewhere[6] and take into account the velocity spread of the beam, the velocity dependence of the ionization efficiency of the mass spectrometer, and the Jacobian factors in the laboratory to CM coordinate transformation. The CO product translational energy distribution obtained by computer fit to the angular distribution data for the $2^1 4^1$ band is shown in Fig. II-4. The error limits indicate the range over which the P(E) can be varied without adversely affecting the fit. The translational energy of the product is very high; the maximum in the distribution is at 55 kcal/mole, or 65% of the total available energy. The resolution of the machine is sufficient to separate products in different vibrational states if the rotational excitation is low,[7] and the locations where peaks for H_2 vibrational levels would fall are marked at the top of Fig. II-4. No vibrational structure was seen.

2. Radiative Lifetime

The quantum yield for dissociation, ϕ_d, is related to the observed fluorescence decay time, τ_{fl}, and the radiative lifetime, τ_r, by

$$\phi_d = 1 - \tau_{fl}/\tau_r,$$

under the assumption that dissociation is the only means of collisionless non-radiative decay. Thus, the relative amount of product obtained after excitation of short- and long-lived rotational states in an S_1 vibrational

Fig. II-4. Product translational energy distributions for the molecular dissociation channel derived from angular distribution data in Fig. II-1. The CM angular distribution is isotropic. Shaded area indicates range for acceptable fit to data (see text). Maximum translational energies with production of vibrationally excited H_2 product are indicated at the top.

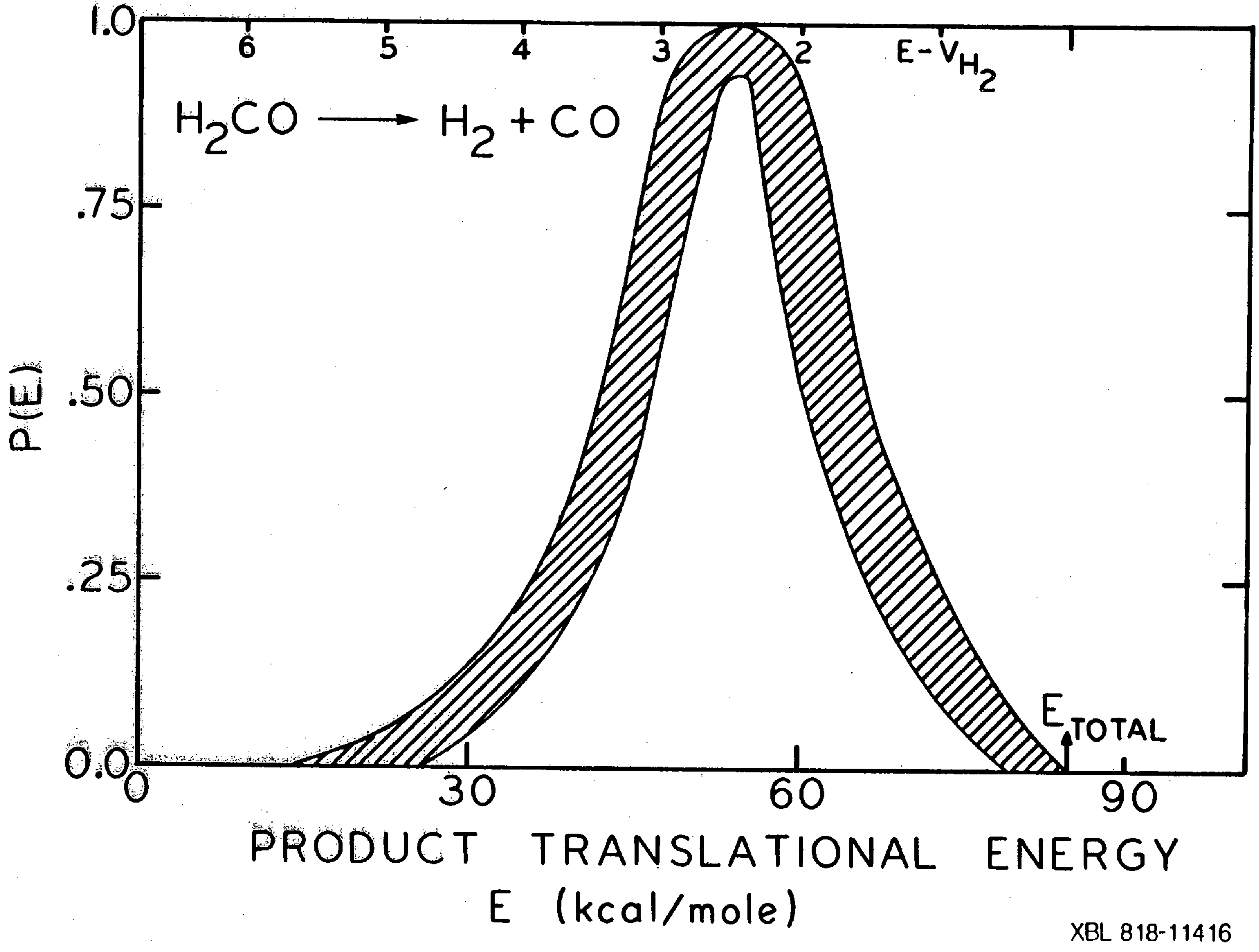
1.0
.75
.50
.25
0.0
P(E)
0
30
60
90
6
5
4
3
2
E-V_{H_2}
$H_2CO \longrightarrow H_2 + CO$
E_{TOTAL}
PRODUCT TRANSLATIONAL ENERGY
E (kcal/mole)
XBL 818-11416

Fig. II-4.

level gives information on the radiative lifetime of that vibrational level.

In the 4^1 vibrational band, TOF spectra at 10° were taken for excitation of the $rR_1(2)0$ line (28340.9 cm^{-1}) which has a 35 ns lifetime,[5] and the $pQ_1(3)E$ line (28302.1 cm^{-1}) which has a 3.1 μs lifetime.[1b] Unfortunately, another line, $pP_1(1)0$ (28302.0 cm^{-1}) was excited along with $pQ_1(3)E$; the separation between the two is less than the laser bandwidth. This state is thought to have a lifetime of about 100 ns,[5,8] and is therefore expected to decay primarily via dissociation. The data at the two excitation frequencies were obtained by alternately measuring spectra for half-hour periods in order to minimize the effect of long term signal variations. The total amount of CO produced at each frequency was obtained by integrating the peaks in the TOF spectrum. After summing 8 half-hour counts at each frequency, the ratio of the product observed at the two frequencies was 1.0 ± 0.2, where the uncertainty given, 1σ, reflects the counting statistics only.

For excitation of a particular rovibrational line i, the dissociation yield $\phi_i \propto p_i A_i(\tau_r - \tau_{fl,i}) I_{l,i}$. p_i is the fraction of molecules in the appropriate rotational state, A_i is the relative absorption strength factor for an asymmetric rotor, τ_r is the radiative lifetime, $\tau_{fl,i}$ is the observed fluorescence decay time and $I_{l,i}$ is the incident laser intensity at that frequency. A value for τ_r can therefore be obtained from the dissociation yields of two or more states if all the other parameters are known. For $pQ_1(3)E + pP_1(1)0$, the laser frequency was set at the maximum of the peak in the gas phase fluorescence excitation spectrum.

This probably centered the laser on $pQ_1(3)E$ since $pQ_1(3)E$ absorbs 3 times more strongly than $pP_1(1)0$ at room temperature, and the fluorescence quantum yield for $pQ_1(3)E$ is greater than for $pP_1(1)0$. Assuming a Guassian lineshape with FWHM = 0.25 ± 0.05 cm^{-1} for the laser, the laser intensity at $pP_1(1)0$ was a factor of 0.64 (+ 0.18, - 0.27) less than that at line center, i.e. at $pQ_1(3)E$.

Table II-2 shows τ_r values calculated from the observed product ratio. The calculation takes into account asymmetric rotor line strength factors, relative rotational populations (Table II-3) and laser intensities. Calculations which span the possible range of rotational temperatures are give in Table II-2, but it can be seen that this is not the major source of uncertainty in the results.

3. Radical Dissociation at 283.9 nm

HCO was detected after excitation of formaldehyde at 283.9 nm, indicating that dissociation to radicals occurs without collisions. Figure II-5 shows the TOF spectrum for HCO measured with the detector 8° from the molecular beam. TOF spectra observed at masses 28 and 29 were the same, indicating that most of the CO^+ detected at mass 28 is due to extensive HCO fragmentation in the ionizer. The integrated signals were within 6% (statistical σ = 12%), and all subsequent data was taken at mass 28. The HCO fragments are considerably slower than the CO products observed for excitation near the S_1 origin. This is as expected since the formation of radicals has a smaller amount of available excess energy (14 kcal/mole vs 85 kcal/mole). An angular

Table II-2. Calculated radiative lifetime (μs).

Product Ratio[a]	Radiative Lifetime[b]	
	T_{rot} = 25 K	T_{rot} = 50 K
0.8	$3.92^{+0.93}_{-0.45}$	$3.91^{+0.62}_{-0.44}$
1.0	$4.77^{+1.49}_{-0.65}$	$4.57^{+0.88}_{-0.44}$
1.2	$6.12^{+2.70}_{-1.04}$	$5.52^{+1.34}_{-0.63}$

a) Total product at $pQ_1(3)E + pP_1(1)0$ divided by total product at $rR_1(2)0$.

b) Error limits come from the uncertainty in the $pP_1(1)0$ contribution. Overall uncertainty is shown by the total range of values in this table.

Table II-3. Parameters used for calculating values of τ_r in Table II-2.

Rotational line	A[a]	τ_{fl} (ns)	population[b] 25 K	50 K
$rR_1(2)0$	0.98	35	8.80	4.84
$pQ_1(3)E$	1.47	3100	8.14	5.50
$pP_1(1)0$	1.00	100	6.96	3.34

a) Relative absorption strength for an asymmetric rotor.

b) Percent of the total population in the appropriate rotational state at the given rotational temperature.

Fig. II-5. Mass 28 time-of-flight spectrum for HCO production at 283.9 nm. The solid curve shown is a computer fit to the data corresponding to the P(E) in Fig. II-6. The dashed curve shows the calculated signal expected for molecular products if equal amounts of HCO and CO products are formed after excitation at 283.9 nm.

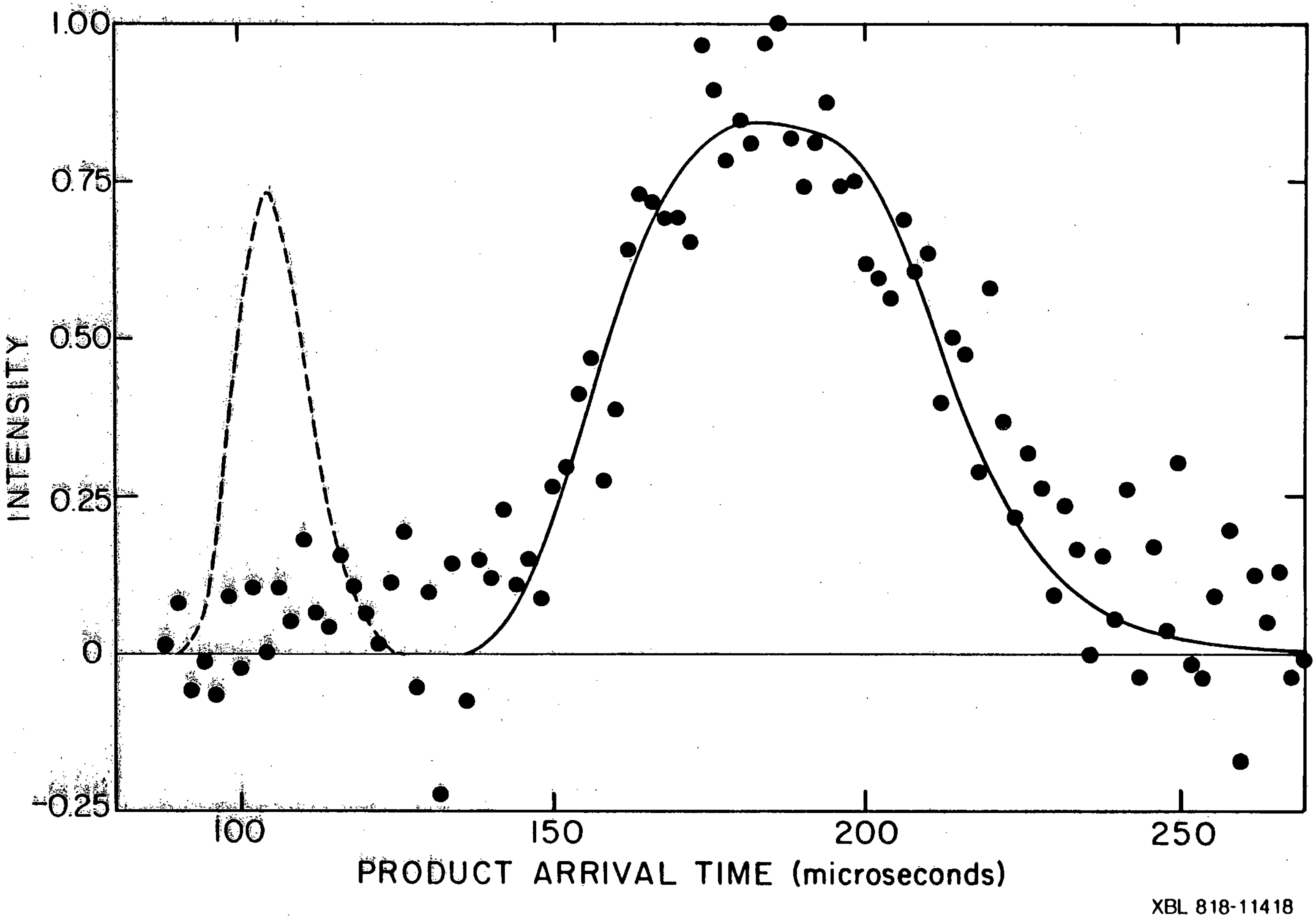
1.00
0.75
0.50
0.25
0
-0.25
INTENSITY
100
150
200
250
PRODUCT ARRIVAL TIME (microseconds)
XBL 818-11418

Fig. II-5

distribution could not be measured because the HCO product is kinematically constrained to a small angle in the laboratory frame of reference by the low translational energy (see Fig. II-3), and the high background from formaldehyde in the beam precludes measurements at laboratory angles less than 8°.

Figure II-6 shows the P(E) that best fit the HCO TOF spectrum. An isotropic angular distribution was assumed since data at a single laboratory angle is not sensitive to the CM angular distribution, and proved adequate to fit the data. The data do not give any information about HCO fragments with less than 2 kcal/mole of translational energy, because such molecules are scattered at angles less than 8° in the laboratory frame.

Since the TOF spectrum for the radical dissociation channel was measured using mass 28, any product from the molecular product channel should also have been detected, separated in time from the HCO signal by the difference in translational energy. Experimentally, however, no evidence for any fast CO product was seen. In order to estimate the branching ratio for the dissociation, the expected signal level for the molecular product channel was calculated assuming equal production of HCO and CO, i.e. $\phi_R = \phi_M$, and using the molecular P(E) obtained in the $2^1 4^1$ band scaled to account for the increased total energy. The observed signal for the radicals was assumed to represent the total radical product, i.e. the radical P(E) was set to zero below 2 kcal/mole. This assumption provides an upper limit for the branching ratio ϕ_M/ϕ_R. Differences in the laboratory angular distribution of the two products caused by the difference in product CM velocities, and the Jacobian factor in the

Fig. II-6. Product translational energy distribution for radical dissociation derived from data in Fig. II-5. An isotropic CM angular distribution is assumed. The data are not sensitive to the P(E) below 2 kcal/mole.

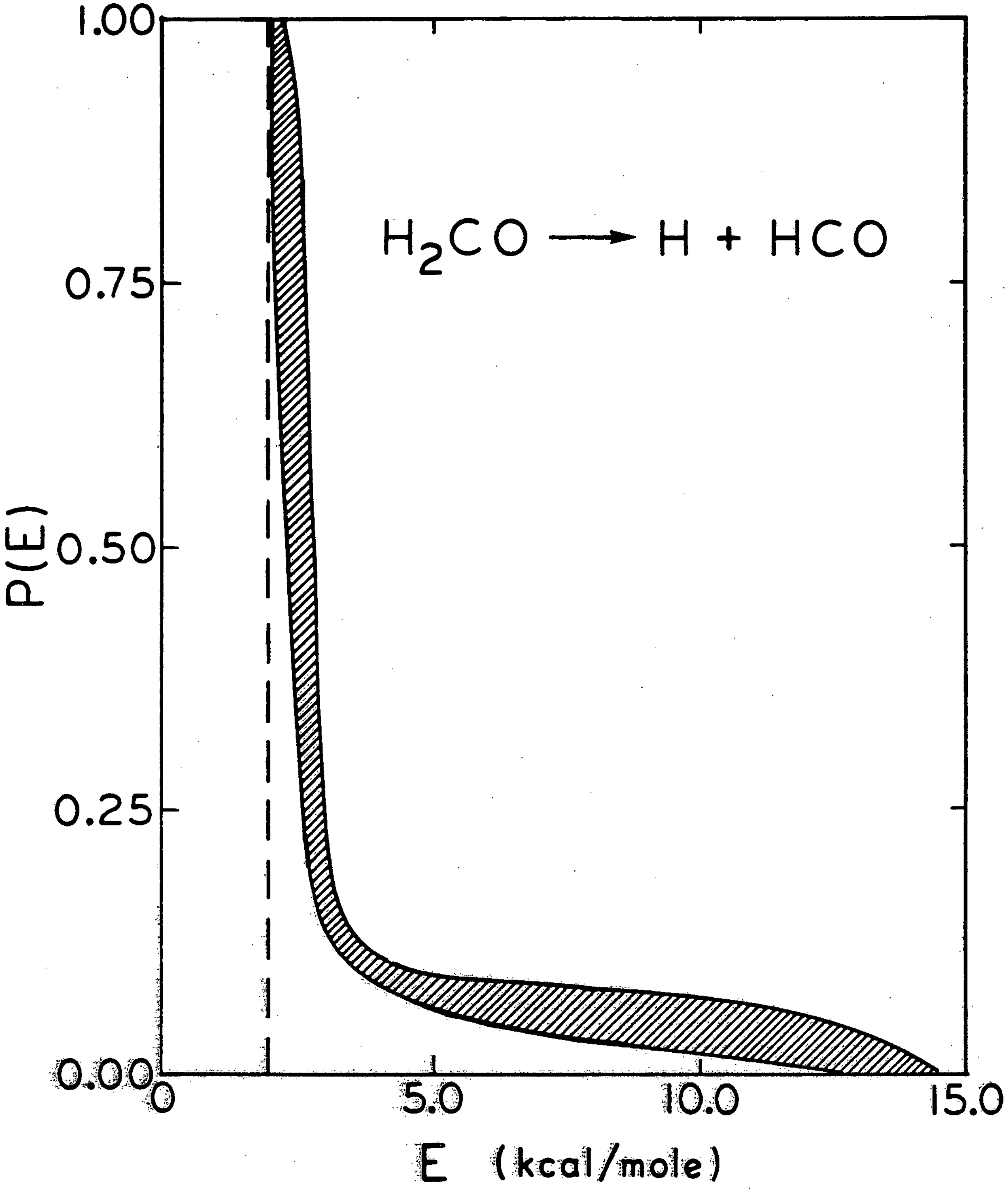

Fig. II-6.

XBL 818-11417

conversion from CM to laboratory frame of reference were taken into account in the calculation, and the result is shown in Fig. II-5. The comparison between the calculated molecular signal level (dashed curve) and the experimental data indicates that $\phi_M < 0.10\ \phi_R$, since a larger ϕ_M would have resulted in a detectable product signal.

D. DISCUSSION

1. Molecular Dissociation near the S_1 Origin

The major result of these experiments is the unequivocal detection of CO products, which confirm the $S_1 \rightarrow S_0 \rightarrow$ product coupling model for collisionless decay of S_1 formaldehyde. The observed TOF signal cannot result from the dissociation of formaldehyde dimer because no signal was seen at masses 29 or 30, and because no evidence for the presence of dimers in the beam was ever seen. The observed signal level (~0.3 counts/pulse) was of the order of magnitude expected from estimates of the beam density, rotational state populations, formaldehyde absorption cross section, fraction of product detected and ionizer efficiency. The similarity of the 4^1 and $2^1 4^1$ TOF spectra is expected since these bands are separated by only 1200 cm^{-1} (4% of the total available energy), and such a small difference in total energy would be unresolvable in the product P(E) unless a change in mechanism had occurred.

The isotropic product angular distribution shows that formaldehyde dissociation occurs on a timescale long compared with rotation. The absorption band of interest is a type b transition, and the transition dipole is perpendicular to the CO bond and in the molecular plane.[9,10] The laser was polarized in the plane of the beams, so molecules with the H - H direction parallel to the molecular beam are preferentially excited. *Ab initio* calculations of the potential energy surface indicate that the path of steepest descent from the transition state to molecular products is in the plane of the molecule.[11] Consequently, CO product from molecules in the plane of the beams at the moment of dissociation is more likely to be detected. If dissociation occurred before rotation averaged all initial orientations, the CO product distribution would show an angular dependence. The isotropic angular distribution is not unexpected since the shortest S_1 formaldehyde decay times (tens of ns)[1,12] are considerably longer than a rotational period.

The absence of structure in the TOF spectrum could indicate that there is sufficient rotational excitation of the products to smear out structure due to vibrational excitation of the H_2 product, and/or that vibrational excitation of CO is disguising any such structure. When 55 kcal/mole is in translation, sufficient energy remains to excite H_2 to $v = 2$ or CO to $v = 4$. Although the translational energy distribution gives no direct information on the distribution of the remaining energy among the internal degrees of freedom, some possibilities are suggested by simple models. In the transition state for H_2CO molecular dissociation calculated by Schaefer,[11] the CO (1.170 Å) and H_2 (1.246 Å) distances are longer than in the free CO (1.128 Å) and H_2 (0.7416 Å) molecules. In particular, the H - H distance in the transition state roughly corresponds to the classical turning point of $v = 3$ in H_2. If the dissociation occurs suddenly and there is no major redistribution of vibrational energy on the strongly repulsive exit channel surface, the products, particularly the H_2, should be vibrationally excited.[13,14] This is consistent with the fact that the maximum of the P(E) roughly falls where H_2 ($v = 2$) should be. This model, however, is only qualitative since the breaking of the C - H bonds is not simultaneous. In the transition state, one C - H bond is already essentially broken ($r =$ 1.586 Å, bond order = 0.2), while the other is nearly normal ($r =$

1.104 Å). Pople's[15] calculated transition state is qualitatively the same as Schaefer's, but the bond distances for the longer of the two C - H bonds and the H - H bond are somewhat greater. A very simple impulse approximation calculation,[16] treating the H_2 as a point mass and assuming that it leaves along the line connecting the H_2 center-of-mass to the C atom in Schaefer's transition state, gives CO with $J = 23$ and $v(\text{average}) = 0.4$ for 55 kcal/mole of product translation energy. Formaldehyde dissociation product energy distributions peaked about $H_2(v = 2, J = 3) + CO(v = 0, J = 23)$ are suggested by these simple models, but many other distributions are similarly consistent with the data.

The CO product vibrational distribution measurements of Houston and Moore[17] showed 11% of the CO in $v = 1$ and 2% in $v = 2$ for photolysis at 337 nm. For photodissociation of the analogous system HFCO, Berry[18] found <7% of the total available energy in HF vibrational excitation. These measurements of low product vibrational energy are in qualitative agreement with the high translational energy of the present result; however, possible effects from collisional processes in these earlier studies may vitiate the comparison. If CO is indeed produced with $J(\text{avg}) = 23$ as implied above, the delay in the CO ($J \sim 10$) appearance observed using a CO laser (Ref. 17 and Chapter III) may be complicated by rotational relaxation. This evidence for the role of an intermediate[17] in formaldehyde dissociation may thus be compromised, but CO infrared fluorescence measurements, also indicate a delay in the CO production.[19]

The product translational energy distribution obtained in this experiment will provide a good test for formaldehyde potential energy surfaces. Dynamical calculations on a good surface should give a P(E) that matches the experimental data. Such calculations would also give more reliable and detailed information on the partitioning of energy among the internal degrees of freedom than could possibly be obtained from the simple models discussed above. Handy and Carter[20] have recently developed an analytical form for the formaldehyde potential surface that should be useful in such calculations.

2. Radiative Lifetime

Table II-2 indicates a best value of ~4.7 μs for τ_r in 4^1, but a fairly wide range of values for τ_r can be consistent with our data. A further complication is introduced in the analysis by the fact that the upper state of $pP_1(1)0$ is J = 0. The molecules in this state will not be rotating so the CO product will not be isotropically distributed in the CM frame. It is not clear whether the signal at 10° would be higher or lower than isotropic. A radiative lifetime of 4.7 μs is in agreement with previous work. The *ab initio* calculation of Kemper et al.[21] yielded τ_r = 4.2 μs for 4^0. This agrees with the longest lifetimes observed by Weisshaar[1] of 4.17 and 3.1 μs for 4^0 and 4^1, respectively, and 3.3 μs value τ_r for 4^1 by Shibuya et al.[12c]

3. Radical Dissociation Channel

In contrast to the molecular dissociation channel, radical products have a very small fraction of the available energy in translation. This is reasonable for a unimolecular reaction with no repulsive energy release in the exit channel, if extensive energy sharing occurs among vibrational degrees of freedom. The calculations of Schaefer[11] and Morokuma[22] indeed suggest that the potential energy surface for the dissociation of S_0 formaldehyde to H + HCO does not have an exit barrier. The P(E) for such a surface would have its maximum at zero translational energy. T_1 may also be involved in radical formation, since 35220 cm^{-1} may be above the barrier for dissociation on the T_1 surface, but the present experiments give no information on this.

The present experiments indicate that dissociation to radicals is dominant over production of H_2 and CO by at least one order of magnitude at 283.9 nm. Statistical calculations were performed in order to compare the experimental branching ratio with a theoretical model. RRKM dissociation rates for the molecular and radical dissociation channels were calculated using a program written by Hase and Bunker.[23] The calculations were done for energies above the radical threshold, so tunneling will have a negligible influence on the rate. The molecular parameters used in the calculation are shown in Table II-4. For the molecular dissociation channel, the geometry and frequencies of the transition state were taken to be those of Goddard and Schaefer.[11a] Their calculations for the radical dissociation channel (inset, Fig. II-7) show that there is no maximum on the potential surface at which to define a transition state. In the absence of a potential maximum in the reaction coordinate,

Table II-4. Parameters used in RRKM calculations.

A. Formaldehyde.[a]

Geometry: planar, r_{CO} = 1.203 Å, r_{CH} = 1.099 Å, <HCO = 121.75 deg

Frequencies (cm^{-1}): 2766.4, 1746.1, 1500.6, 1167.3, 2843.4, 1251.2.

Moments of inertia (amu $Å^2$): 1.79, 13.04, 14.83.

B. Molecular transition state.[b]

Geometry: planar, r_{CO} = 1.151 Å, r_{CH} = 1.104 Å, $r_{CH'}$ = 1.586 Å,

r_{HH} = 1.203 Å, <H'CO = 112.5 deg.

Frequencies (cm^{-1}): 2760, 1654, 592, 800, 1137.

Moments of inertia (amu $Å^2$): 1.71, 13.73, 15.44.

C. Radical critical configuration.

Geometry:[c] planar, r_{CO} = 1.203 Å, r_{CH} = 1.099 Å, <HCH' = 116.5 deg.,

<HCO = 121.75 deg.

$r_{CH'}$	1.5 Å	2.0 Å	2.5 Å	3.0 Å	3.5 Å
n[d]	0.214	0.031	0.005	6.7×10^{-5}	9.7×10^{-5}
Frequencies[e]	2600	2600	2600	2600	2600
cm^{-1}	1800	1800	1800	1800	1800
	1100	1100	1100	1100	1100
	578	221	84	32	12
	578	221	84	32	12
Moments of	2.46	3.48	4.53	5.49	6.27
inertia	13.50	14.52	16.00	18.05	20.76
	15.95	18.00	20.53	23.54	27.03

Table II-4. continued

a) Parameters from Refs. 27, 29.
b) Parameters from Ref. 11a.
c) Geometry is that of H_2CO (Ref. 27) with one C - H bond extended.
d) n = bond order. $\ln n = [r_{C-H} - 1.099 \text{ Å}]/-0.26$.
e) The first three frequencies correspond to the HCO freqencies. The C - H stretch is estimated from the frequency measured in a matrix (Ref. 28), the C - O and bend frequencies are from Ref. 29. See text for the explanation of the models for the remaining two frequencies.

Fig. II-7. Calculated RRKM rates for $H_2CO \rightarrow H_2 + CO$ and $H_2CO \rightarrow H + HCO$ (using different models for the critical configuration for radical dissociation--see text). The parameters used are given in Table II-4. Inset shows potential energy surface for $H_2CO \rightarrow H + HCO$ calculated by Goddard and Schaefer.[11a] E^* is the energy of the dissociating molecule referenced to the zero-point energy of the molecule.

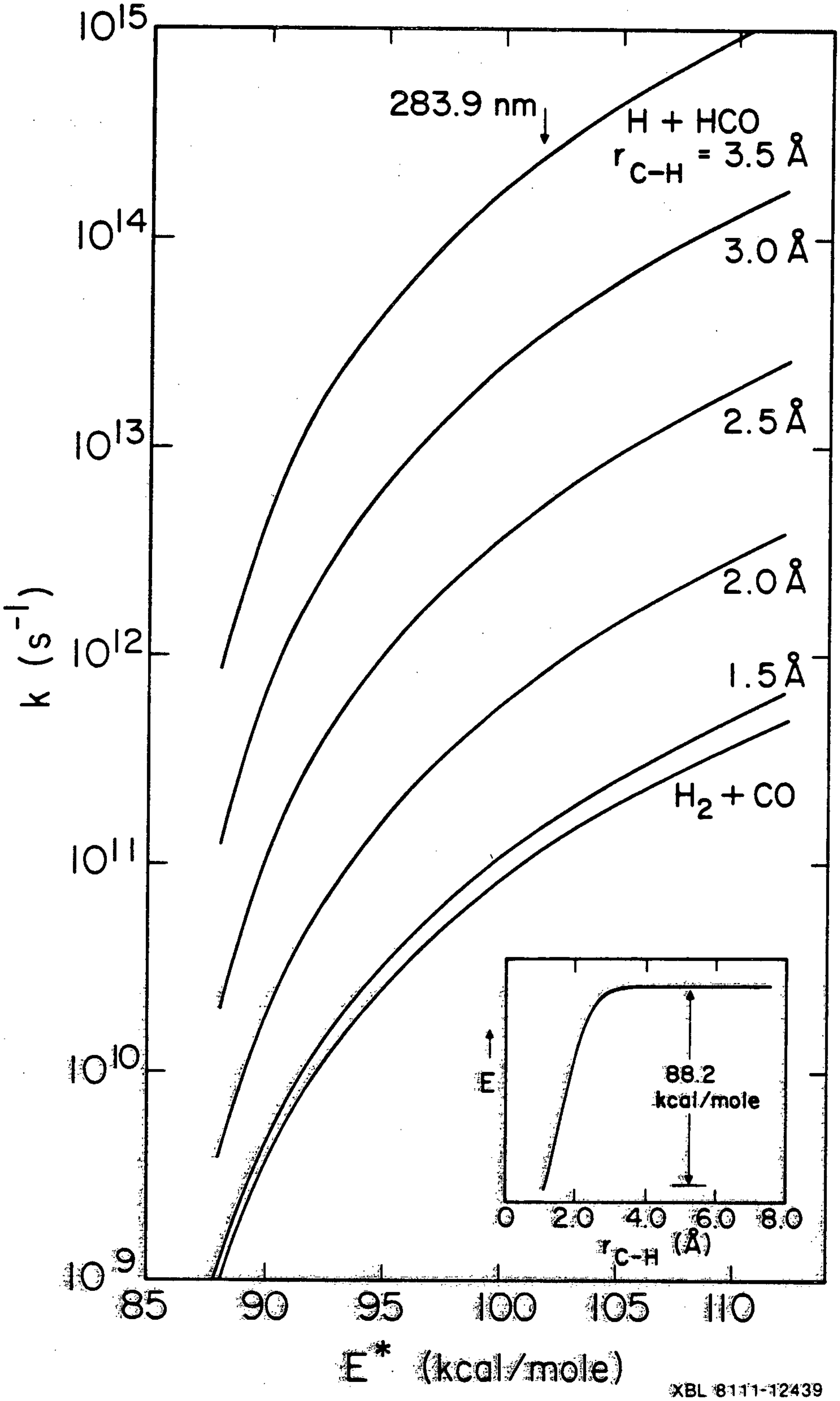
10^{15}
10^{14}
10^{13}
10^{12}
10^{11}
10^{10}
10^{9}
$k\ (s^{-1})$
283.9 nm
H + HCO
r_{C-H} = 3.5 Å
3.0 Å
2.5 Å
2.0 Å
1.5 Å
$H_2 + CO$
85
90
95
100
105
110
E^* (kcal/mole)
E
88.2 kcal/mole
0
2.0
4.0
6.0
8.0
r_{C-H} (Å)
XBL 8111-12439

Fig. II-7.

various methods for locating the critical configuration, such as the minimization of state density,[24] result in a critical configuration at large values of the reaction coordinate.[24,25] For $H_2CO \rightarrow H + HCO$, it is expected that the critical configuration will have the C - H bond stretched to 2-3 times the normal C - H bond distance. For a loose complex such as this, the critical configuration for dissociation should resemble the product more than the reactants. Three frequencies of the critical configuration were chosen to match the free HCO frequencies; one C - H stretch becomes the reaction coordinate, and the remaining two frequencies correspond to bends in H_2CO that become rotations of the products. Although it is not strictly applicable to bending vibrations, the BEBO method[26] was used to determine these two frequencies for several models of the radical critical configuration with different C - H bond distances. The frequency in the critical configuration, ν, is obtained from the single bond frequency in the molecule, ν_s, via $\nu = \nu_s\sqrt{n}$. The bond order n is given by $\ln n = [r_{CH} - r_s]/-0.26$, and r_s = bond length for a single C - H bond. The results of the calculations are shown in Fig. II-7. For the most reasonable models of the radical critical configuration, r_{CH} = 2-3 Å, dissociation of H_2CO to radicals dominates the molecular channel by more than one order of magnitude. Recently, Goddard, et al.[11b] have published more complete calculations for the molecular transition state. Their frequencies are higher than those in Table II-4, which would decrease the calculated molecular dissociation rate. Thus, the RRKM calculations indicate that it is not unreasonable for the radical channel to dominate at an energy 14 kcal/mole above the threshold for radical formation. This estimate for the molecule/radical branching ratio is not in good agreement with previous quantum yield measurements. Values of ϕ_R from 0.4 to 0.9[30-32] have been obtained for wavelengths between 280 and 300 nm. $\phi_M + \phi_R = 1$, so the molecule/radical branching ratios from these experiments are >0.1. Since not all works show a smooth dependence on ϕ_R on wavelength (see Fig. 3 of Ref. 31), comparison to the present work at 283.9 nm may not be valid. The previous measurements were done at high pressures (>5 Torr) using radical scavengers, so the discrepancy might also be attributed to the difference in pressure regime, i.e. collisional effects.

E. CONCLUSIONS

The major conclusion of this work is that formaldehyde does indeed dissociate without collisions after excitation near the S_1 origin. This strongly supports the model derived from low pressure fluorescence decay times for S_1 decay through a lumpy continuum of S_0 levels broadened by dissociation. At higher photolysis energies, dissociation to radicals is the dominant channel and also takes place without collisions. Molecular products have a large fraction of the total available energy in translation, while the radical products have little translational energy.

The photopredissociation of formaldehyde near the S_1 origin is now quite well understood in the collisionless regime. Incorporation of collisional effects into this understanding requires further investigation.

REFERENCES

1. a) J. C. Weisshaar and C. B. Moore, J. Chem. Phys. 70, 5135 (1979); b) 72, 5415 (1980); c) J. C. Weisshaar, D. J. Bamford, E. Specht, and C. B. Moore, J. Chem. Phys. 74, 226 (1981).
2. Y. T. Lee, J. D. McDonald, P. R. LeBreton, and D. R. Herschbach, Rev. Sci. Instrum. 40, 1402 (1969).
3. D. A. Ramsay, private communication.
4. The notation $rQ_{K''}(J'')$ denotes a $\Delta K = +1$, $\Delta J = 0$ transition in absorption from the J"K" ground state. O and E indicate whether J" + K_A" + K_C" is odd or even. See also Rev. 1a.
5. D. J. Bamford, P. Ho, Aa. S. Sudbo, and C. B. Moore, in preparation.
6. R. J. Buss, Ph.D. Thesis, University of California, Berkeley (1979).
7. R. K. Sparks, L. R. Carlson, K. Shobatake, M. L. Kowalczyk, and Y. T. Lee, J. Chem. Phys. 72, 1401 (1980).
8. J. C. Weisshaar, unpublished data.
9. D. C. Moule and A. D. Walsh, Chem. Rev. 75, 67 (1975).
10. G. H. Dieke and G. B. Kistiakowsky, Phys. Rev. 45, 4 (1934).
11. a) J. D. Goddard and H. F. Schaefer, J. Chem. Phys. 70, 5117 (1979); b) J. D. Goddard, Y. Yamaguchi, and H. F. Schaefer, J. Chem. Phys. 75, 3459 (1981).
12. a) K. Shibuya, R. A. Harger, and E. K. C. Lee, J. Chem. Phys. 69, 751 (1978); b) K. Shibuya and E. K. C. Lee, J. Chem. Phys. 69, 5558 (1978); c) K. Shibuya, P. W. Fairchild, and E. K. C. Lee, J. Chem. Phys. 75, 3397 (1981); d) P. W. Fairchild, K. Shibuya, and E. K. C. Lee, J. Chem. Phys. 75, 3407 (1981).

13. M. J. Berry, Chem. Phys. Lett. 29, 329 (1974).

14. R. L. Jaffe and K. Morokuma, J. Chem. Phys. 64, 4881 (1976).

15. M. J. Frisch, R. Krishnan, and J. A. Pople, J. Phys. Chem. 85, 1467 (1981); L. B. Harding, H. B. Schlegel, R. Krishnan, and J. A. Pople, J. Phys. Chem. 84, 3394 (1980).

16. G. E. Busch and K. R. Wilson, J. Chem. Phys. 56, 3626 (1972).

17. P. L. Houston and C. B. Moore, J. Chem. Phys. 65, 757 (1976).

18. D. E. Klimek and M. J. Berry, Chem. Phys. Lett. 20, 141 (1973).

19. M. B. Zughul, Ph.D. Thesis, University of California, Berkeley, 1978.

20. N. C. Handy and S. Carter, Chem. Phys. Lett. 79, 118 (1981).

21. M. J. H. Kemper, J. M. F. van Dijk, and H. M. Buck, J. Chem. Phys. 70, 2854 (1979).

22. D. M. Hayes and K. Morokuma, Chem. Phys. Lett. 12, 539 (1972).

23. W. L. Hase and D. L. Bunker, Program #234, Quantum Chemistry Program Exchange, Indiana University.

24. D. L. Bunker and M. Pattengill, J. Chem. Phys. 48, 772 (1968).

25. P. J. Robinson and K. A. Holbrook, Unimolecular Reactions, Wiley-Interscience, London, 1972, Ch. 6.

26. H. S. Johnston, Gas Phase Reaction Rate Theory, Ronald, New York, 1966, Ch. 4.

27. K. Yamada, T. Nagakura, K. Kuchistu and Y. Morino, J. Mol. Spectrosc. 38, 70 (1971).

28. D. E. Milligan and M. E. Jacox, J. Chem. Phys. 41, 3032 (1964).

29. G. Herzberg, Molecular Spectra and Molecular Structure. Vol. III, Van Nostrand Reinhold, New York, 1966.

30. J. H. Clark, C. B. Moore, and N. S. Nogar, J. Chem. Phys. 68, 1264 (1978).

31. K. Y. Tang, P. W. Fairchild, and E. K. C. Lee, J. Phys. Chem. 83, 569 (1979).

32. A. Horowitz and J. G. Calvert, Int. J. Chem. Kinet. 10, 805 (1978).

CHAPTER III. CO APPEARANCE RATES

A. INTRODUCTION

The present understanding of the role of collisions is incomplete; Houston[1] and Zughul[2] observed a delay in the appearance of CO relative to the decay of $H_2CO(S_1)$. Within the experimental uncertainty, the appearance rate was the same for 337 and 355 nm excitation, and extrapolated to zero at zero pressure. A model postulating that $H_2CO(S_1)$ decays to an intermediate state, I, which then collisionally dissociates to H_2 + CO was constructed to explain these observations. This can be reconciled with the observation of CO product formation in a molecular beam if collisions quench S_1 to I very efficiently.

The major unknown in the collisional dissociation of formaldehyde is the identity of this intermediate. The T_1 and S_0 states of H_2CO, as well as the isomer HCOH have all been suggested. The experiments described in this chapter were designed to study the behavior of the intermediate as a function of energy. Such information would be useful in sorting through these candidates. Measurements of the CO appearance rate were extended to shorter wavelengths using the method of transient absorption of CO laser emission used by Houston.[1]

B. EXPERIMENTAL

Much of the experimental apparatus has been previously described by Houston.[1] Modifications and additional details will be described in this account.

Figure III-1 shows a schematic diagram of the experiment. The pulsed uv photolysis laser and the cw CO probe laser beams are overlapped in a cell containing formaldehyde. The 2 laser beams are combined and separated by dichroic mirrors. Transient absorptions of the ir laser by CO from formaldehyde dissociation are monitored by a fast infrared detector. A transient digitizer and hardwired signal averager are used for signal processing.

1. CO Laser

A description of the CO laser discharge tube has been given by Houston;[1] the laser is similar to those described by Djeu[3] and by Gerlach and Amer.[4] The cooling system and feedback circuit have been modified to improve the stability of the laser.

Figure 2 of Ref. 1 is a schematic of the CO laser tube. Plexiglas window holders, cut at Brewster's angle, fit over the (square-cut) ends of the laser tube and were sealed on the Apiezon W (black wax). Calcium fluoride windows (38 mm diameter x 5 mm thick) were sealed with o-rings and held on by vacuum. When the discharge tube was cold, the windows were flushed with dry nitrogen to prevent water condensation. The windows were periodically cleaned with lens paper and spectral grade methanol; this was crucial to good laser performance. The teflon

Fig. III-1. Schematic of the CO appearance rate experiments. DM = dichroic mirror, M = mirror, I = iris, F = bandpass ir filter. See text for description.

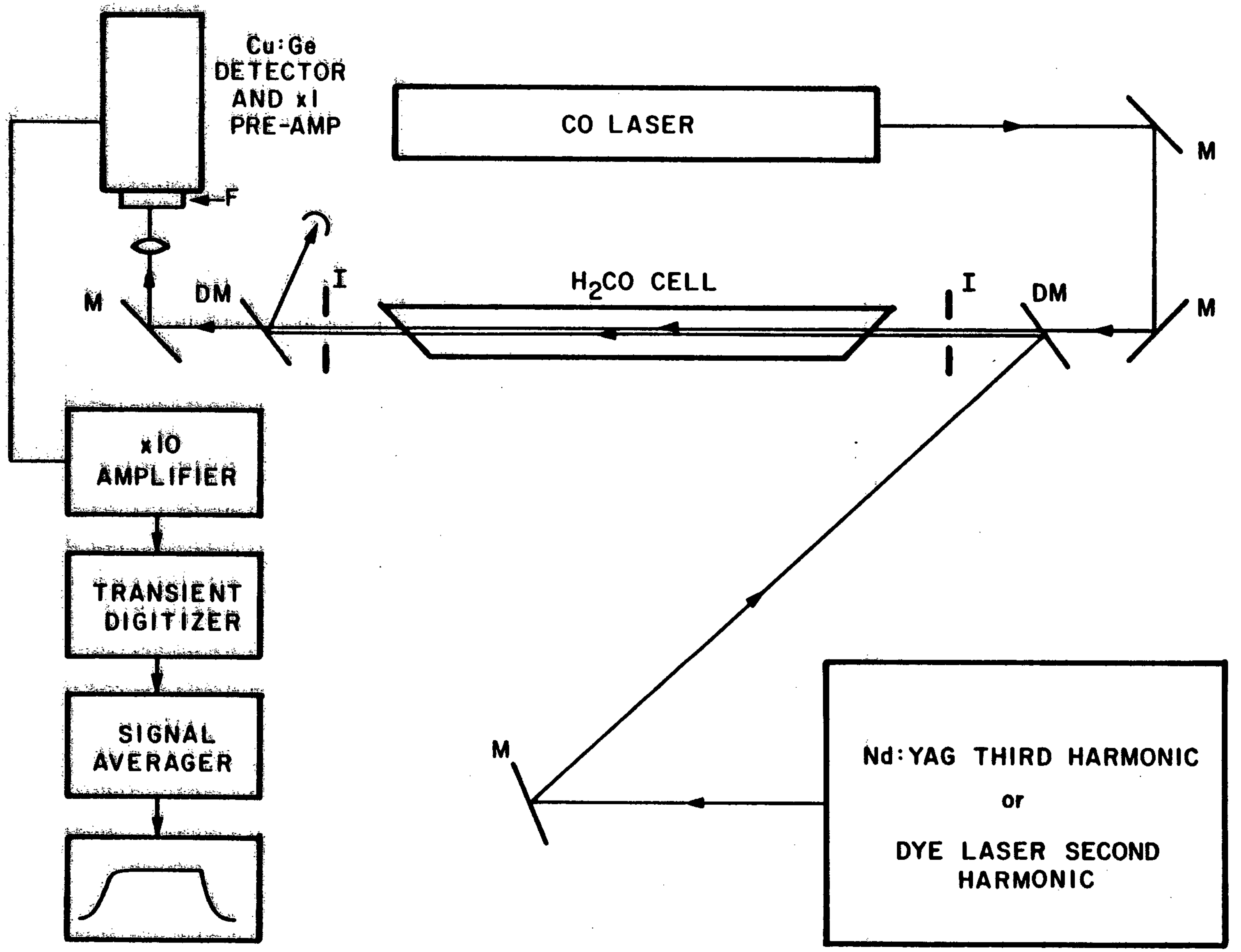

Fig. III-1

XBL 8111-12444

plugs near the ends of the discharge tube reduce diffusion of CO to the unexcited regions near the windows, where it would quench lasing in the v = 1-0 band. A portion of the line connecting the discharge tube and the vacuum pump was water cooled to reduce oil backstreaming. The discharge tube could be cleaned by removing the window holders and teflon plugs, rinsing the inside with acetone, dilute nitric acid, etc. to remove deposits, and then baking the entire tube in the glass annealing oven.

Nitrogen boiloff from the cooling jacket of the discharge tube was vented through small (~12 mm diameter) openings near each electrode, similar to those described by Gerlach.[4] A manifold of glass and tygon tubing carried the cold gas away from the steel I beam (6" x 6" x 8') which served as an optical rail. This reduced perturbations in the laser alignment caused by thermal contractions of the rail. The liquid nitrogen jacket was enclosed in Armstrong Armalok insulation; 50 liters of ℓN_2 lasted approximately 5 hrs. Variations in the cooling jacket ℓN_2 level were held to within ±1 cm. Figure III-2 is a circuit diagram for the ℓN_2 level controller, which shut off the N_2 flow to the ℓN_2 dewar when the cooling jacket was full. The previously used thermal expansion sensor was replaced with a resistance temperature sensor. Careful control of the discharge temperature reduced fluctuations in the laser power. After each use of the laser, the cooling jacket was flushed with dry nitrogen during warming. This kept water from condensing in the cooling jacket and cracking the tube upon subsequent cooling.

Fig. III-2. Circuit diagram for liquid nitrogen controller. When the ℓN_2 level in the laser cooling jacket is high, current flows through the magnetic valve, shutting off the nitrogen flow to the ℓN_2 dewar.

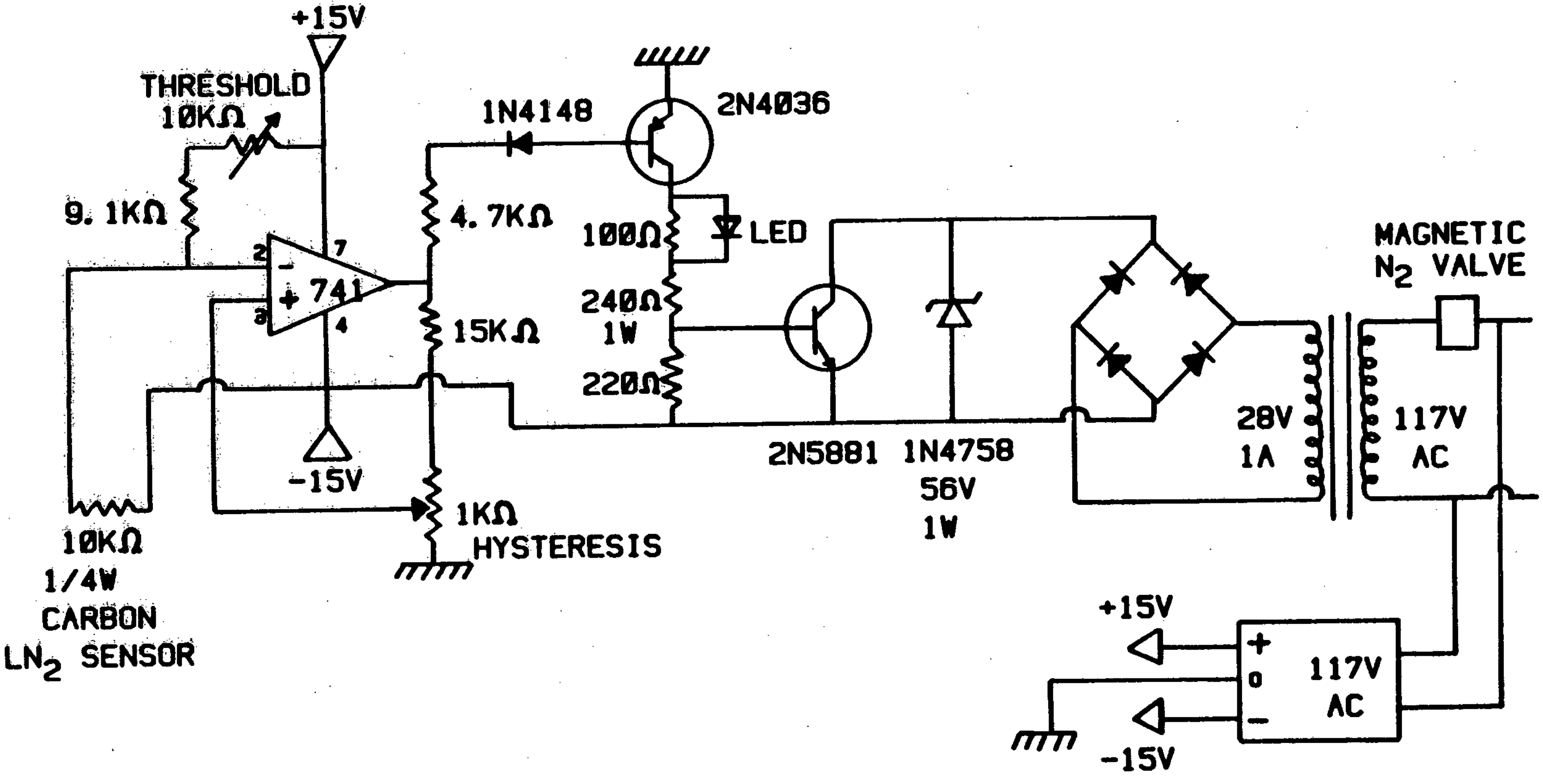

XBL 8111-12340

Fig. III-2.

The laser cavity was formed by a grating (Bausch and Lomb, 4 μ, 300 lines/mm) and a 3 m radius-of-curvature output mirror coated for 98% reflection at 4.8 μ (Coherent). Cavity alignment was done with the eighth order reflection of a HeNe laser. An intracavity iris could be closed down to give single mode operation. Figure III-3 shows the components of the feedback circuit used to lock the laser to the peak of its gain curve; Houston[1] also discusses the stabilization scheme. The reference channel of a lock-in amplifier (PAR, JB-5) provided a 400 Hz signal. This was fed to a Burleigh RC 42 ramp generator that served as a programmable high voltage power supply. The output of the ramp generator was applied to a piezoelectric transducer (Burleigh PZ-80) which modulated the position of the output mirror of the CO laser along the optical axis. A small change in the cavity length changes the position of the laser's longitudinal modes within the gain curve of the discharge. Modulation of the mirror position therefore leads to a similar modulation in laser power, the amplitude and sign of which are determined by the slope of the gain curve. The laser output along the zeroth order reflection of the grating was monitored with a PbSe detector (Optoelectronics) which was connected to the signal channel of the lock-in. The lock-in amplifier was used with a filter time constant of 3 s and 6 dB/octave rolloff. The double-ended DC signal from the monitor terminals of the lock-in was converted to a single-ended signal by the differential amplifier shown in Fig. III-4. The gain of the differential amplifier was typically set at 20 or 50, and the limiter at ±9V. This signal was fed to the ramp generator as a small "correction" to the output DC level. This "correction" drives the laser toward the

Fig. III-3. Schematic of the feedback circuit used for laser stabilization.

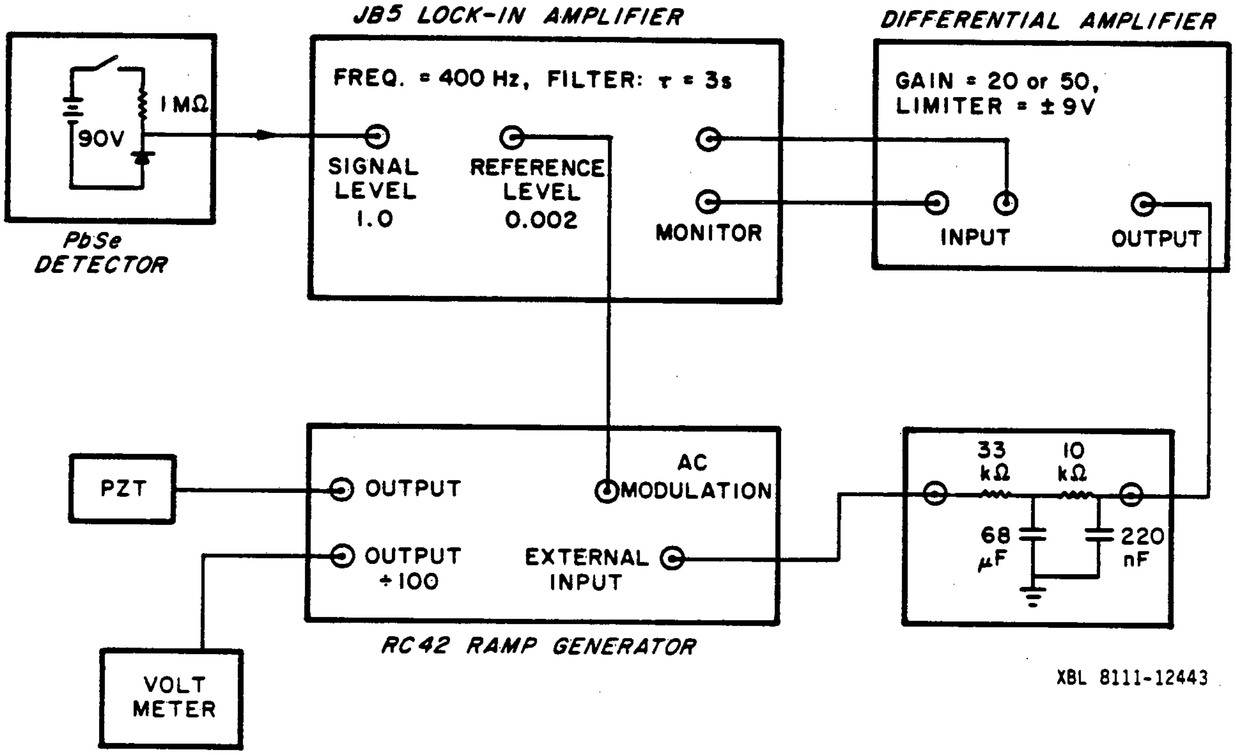

XBL 8111-12443

Fig. III-3.

Fig. III-4. Circuit diagram for differential amplifier. ZD = zener diodes used as voltage limiters; ±3,6,9,12 or ∞ V.

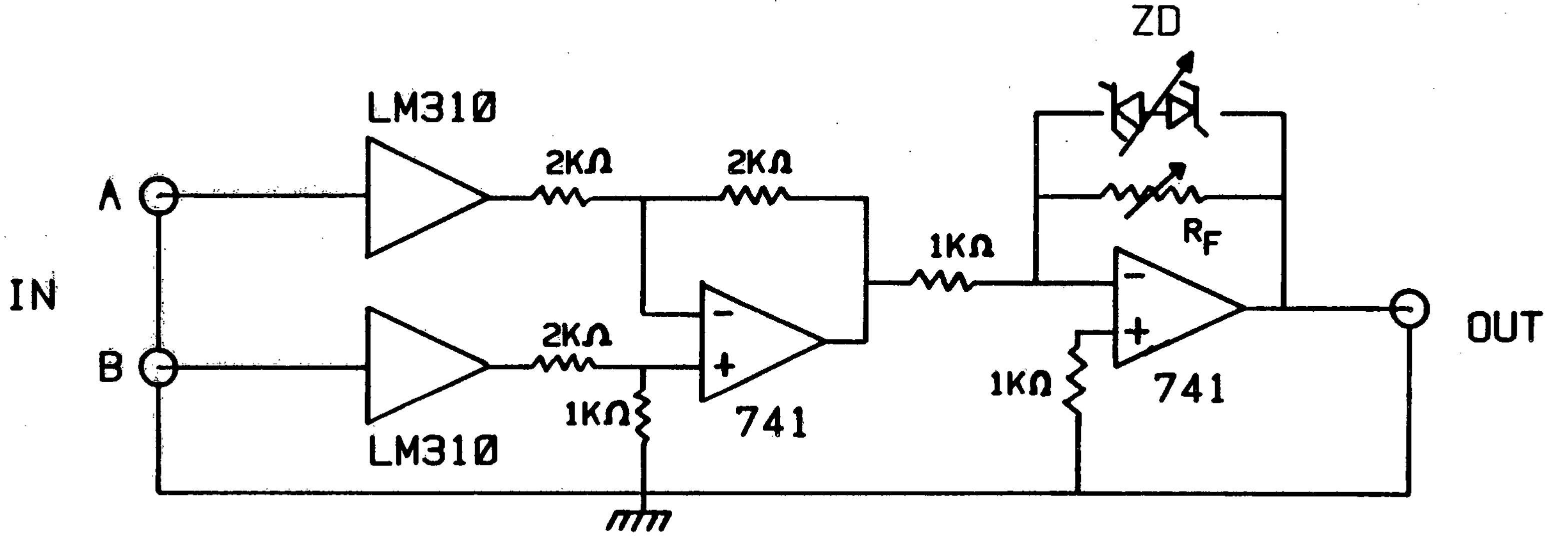

XBL 8111-12341

Fig. III-4.

peak of the gain curve; the size of the correction is proportional to the slope of the gain curve. The DC level of the ramp generator output was monitored with a voltmeter. Large adjustments and the initial setting of the DC level (0 to 1000 V) were done manually with the ramp bias (or offset) control on the ramp generator. Under optimized conditions, the laser power stability was better than ~1% on a μs time scale. On a ms time scale, larger (5-10%) fluctuations were observed, and are attributed to vibrations of the laser table.

A gas handling manifold was constructed of soldered 1/4" copper tubing, 1/4" diameter polyflow tubing, and Gyrolok fittings. Each gas inlet was equipped with a shut-off valve and a needle valve. The relative gas flow to the halves of the laser could be varied with needle valves. CO and air were pre-mixed in a section of the manifold containing a 0-1 atm pressure gauge, and added to the other gases through another needle valve. Hoses of 3/8" diameter polyflow tubing (several meters long) connected the manifold to the discharge tube; the connection to the glass was made with nylon Ultratorr fittings. The purities of the gases used in the discharger were: He - 99.995%, N_2 - 99.999% and CO - 99.0% (Matheson Technical Grade).

The recommended procedure for starting the CO laser is: Allow the lock-in amplifier to warm up for about one hour and adjust the AC balance. During this time, open the CO needle valves to give a measurable pressure (~500-600 Torr) on the gauge, and a pressure in the laser of ~0.1 Torr (barely measurable on the oil manometer at the laser outlet). After the CO flow reaches steady state, as evidenced by a constant reading on the gauge, add air (~5%) to the CO. Then cool the laser tube with ℓN_2. Add ~1 Torr N_2 to the CO/air mixture before turning on the power supply. Figure III-5 is a schematic of the laser power supply; typical operating conditions were 12 kV and 20 mA. Slowly add 1 Torr He to the CO/air/N_2 discharge, then 3 Torr He to the outer ports. If either half of the discharge goes out, reduce the He and balance the gas flows. If the discharge does not re-light when the He is shut off, turn down the high voltage and try again. Look for lasing with a liquid crystal sheet while adjusting the grating settings. With the gas mixture given here, the longer wavelength transitions ($v \geqq 3$) lase. Lasing in the $v = 1$-0 band is obtained by adding more N_2 to the discharge and reducing the CO as the grating is tuned to shorter wavelengths. Conversely, increasing the CO and decreasing the N_2 results in many longer wavelength transitions, and improves their output powers. Once lasing on the desired transition is obtained, the gas mixture and grating setting should be adjusted for maximum power using either a thermopile or the ir detector (and chopping the beam) to monitor the power level. Then turn on the feedback electronics and adjust the gain and limiter voltage for the most stable output. Table III-1 lists some of the laser lines observed and typical output powers. Lasing was also observed from higher vibrational levels ($v = 5$-10), but these transitions were not used in the present experiments. Wavelengths were measured with a 3/4 m Spex monochromator; $v = 1$-0 transitions could also be identified with a CO gas filter cell. Absolute powers were measured with an Eppley thermopile. Relative power levels could also be obtained by chopping the laser beams and noting the amplitudes of the square-wave signals from the ir detector.

Fig. III-5. Circuit diagram for the CO laser power supply.

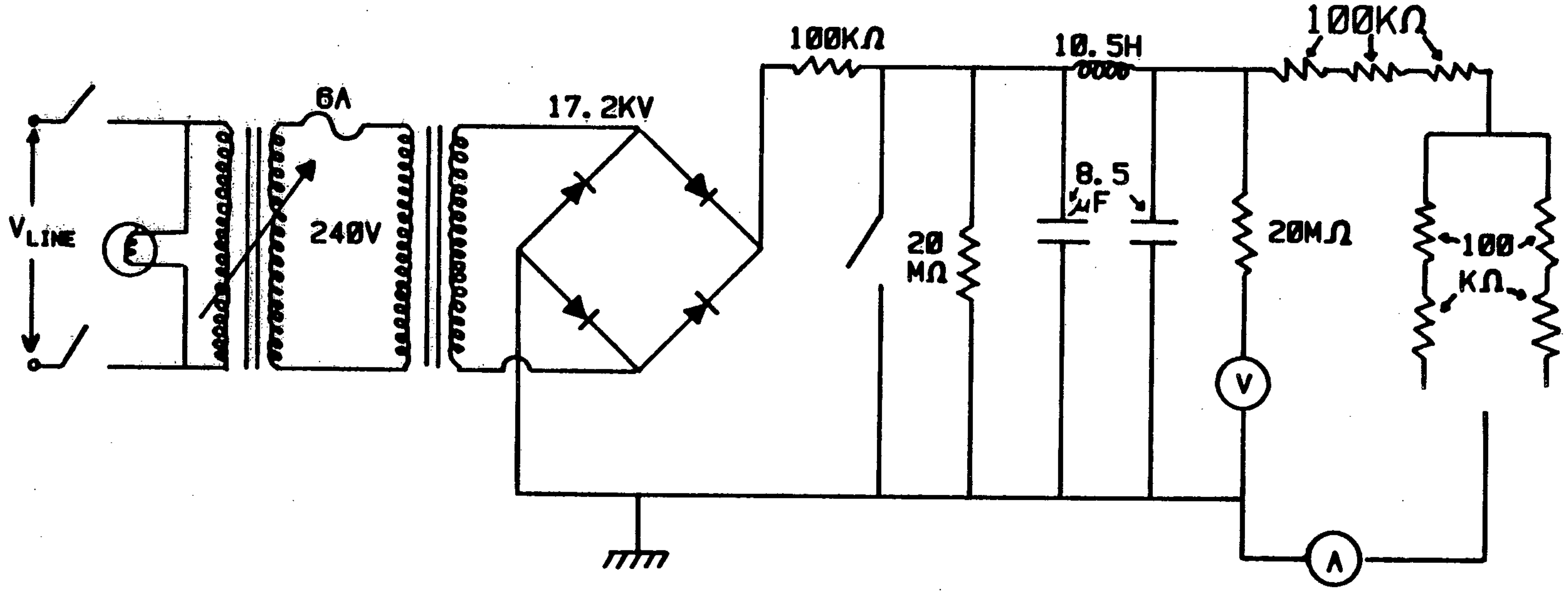

XBL 8111-12339

Fig. III-5.

Table III-1. CO laser lines observed.[a]

Laser Line	Frequency cm^{-1}	Power mW
$P_{1-0}(11)$	2099.08	6
$P_{1-0}(12)$	2094.86	8
$P_{1-0}(13)$	2090.60	4
$P_{2-1}(9)$	2081.23	20
$P_{2-1}(10)$	2077.11	20
$P_{2-1}(11)$	2072.96	20
$P_{2-1}(12)$	2068.78	30
$P_{2-1}(13)$	2064.55	20
$P_{3-2}(8)$	2059.20	20
$P_{3-2}(9)$	2055.15	30
$P_{3-2}(10)$	2051.07	35
$P_{3-2}(11)$	2046.95	35
$P_{3-2}(12)$	2042.80	35
$P_{4-3}(7)$	2037.12	35
$P_{4-3}(8)$	2033.14	35
$P_{4-3}(9)$	2029.12	40

a) Partial list. Transitions from higher vibrational levels were also observed.

2. Photolysis Lasers

Two different laser systems were used for the formaldehyde photolysis. For the studies at 354.7 nm, a Raytheon model SS404 Nd:YAG oscillator/amplifer system was used. The output of this laser is in the TEMOO mode with a beam diameter of ~3 mm. Typically, 5 mJ of 1064.1 nm output from the master oscillator yields ~200 mJ after three amplifiers. A type I KD*P crystal generates the 532 nm second harmonic, and a type II KD*P crystal mixes fundamental with second harmonic to generate the 354.7 nm third harmonic. Reference 2 gives a more detailed description of this laser. A maximum of 30 mJ of 354.7 nm light can be obtained, but 5-10 mJ were typically used. Laser energies were measured after a 60 deg quartz dispersing prism with a Scientech thermopile.

The second photolysis laser, a Quanta-Ray Nd:YAG-pumped dye laser system, was used for the shorter wavelength studies. 317.0, 298.5 and 298.3 nm light was obtained by doubling the output from Rh 640, DCM and Rh 590 (Exciton), respectively, which were pumped with ~200 mJ of YAG second harmonic. Generally, 3-4 mJ of uv light were used; laser energies were measured after a uv pass/vis block filter (Corning 7-54) and one 90 deg quartz prism. More detailed information on this laser system can be obtained from the instrument manuals and from Quanta-Ray.

3. Optical Configuration

The ir and uv laser beams were overlapped and then separated with dichroic mirrors (DM on Fig. III-1). One set of mirrors, used for the experiments at 354.7 nm, reflected ~80% of the uv and transmitted ~90% of the ir. The other mirrors were used for the 317.0, 298.5 and 283.9

nm experiments, and reflected >90% of the uv and transmitted >90% of the ir.

Aluminum and gold front surface mirrors were used to direct the CO laser beam through the formaldehyde cell and onto the detector. The ir beam was (generally) focussed onto the detector element with an As_2S_3 lens (2" diameter, f/1). This lens also attenuated the uv light that leaked through the second dichroic mirror. Scattered photolysis laser light and other background were further reduced with ir filters. A W4741 filter (half-maximum transmission points 1930 and 2420 cm^{-1}) was used inside the detector dewar (ℓN_2 cooled), and a N474 filter (half-max 2050-2190 cm^{-1}) outside the dewar (also see Fig. III-18). This arrangement satisfactorily eliminated scattered light except under conditions of high uv energy (~12 mJ/pulse) and low signals (i.e. H_2CO pressures $\lesssim$0.1 Torr).

The photolysis lasers were not in the same room as the CO laser, so multiple reflections were required to direct the uv beam to the formaldehyde cell. This had a deleterious effect on the shape and size of the laser beams. For the 354.7 nm experiments, after the three dielectric mirrors, the dichroic mirror and cell window, the uv pulse energy in the H_2CO cell is only 50-60% of the energy measured after the 60 deg dispersing prism. For the shorter wavelengths, the losses at the right-angle quartz prisms used for beam steering, the dichroic mirror and cell window were such that the useful uv energy was roughly 65% of the value measured after the first prism. A 1 m focal length CaF_2 lens and/or a 2 m f.l. quartz lens were (sometimes) used to collimate and/or focus the uv beams. These lenses were placed at distances ranging from ~30 cm to 2.5 m from the cell.

Irises were placed at both ends of the cell for beam definition and as an aid in overlapping the laser beams. The diameter of the first aperture matched that of the larger of the two laser beams. The second aperture was never larger than the smaller of the two beams, but was closed down when using strong CO laser transitions, so that the signal from the ir detector did not saturate the electronics. This was done by chopping the CO laser beam and observing the output waveform on an oscilloscope.

4. Detector and Electronics

The intensity of transmitted CO laser light was monitored with a liquid-helium cooled copper-doped germanium detector (SBRC). A detailed description of this ir detector and its dewar can be found in Ref. 5. Reference 6 gives the circuit diagram for the detector and its preamplifier. The response of the detector and pre-amp to a 8 ns laser pulse (3.5 μ) indicated a 150 ns response time with a 28.9 kΩ load resistor.[6] The data at 354.7 nm and 298.5 nm were taken with a 28.7 kΩ load resistor; an 8 kΩ resistor was used for the data at 283.9 and 317 nm. Using the 28.7 kΩ load, the fastest risetimes (~280 ns) would be slowed ~15% by detector response time. Experiments using the smaller load resistor seemed to give risetimes about 20% faster than comparable traces with the 28.7 kΩ load, but this difference is on the order of the scatter and uncertainty in the data.

In addition to the x1 pre-amplifier built onto the detector dewar, one stage of a Keithley 104 wide band amplifer was used for x10 amplification. The signal was then input to a Biomation 8100 transient digitizer (2048 channels, 10 ns/channel minimum) interfaced with a Northern 575 signal averager. The transient digitizer has dual-timebase and pre-triggered modes and was triggered by a photodiode which looked at scattered YAG second harmonic. Signals were accumulated for 128-2048 shots, and the data output on an X-Y plotter. Data could also be stored on magnetic tape and transferred to floppy disk.

5. Gas Handling

Formaldehyde monomer was prepared from paraformaldehyde (Matheson, Coleman and Bell) by the method of Spence and Wild;[7] further details are given in Ref. 8. NO used in the radical scavenging experiments was purified by passing it over silica gel held at dry-ice temperature.[9]

Gases were handled in a standard glass-and-grease vacuum line, which was pumped to 10^{-6} Torr before each experiment. Gas pressures were measured with a calibrated Pace capacitance manometer with a 50 Torr range. At pressures $\leq$ 1 Torr, a MKS Baratron manometer was also used.

The formaldehyde cell was made of pyrex and was 1 m long. The center section was 80 cm long and ~5 cm in diameter. The end sections were each 10 cm long and 1.5 cm in diameter with sapphire windows (1 mm x 25 mm diameter) epoxied on at Brewster's angle.

C. RESULTS AND ANALYSIS

1. Appearance Rates

The appearance rates of CO produced by dissociation of H_2CO at 354.7 nm (tripled YAG), 317.0, 298.5 and 283.9 nm were measured by the CO laser absorption technique. A typical trace is shown in Fig. III-6. The rise of CO was treated as exponential and an appearance rate determined from a log plot (Fig. III-7, line b). The observed rises are not exactly exponential; the first part of the rise is too slow. This was most noticable for photolysis at 354.7 nm and for low formaldehyde pressures.

If formaldehyde dissociation to H_2 + CO occurs via sequential first order processes, namely

$$H_2CO(S_1) + M \rightarrow I + M \qquad (1)$$

$$I + M \rightarrow H_2 + CO(v,J)_{obs} + M, \qquad (2)$$

then the concentration of CO at a time t should be given by:

$$\frac{[CO]_t}{[CO]_{max}} = 1 + \frac{1}{k_1[M] - k_2[M]}\left(k_2[M]e^{-k_1[M]t} - k_1[M]e^{-k_2[M]t}\right)$$

where CO_{max} = the initial concentration of $H_2CO(S_1)$. For a few traces, curves of this form were computer fit to the data by a least-squares method: Table III-2 gives the results. If the model involving collisional decay of S_1 to an intermediate is correct, $k_1[M]$ should be the observed $H_2CO(S_1)$ decay rate. In Fig. III-8, the dot-and-dash line is the CO rise calculated with $k_1[M] = 10\ \mu s^{-1}$ (the measured S_1 decay rate for 0.5 Torr H_2CO excited at 354.7 nm[10]), and a decay rate for the intermediate (I) of 2 μs^{-1} $Torr^{-1}$ (i.e. $k_2[M] = 1.0\ \mu s^{-1}$, which

Fig. III-6. Time-resolved absorption of the $P_{1-0}(12)$ CO laser line by CO produced from 354.7 nm photolysis of 1.00 Torr H_2CO. The decay is diffusion of the CO out of the probe beam.

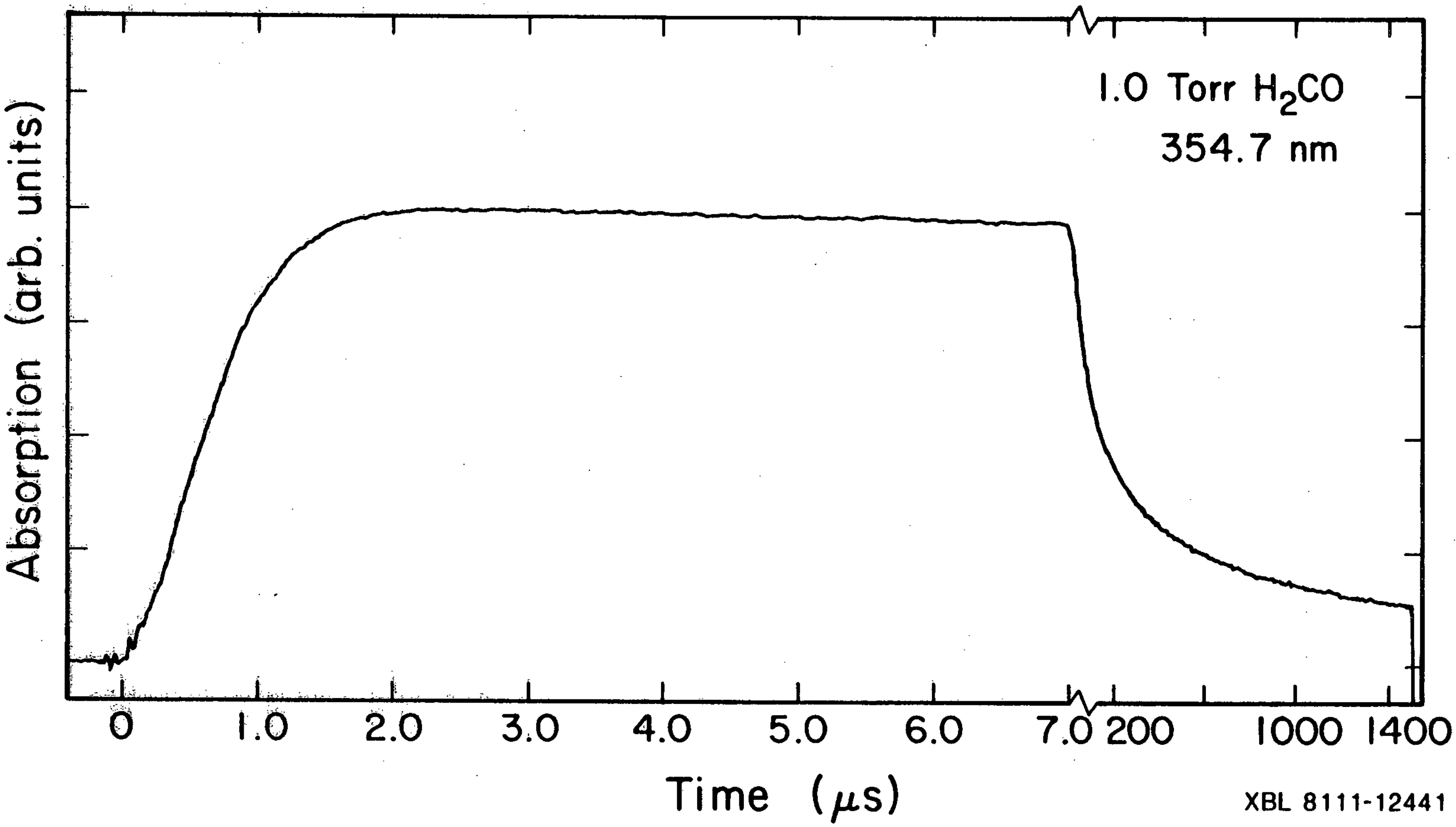
1.0 Torr H_2CO
354.7 nm
Absorption (arb. units)
0
1.0
2.0
3.0
4.0
5.0
6.0
7.0
200
1000
1400
Time (μs)
XBL 8111-12441

Fig. III-6.

Fig. III-7. Graphical analysis of the CO rise shown in Fig. III-6. Line b gives a 2.00 μs^{-1} appearance rate for the CO (the initial, slow part of the rise is not fit--see text for discussion). Lines a and c indicate the range of lines that can reasonably be fit to the data and yield uncertainties for the appearance rates of +15% and -8%.

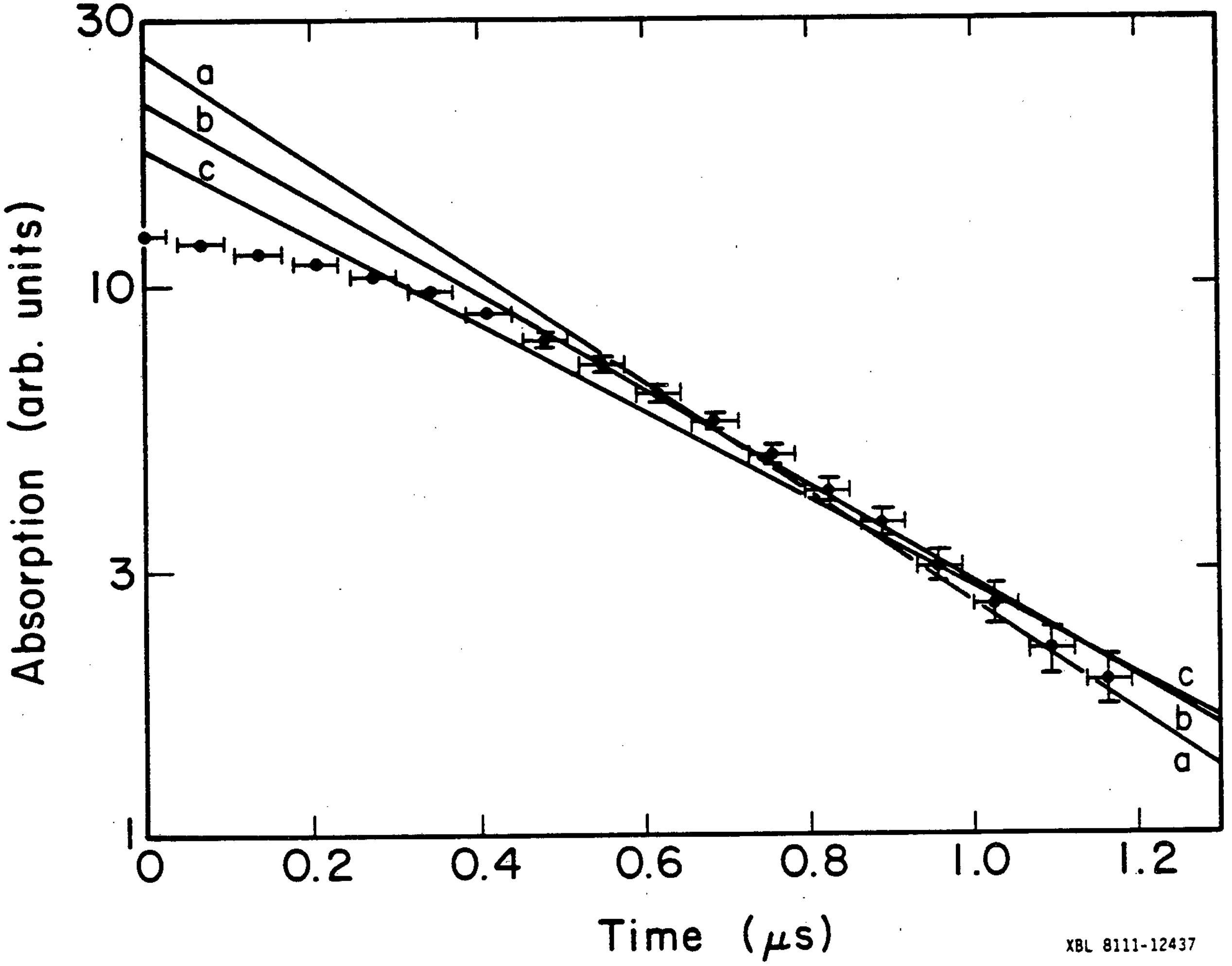
Absorption (arb. units)
30
10
3
1
0
0.2
0.4
0.6
0.8
1.0
1.2
Time (μs)
a
b
c
c
b
a
XBL 8111-12437

Fig. III-7.

Table III-2. Curve fitting results.

λ, (nm)	H_2CO pressure, (Torr)	$k_1[M]$, (μs^{-1})	$k_2[M]$, (μs^{-1})	s^a	$k_2[M]gr$,^{b} (μs^{-1})
354.7	0.103	7.00^c	0.325	0.037	0.40
	0.103	1.60	0.404	0.008	0.40
	0.50	10.00^c	0.667	0.056	0.94
	0.50	2.10	0.990	0.013	0.94
	0.50	10.00^c	0.736	0.055	1.06
	0.50	2.45	1.040	0.017	1.06
	1.00	14.00^c	1.400	0.066	2.00
	1.00	2.85	2.589	0.022	2.00
	1.00	3.33	2.419	0.023	2.00
317.0	0.49	171.3^d	0.970	0.010	1.06
	0.49	774.0^d	0.964	0.010	1.06
	1.05	5.745	1.875	0.019	1.95

a) s = the variance.
b) Value for $k_2[M]$ derived from graphical analysis ignoring the first part of the rise.
c) Least squares fit with $k_1[M]$ constrained to the $H_2CO(S_1)$ decay rate from Ref. 10.
d) This fit is insensitive to $k_1[M]$--the rise is virtually a single exponential. See Fig. III-9.

Fig. III-8. Curve fitting results--modelling the CO rise as two sequential first order processes (see text). H_2CO pressure = 0.5 Torr, 354.7 nm photolysis, monitoring CO(v=0, J=12). x = experimental points. —·— = calculated rise for $k_1[M] = 10\ \mu s^{-1}$ = the observed S_1 decay rate, $k_2[M] = 1.00\ \mu s^{-1}$. - - - - - = best fit with $k_1[M]$ constrained to $10\ \mu s^{-1}$, $k_2[M] = 0.67\ \mu s^{-1}$. ——— = best fit obtained, $k_1[M] = 2.10\ \mu s^{-1}$, $k_2[M] = 0.99\ \mu s^{-1}$.

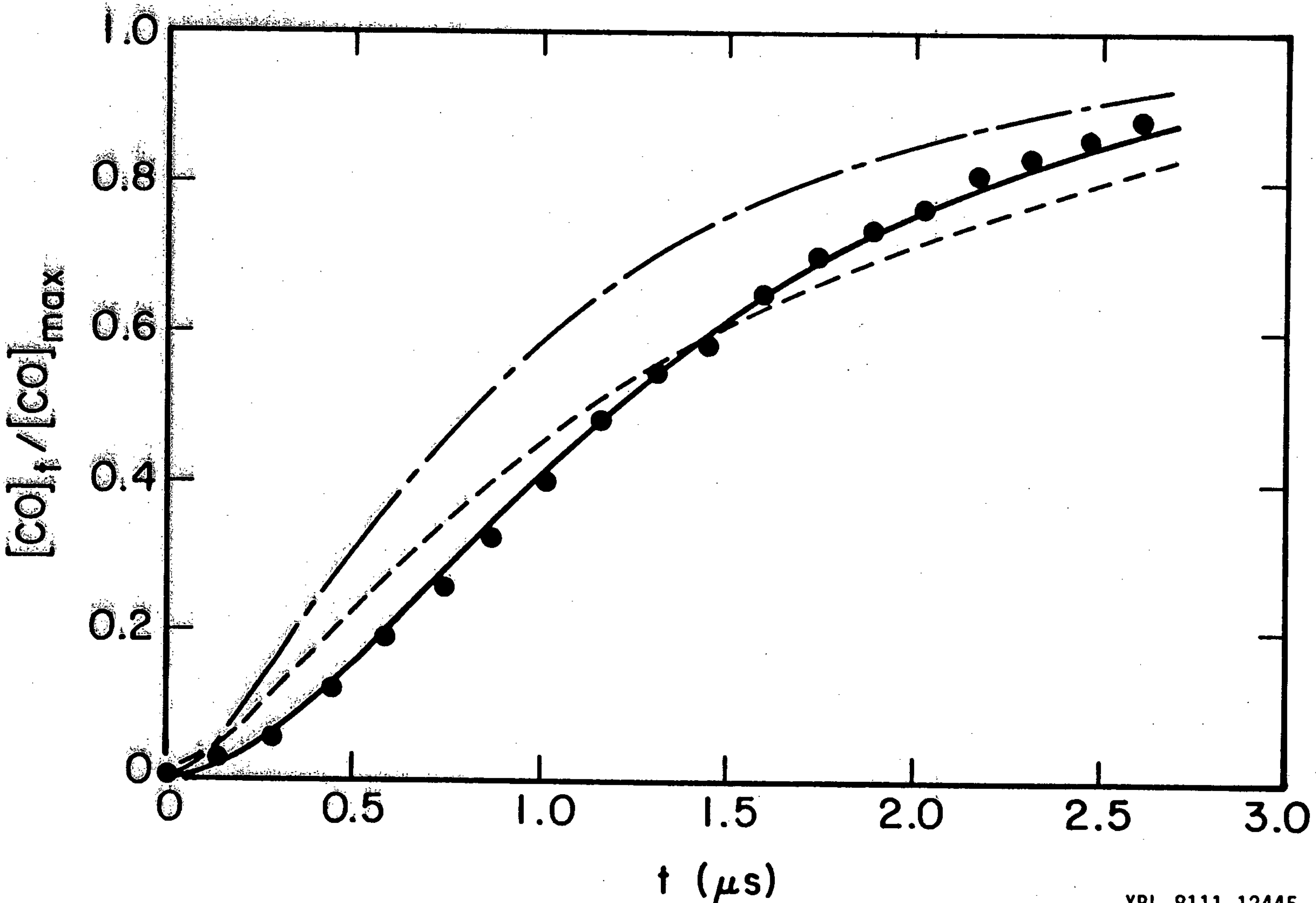

XBL 8111-12445

Fig. III-8.

is the value of $k_2[M]$ obtained from the best overall fit and from the graphical analysis). The dashed curve is the best fit obtained under the constraint $k_1[M] = 10\ \mu s^{-1}$; $k_2[M] = 0.67\ \mu s^{-1}$. The solid curve is the best fit obtained if both rates are allowed to vary; $k_1[M] = 2.10\ \mu s^{-1}$ and $k_2[M] = 0.99\ \mu s^{-1}$. At 354.7 nm, the fit to the experimental data is clearly improved when $k_1[M]$ is allowed to change. This is not as crucial at 317 nm; the 0.50 Torr rise is virtually a single exponential (Fig. III-9).

The values of $k_2[M]$ from the best computer fits are in agreement with the results of graphical analysis in which the early, slow part of the rise was ignored (see Fig. III-7). Most of the data was graphically analyzed. The uncertainties in the appearance rates determined in this manner were taken from the slopes of the extreme lines that could be drawn through the points on the log plot (Fig. III-7, lines a and c). These uncertainties are given in the tables of results (Tables III-3 through 7) and are on the order of ±20%. The error bars for the individual points in a trace are based on estimates of the noise in the signal and possible uncertainties in the location of the baseline and the t=0 point. Both methods of analysis are subject to these uncertainties in baseline determination.

The amplitude of the absorption signal was linearly proportional to the formaldehyde pressure (Fig. III-10), photolysis laser energy (Fig. III-11) and the number of laser shots averaged (Fig. III-12). Table III-3 gives the measured CO appearance rates for 354.7 nm photolysis, and Fig. III-13 shows the linear dependence on pressure.

Fig. III-9. Curve fitting results. H_2CO pressure = 0.49 Torr, 317 nm photolysis. x = experimental points. The solid curve represents the best fit to the experimental data; the calculated curves with $k_1[M] = 171.3\ \mu s^{-1}$ and $k_2[M] = 0.970\ \mu s^{-1}$ and with $k_1[M] = 774.0\ \mu s^{-1}$ and $k_2[M] = 0.964\ \mu s^{-1}$ are identical.

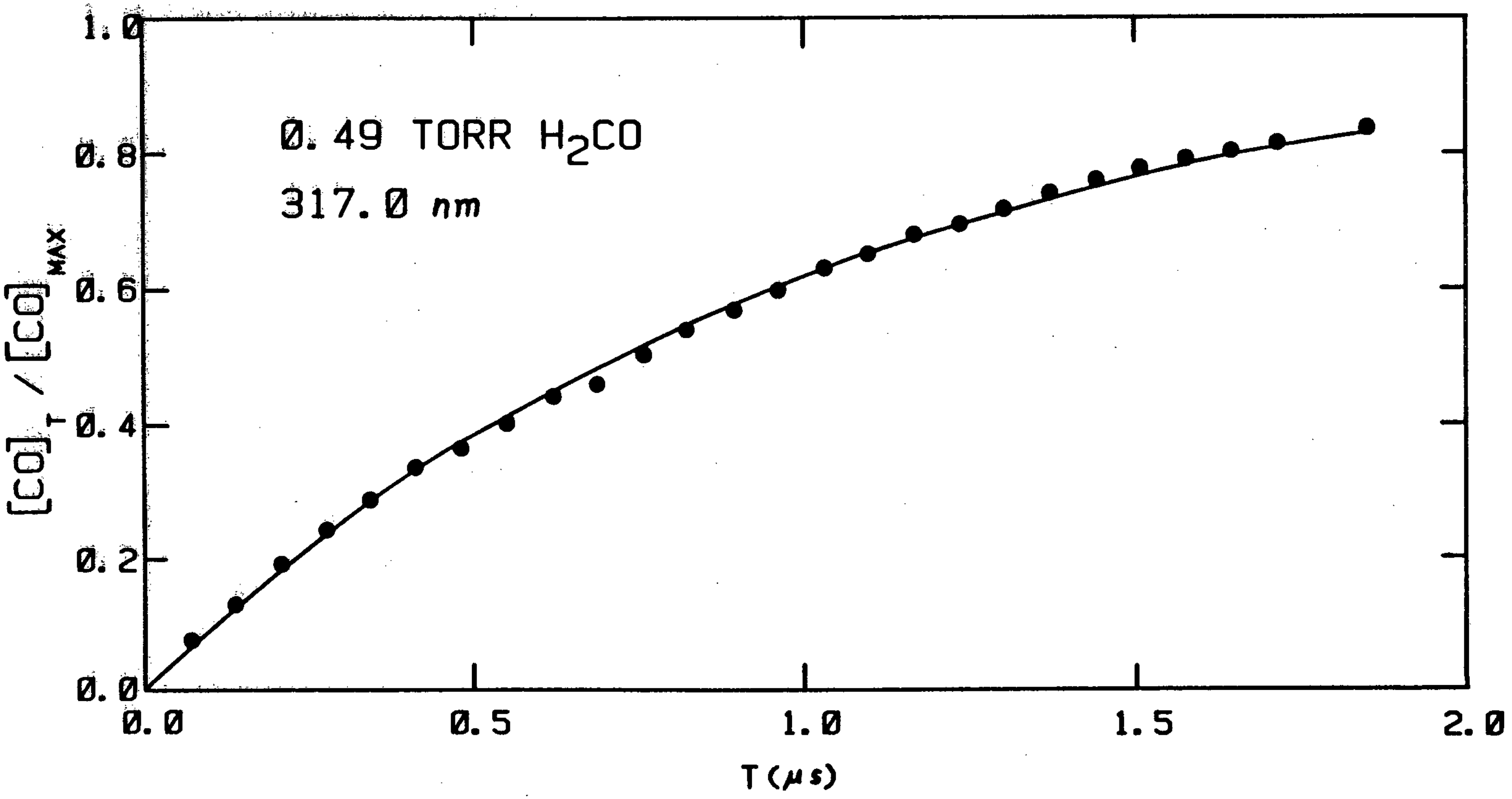

XBL 8111-12338

Fig. III-9.

Fig. III-10. Absorption signal amplitude as a function of H_2CO pressure.

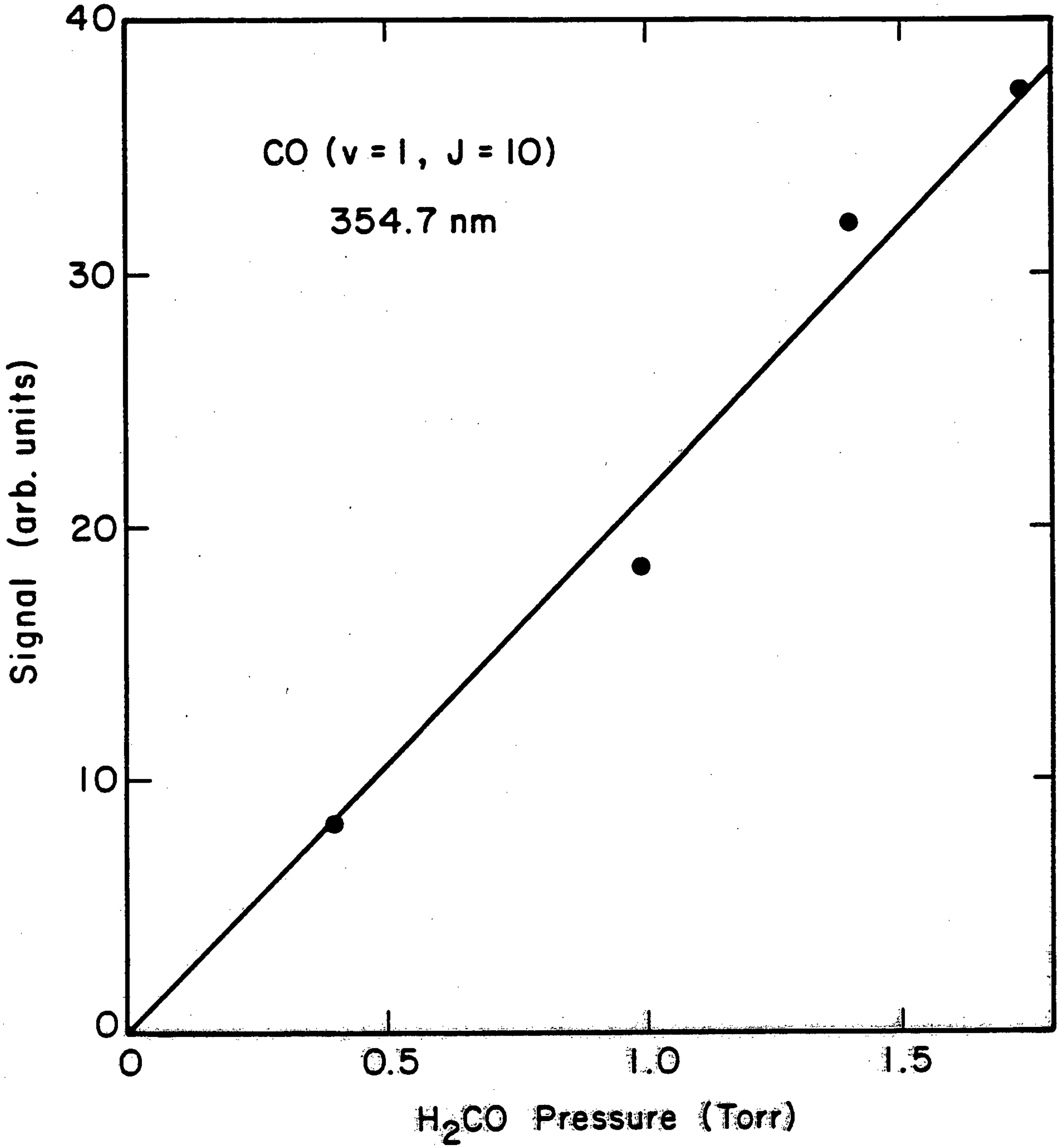

XBL 8111-12435

Fig. III-10.

Fig. III-11. Absorption signal amplitude as a function of photolysis energy (354.7 nm).

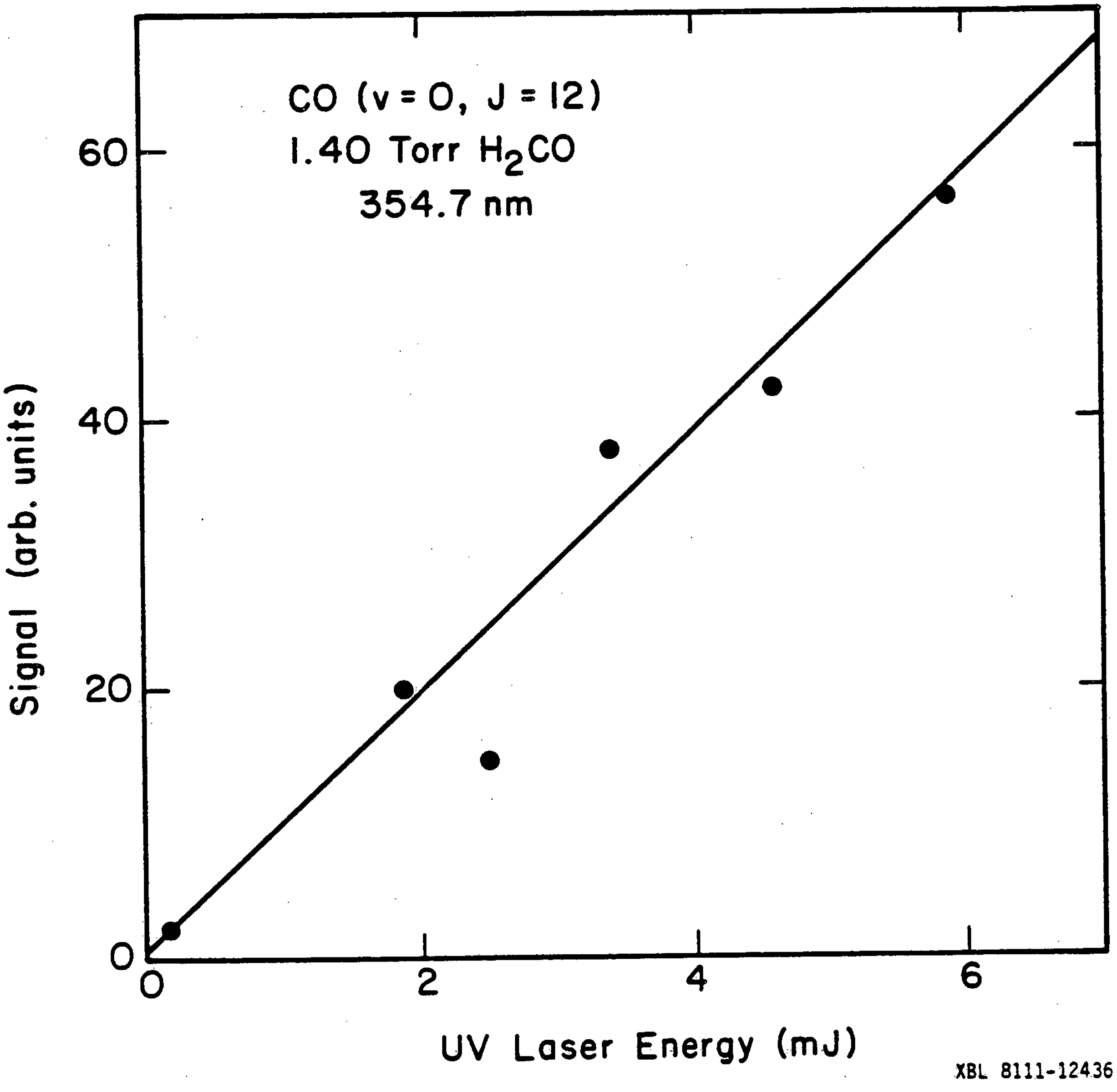

XBL 8111-12436

Fig. III-11.

Fig. III-12. Absorption signal amplitude as a function of the number of laser shots averaged. 1.03 Torr H_2CO (same sample used for all points), 354.7 nm, CO(v=0, J=12).

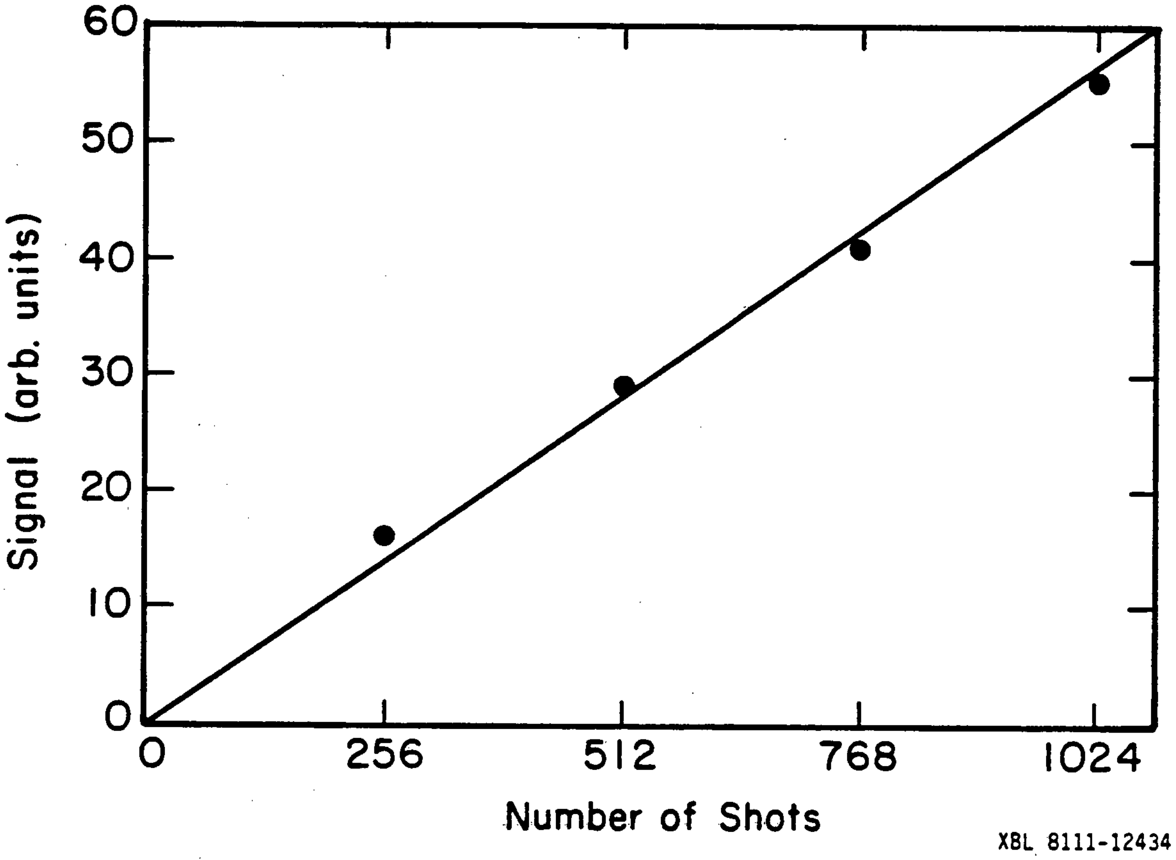
Signal (arb. units)
60
50
40
30
20
10
0
0
256
512
768
1024
Number of Shots
XBL 8111-12434

Fig. III-12.

Table III-3. CO appearance rates following H_2CO photolysis at 354.7 nm.[a]

Laser line	P, (Torr)	τ^{-1}, (μs^{-1})	$(P\tau)^{-1}$, $Torr^{-1}\ \mu s^{-1}$	Uncertainty
$P_{1-0}(12)$	0.103	0.40	3.88	-18%, -15%
	0.25	0.65	2.60	+12%, - 9%
	0.35	0.80	2.29	+16%, -10%
	0.40	0.84	2.10	+10%, - 4%
	0.50	0.94	1.88	+ 7%, - 5%
	0.50	1.03	2.06	+10%, -10%
	0.50	1.06	2.12	+ 9%, - 6%
	0.64	1.17	1.83	+ 9%, - 9%
	0.74	1.46	1.97	+ 3%, -23%
	0.80	1.48	1.85	+ 9%, - 9%
	0.96	1.87	1.95	+13%, -10%
	1.00	1.90	1.90	+14%, - 8%
	1.00	2.00	2.00	+15%, - 8%
	1.03	2.23	2.17	+15%, -13%
	1.04	1.86	1.79	+11%, - 5%
	1.07	2.37	2.21	+11%, -11%
	1.07	2.25	2.10	+ 6%, - 9%
	1.12	2.02	1.80	-10%
	1.12	2.19	1.96	+ 6%, - 9%
	1.12	2.04	1.82	+14%, -13%
	1.14	1.89	1.66	+14%, - 3%

Table III-3. Continued

	1.14	2.06	1.81	+12%, -12%
	1.14	1.94	1.70	+12%, - 8%
	1.20	2.19	1.83	-15%
	1.40	2.47	1.76	+12%, - 9%
	1.40	2.76	1.97	+11%, -11%
	1.41	2.54	1.80	+ 9%, - 6%
	1.42	2.58	1.82	+11%, - 9%
	1.42	2.57	1.80	+13%, -11%
	1.64	2.66	1.62	+17%, - 0%
	1.84	3.24	1.76	+10%, -12%
	2.00	3.37	1.69	+12%, -16%
$P_{2-1}(10)$	0.40	0.72	1.80	+14%, -11%
	0.70	1.18	1.69	+19%, -15%
	0.99	1.58	1.60	+13%, -18%
	1.40	2.22	1.59	+24%, -15%
	1.73	2.77	1.60	+ 9%, -18%

a) 28.7 kΩ load resistor used.

Fig. III-13. CO appearance rates as a function of H_2CO pressure for 354.7 nm photolysis (data in Table III-3). The lines shown are least-squares fits to the data, uncertainties are one sigma and reflect the scatter in the data only.

Line a: CO(v=0, J=12) slope = 1.623 ± 0.063 μs^{-1} $Torr^{-1}$
intercept = 0.254 ± 0.057 μs^{-1}
Line b: CO(v=1, J=10) slope = 1.531 ± 0.033 μs^{-1} $Torr^{-1}$
intercept = 0.095 ± 0.038 μs^{-1}
Line c: combined data slope = 1.604 ± 0.059 μs^{-1} $Torr^{-1}$
intercept = 0.239 ± 0.066 μs^{-1}

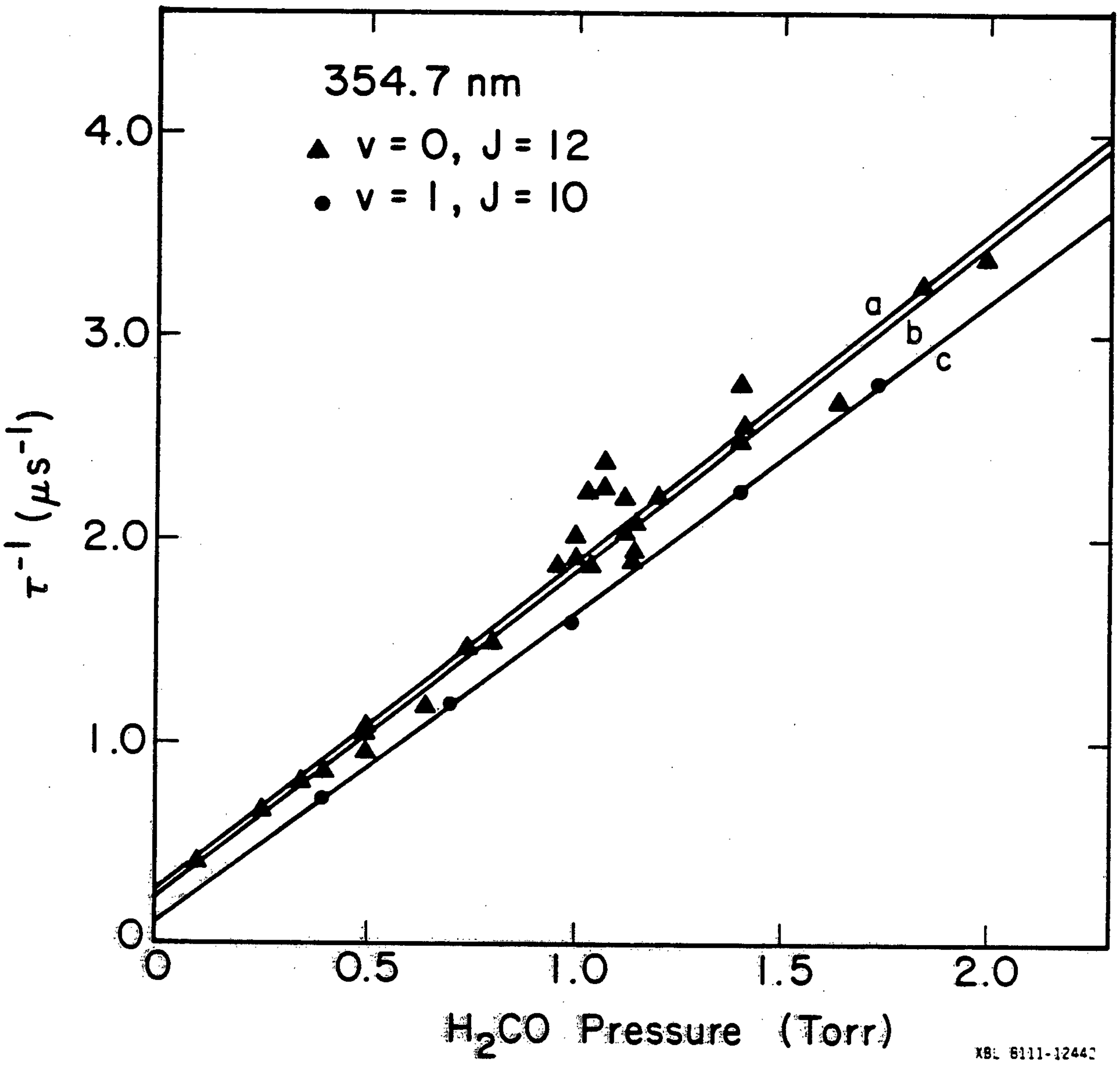
354.7 nm
▲ v = 0, J = 12
● v = 1, J = 10
a
b
c
τ^{-1} (μs^{-1})
0
1.0
2.0
3.0
4.0
0
0.5
1.0
1.5
2.0
H_2CO Pressure (Torr)
XBL 8111-12442

Fig. III-13.

Lines a and b are least squares fits to the data for CO, v = 0 and 1, respectively; line c is a fit to all the data. The appearance rates for CO(v=1, J=10) are ~15% smaller than those for CO(v=0, J=12), but the differences are comparable to the uncertainty in the data. CO appearance rates were also measured after formaldehyde excitation at 317.0, 298.5 and 283.9 nm, and are given in Tables III-4 through III-6. Figures III-14 through III-16 show the pressure dependence of these appearance rates. The lines shown in the figures are linear least-squares fits to the data; the uncertainties in the slopes and intercepts given (1σ) are derived from the scatter in the data. Given the sparsity of the data--particularly at 298.5 nm, however, these numbers should be viewed with caution. As Fig. III-17 shows, the appearance rates at all four wavelengths studied in these experiments are basically the same--the appearance rates have no obvious dependence on wavelength.

Table III-7 gives appearance rates for CO produced in v = 1, J = 9-13 with 298.5 and 354.7 nm excitation of H_2CO. These risetimes show no significant dependence on rotational level--observed differences are within the experimental uncertainty.

2. Vibrational Distribution

Information on the vibrational distribution of the CO produced by formaldehyde photolysis can be obtained from the relative amplitudes of the absorption of different CO laser transitions. The present data at 354.7 and 317.0 nm supplements previous work.[1] Following the analysis

Table III-4. CO appearance rates following H_2CO photolysis at 317.0 nm.[a]

Laser line	P, (Torr)	τ^{-1}, (μs^{-1})	$(P\tau)^{-1}$, $Torr^{-1}\ \mu s^{-1}$	Uncertainty
$P_{1-0}(12)$	0.31	0.78	2.52	+14%, - 4%
	0.49	1.06	2.16	+ 7%, - 9%
	0.73	1.72	2.36	+15%, -13%
	1.05	2.08	1.98	+19%, -15%
	1.54	3.14	2.04	+18%, - 7%
	2.00	4.15	2.08	+11%, -13%
$P_{2-1}(10)$	0.31	0.62	2.00	+13%, -10%
	0.49	0.92	1.88	+11%, -13%
	0.73	1.39	1.90	+14%, -15%
	1.05	2.01	1.91	+10%, -12%
	1.54	3.10	2.01	+23%, -30%
	2.00	4.38	2.19	+13%, -22%
$P_{3-2}(8)$	0.31	0.83	2.68	+14%, -11%
	0.49	1.25	2.55	+14%, -15%
	0.73	1.76	2.41	+18%, -14%

a) 8 kΩ load resistor used.

Fig. III-14. CO appearance rates as a function of H_2CO pressure for 317.0 nm photolysis (data in Table III-4). The line is a least-squares fit to all the data: slope = 2.034 ± 0.070 μs^{-1} $Torr^{-1}$, intercept = 0.079 ± 0.075 μs^{-1}.

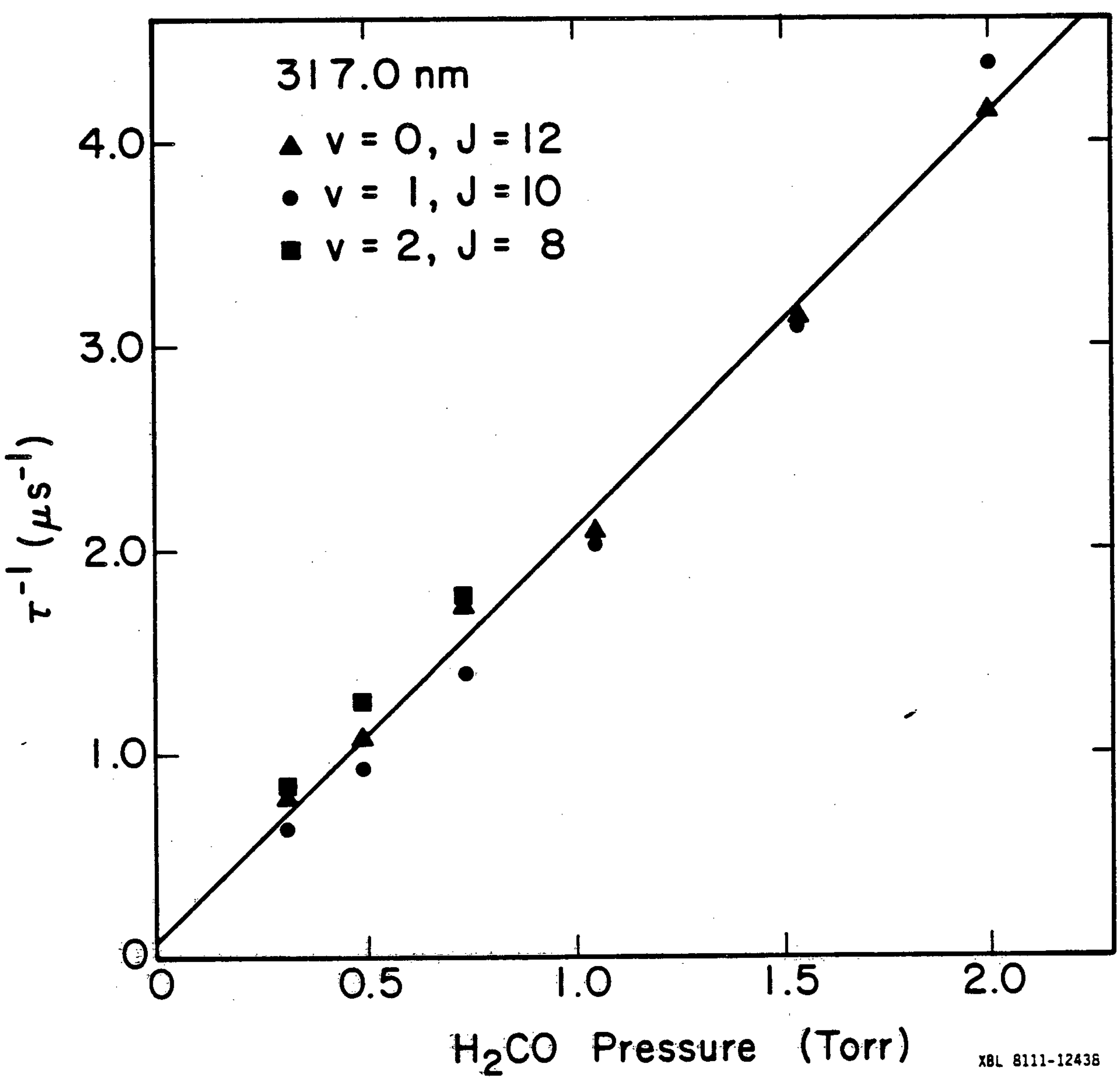
317.0 nm
▲ v = 0, J = 12
● v = 1, J = 10
■ v = 2, J = 8
τ^{-1} (μs^{-1})
4.0
3.0
2.0
1.0
0
0
0.5
1.0
1.5
2.0
H_2CO Pressure (Torr)
XBL 8111-12436

Fig. III-14.

Table III-5. CO appearance rates following H_2CO photolysis at 298.5 nm.[a]

Laser line	P, (Torr)	τ^{-1}, (μs^{-1})	$(P\tau)^{-1}$, $Torr^{-1}\ \mu s^{-1}$	Uncertainty
$P_{1-0}(12)$	0.38	1.08	2.84	+13%, -15%
	0.50	1.50	3.00	+11%, -11%
	0.52	1.61	3.10	+29%, -20%
	0.70	1.72	2.46	+21%, -19%
	1.52	2.69	1.77	+15%, -21%
$P_{2-1}(10)$	0.56	1.02	1.82	+22%, -21%
	0.77	1.28	1.66	+22%, -22%
	1.02[b]	2.08	2.04	+11%, -13%
	1.04	1.73	1.66	+16%, -10%
	1.05	1.95	1.86	+27%, -26%

a) 28.7 kΩ load resistor used.
b) 8 kΩ load resistor used.

Fig. III-15. CO appearance rates as a function of H_2CO pressure for 298.5 nm photolysis (data in Table III-5). The line is a least-squares fit to all the data: slope = 1.262 ± 0.238 μs^{-1} $Torr^{-1}$, intercept = 0.649 ± 0.207 μs^{-1}.

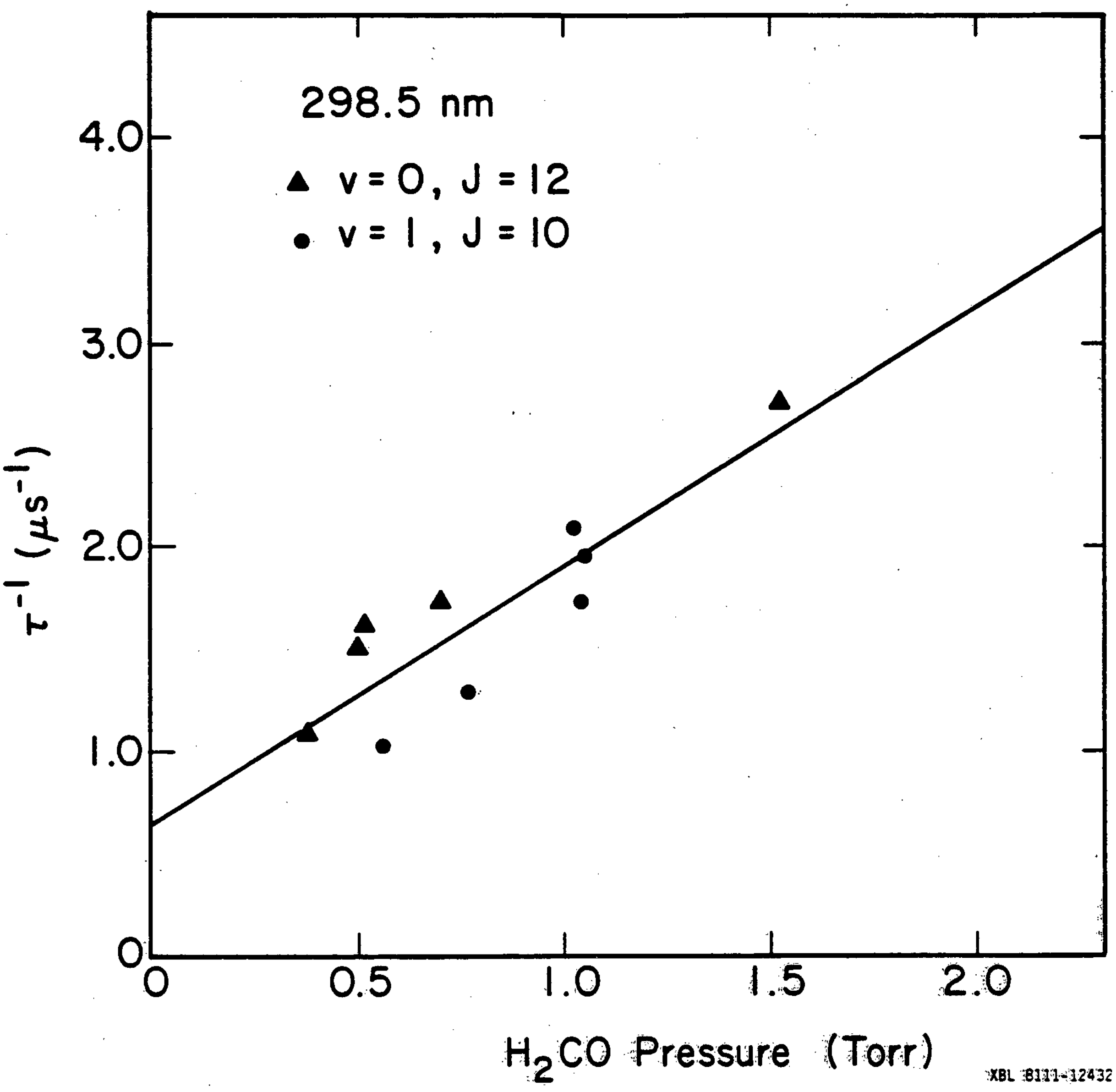
298.5 nm
▲ v = 0, J = 12
● v = 1, J = 10
τ^{-1} (μs^{-1})
0
1.0
2.0
3.0
4.0
0
0.5
1.0
1.5
2.0
H_2CO Pressure (Torr)
XBL 8111-12432

Fig. III-15.

Table III-6. CO appearance rates following H_2CO photolysis at 283.9 nm.[a]

Laser line	P, (Torr)	τ^{-1}, (μs^{-1})	$(P\tau)^{-1}$, $Torr^{-1}\ \mu s^{-1}$	Uncertainty
$P_{1-0}(12)$	0.52	1.51	2.90	+19%, -11%
	0.75	1.83	2.44	+15%, -13%
	1.05	1.92	1.83	+18%, - 9%
	1.31	2.79	2.13	+11%, -11%
	1.77	3.77	2.13	+18%, - 9%
$P_{2-1}(10)$	0.52	1.01	1.94	+19%, -18%
	0.75	1.35	1.80	+15%, -13%
	1.05	2.12	2.02	+11%, -12%
$P_{3-2}(8)$	0.52	1.38	2.65	+14%, -14%
	0.75	1.45	1.93	+18%, -10%

a) 8 kΩ load resistor used.

Fig. III-16. CO appearance rates as a function of H_2CO pressure for 283.9 nm photolysis (data in Table III-6). The line is a least-squares fit to all the data: slope = 1.953 ± 0.196 μs^{-1} $Torr^{-1}$, intercept = 0.157 ± 0.192 μs^{-1}.

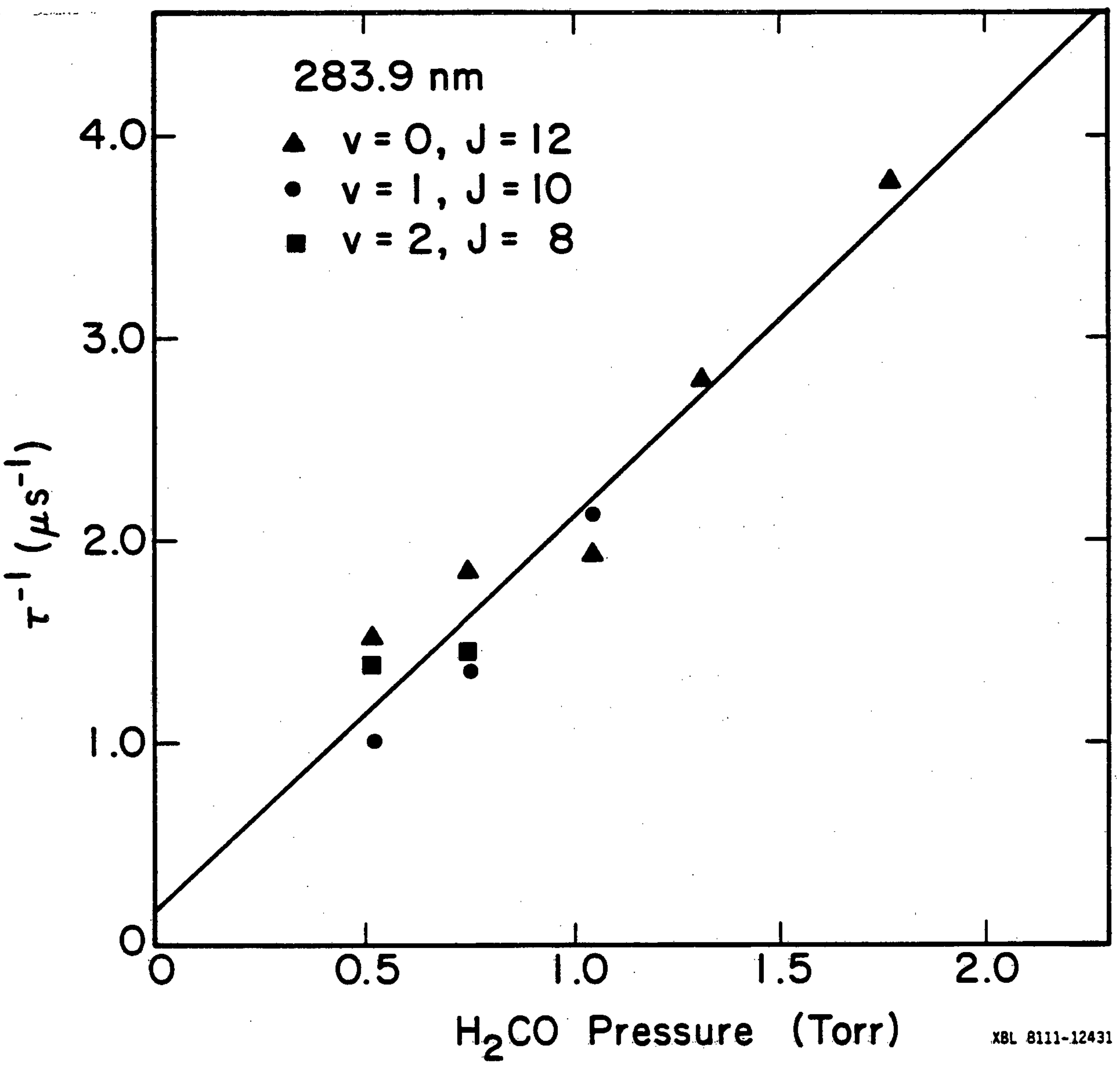

XBL 8111-12431

Fig. III-16.

Fig. III-17. CO appearance rates as a function of pressure: all photolysis wavelengths. The line is a least-squares fit to all the data: slope = 1.723 ± 0.061 μs^{-1} $Torr^{-1}$, intercept = 0.226 ± 0.064 μs^{-1}. The uncertainties are 1σ and reflect the scatter in the data only.

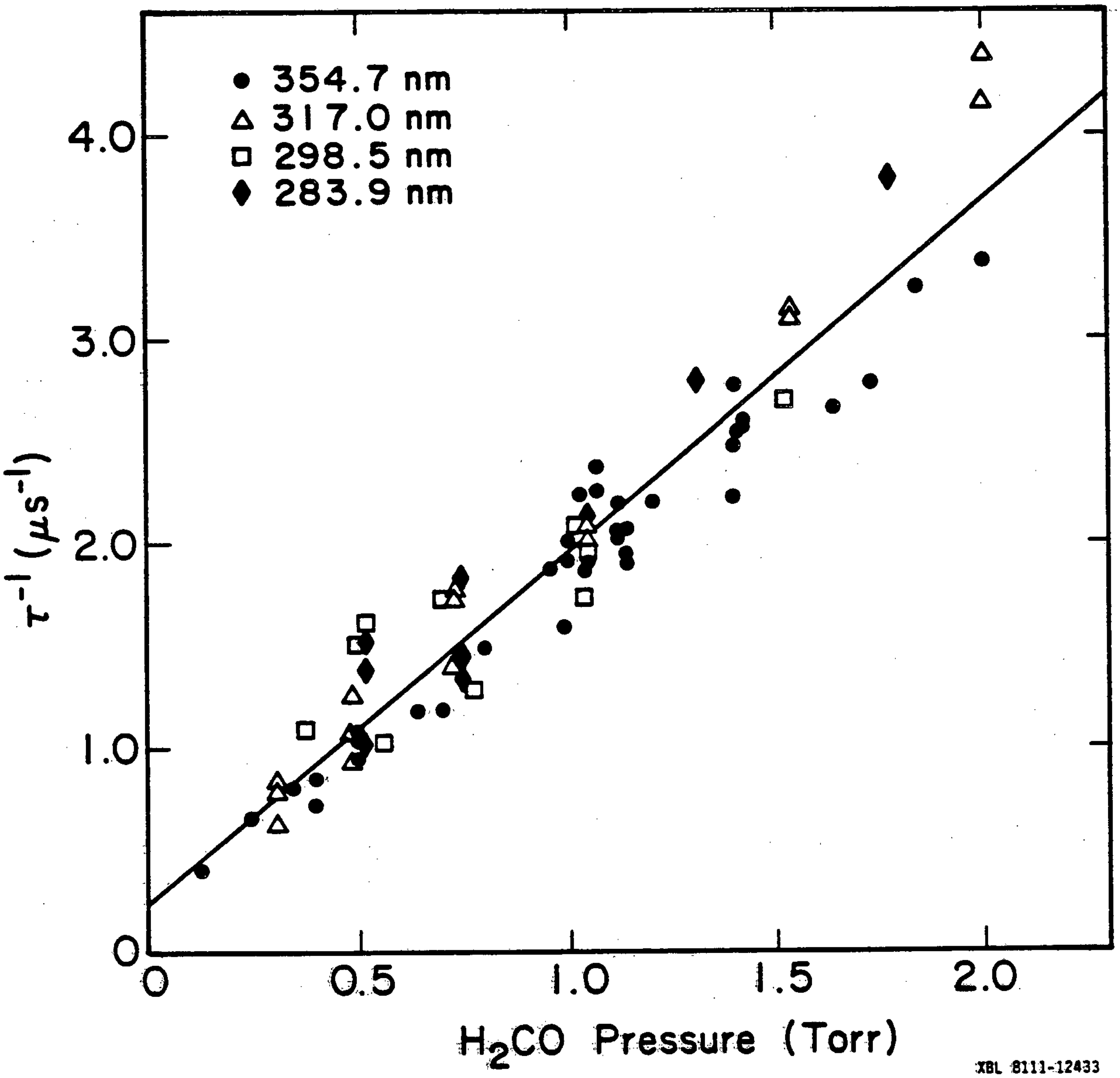

● 354.7 nm
△ 317.0 nm
□ 298.5 nm
◆ 283.9 nm
τ^{-1} (μs^{-1})
0
1.0
2.0
3.0
4.0
0
0.5
1.0
1.5
2.0
H_2CO Pressure (Torr)
XBL 8111-12433

Fig. III-17.

Table III-7. CO appearance rates for different rotational states.

A. 298.5 nm.

Laser line	P, (Torr)	τ^{-1}, (μs^{-1})	$(P\tau)^{-1}$ Torr^{-1} μs^{-1}	Uncertainty
$P_{2-1}(9)$	1.05	1.96	1.86	+54%, -16%
$P_{2-1}(10)$	1.05	1.95	1.86	+27%, -26%
$P_{2-1}(11)$	1.05	2.40	2.29	+ 8%, -17%
$P_{2-1}(12)$	1.05	2.43	2.32	+19%, -19%
$P_{2-1}(13)$	1.05	2.06	1.97	+19%, -24%
$P_{2-1}(13)$	1.26	2.29	1.81	+21%, -24%

B. 354.7 nm.

Laser line	P, (Torr)	τ^{-1}, (μs^{-1})	$(P\tau)^{-1}$ Torr^{-1} μs^{-1}	Uncertainty
$P_{1-0}(12)$	1.30	2.34	1.80	+22%, -11%
$P_{2-1}(10)$	1.30	2.11	1.62	+21%, -16%
$P_{2-1}(11)$	1.30	2.28	1.75	+19%, -23%

of Houston,[1] the height of an absorption signal, $H_{n''}$, is related to the populations of the upper and lower states by

$$H_{n''} \propto \left(\frac{N''}{g''} - \frac{N'}{g'}\right)\nu_{n',n''}|\mu_{n',n''}|^2 \tag{3}$$

For the absorption of the P(J"), v + 1 → v laser line, $g' = 2J' + 1 = 2J'' - 1$ and $g'' = 2J'' + 1$. The transition frequency, $\nu_{n',n''}$ is effectively independent of v, and in the harmonic oscillator approximation, $|\mu_{n',n''}|^2 \propto v' = v + 1$. Thus (3) becomes

$$N_{v,J''} - N_{v+1,J''-1} \cdot \frac{(2J''+1)}{(2J''-1)} \propto H_{v,J''} \cdot \frac{(2J''+1)}{v+1} \tag{4}$$

with the boundary condition that for some $v = v_{max}$, $N_{v+1,J} = 0$. Using a Boltzmann distribution to relate $N_{v,J\pm1}$ to $N_{v,J}$, (4) can be repetitively applied to the observed signal heights to obtain relative vibrational state populations.

For 354.7 nm photolysis, averaging two sets of data gives relative signal heights of 74.8 ± 2.8, 20.8 ± 1.1 and 4.5 ± 1.8 for the $P_{1-0}(12)$, $P_{2-1}(10)$ and $P_{3-2}(8)$ laser lines, respectively. These signal heights are normalized to a total of 100, and differences in laser powers, numbers of shots averaged and scale factors have been taken into account. These data indicate a CO product vibrational distribution of (91.1 ± 4.0)% in v = 0, (8.2 ± 0.7)% in v = 1 and (0.7 ± 0.3)% in v = 2 for photolysis at 354.7 nm. Similarly, at 317.0 nm, averaging the normalized results of 5 experiments gives relative signal heights of 42.8 ± 5.7, 36.8 ± 4.5 and 20.2 ± 4.0 for the $P_{1-0}(12)$, $P_{2-1}(10)$ and $P_{3-2}(8)$ laser lines. These give a product vibrational distribution of (76.9 ± 10.9)% in v = 0, (19.3 ± 2.7)% in v = 1 and (3.8 ± 0.7)% in v = 2.

The above calculations contain two assumptions. The first assumption is that essentially no product is formed in $v = 3$ or higher. This is probably a good assumption--Houston[1] found little or no product in $v = 3$ at similar wavelengths (see section D-2 of this chapter). Secondly, the rotational distribution within each vibrational state was assumed to be thermal. This should also be a fairly good assumption: the absorption signal heights used in these calculations are measured after the absorption has leveled off (see Fig. III-6), and several μs should be sufficient for nearly complete rotation-translation equilibrium.

3. Radical/Molecule Branching Ratio

At the shorter excitation wavelengths used, formaldehyde dissociates to H + HCO as well as to H_2 + CO. Table III-8 gives rates and timescales (τ's) for the relevant radical reactions in pure formaldehyde and in the presence of NO. In pure formaldehyde, radical recombination is two orders of magnitude slower than the timescale of these experiments and thus presents no complications. Use of the proper amount of the radical scavenger NO produces CO from HCO on an observable timescale. Figure III-18 is a trace taken for 283.9 nm excitation of 1 Torr H_2CO + 0.23 Torr NO, Fig. III-19 shows the graphical analysis. The initial rise corresponds to CO produced by molecular dissociation of H_2CO: the risetime (2.0 μs^{-1}) is in accord with the previous pure formaldehyde measurements. The slower rise corresponds to CO from the reaction of HCO + NO. Although the observed risetime does not exactly match the

Table III-8. Radical reaction rates for 1.00 Torr H_2CO + 0.23 Torr NO.[a]

Reaction	k[b]	Initial rate[c]	τ[d]
$H + HCO \rightarrow H_2 + CO$	5.5×10^{-10}	5.5×10^{16}	312 μs
$H + H_2CO \rightarrow H_2 + HCO$	5.0×10^{-14}	1.6×10^{16}	606 μs
$2HCO \rightarrow H_2CO + CO$	6.3×10^{-11}	6.3×10^{15}	2.7 ms
$HCO + NO \rightarrow HNO + CO$	1.2×10^{-11}[e]	8.7×10^{17}	11.5 μs
$H + NO + M \rightarrow HNO + M$	4.5×10^{-31}[f]	1.1×10^{15}	8.8 ms
$CO(V=1) + NO(v=0) \rightarrow CO(v=0) + NO(v=1)$	2.0×10^{-14}[g]		6.6 ms

a) H_2CO absorption cross section at 283.9 nm = 3×10^{-20} cm^2. For 2 mJ uv, $[H]_o = [HCO]_o = 1 \times 10^{13}$ molecule cm^{-3}.
b) From Ref. 11. Units are cm^3 $molecule^{-1}$ s^{-1}.
c) Units are molecule cm^{-3} s^{-1}.
d) τ is the timescale for the reaction. For pseudo first order kinetics $\tau = 1/k[M]$. For second order kinetics, $\tau = (e-1)/k[X]_o$, where X is the reactant.
e) For Ref. 12.
f) Units are cm^6 $molecule^{-2}$ s^{-1}
g) From Ref. 13.

Fig. III.-18. Time-resolved absorption of the $P_{1-0}(12)$ CO laser line following 283.9 nm photolysis of 1.0 Torr H_2CO in the presence of 0.23 Torr NO. The initial rise corresponds to CO formed via dissociation of H_2CO to molecular products. The slower rise is from CO produced in the reaction of HCO with NO. See text for further discussion.

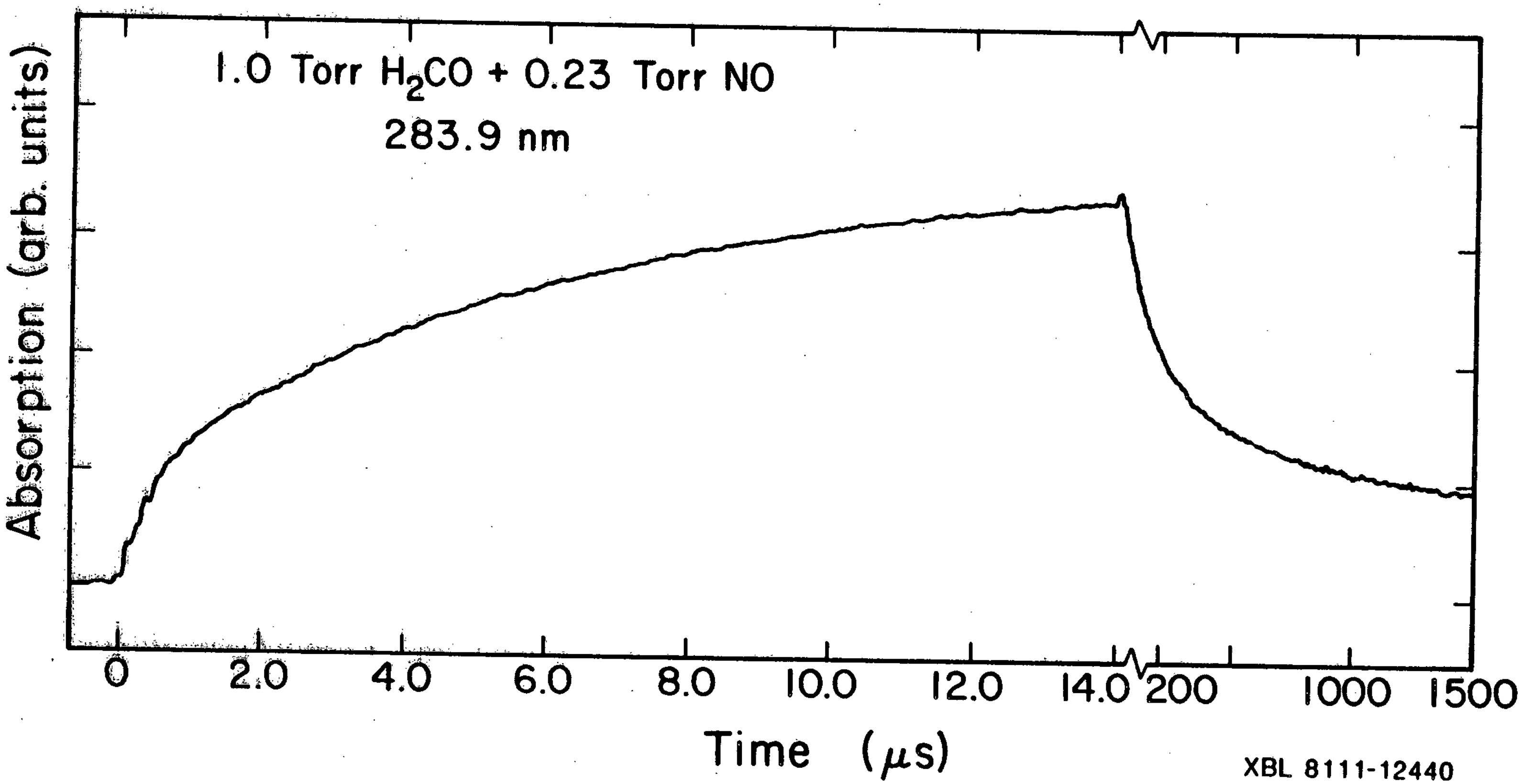

XBL 8111-12440

Fig. III-18.

Fig. III-19. Graphical analysis of the CO rise shown in Fig. III-18. Lines B gives a value of 0.19 μs^{-1} for the slow rise, τ_s^{-1}. Lines A and C indicate the range of lines that can reasonably be fit to the data and yield uncertainties for τ_s^{-1} of +18% and -7%. The inset shows the fast rise obtained after subtracting each of the fits for the slow rise. $\tau_f^{-1} = 2.0\ \mu s^{-1}$, +30%, -5%. The ratio of the amplitudes of the rises, $A_s/A_f = 3.2$, +50%, -20%.

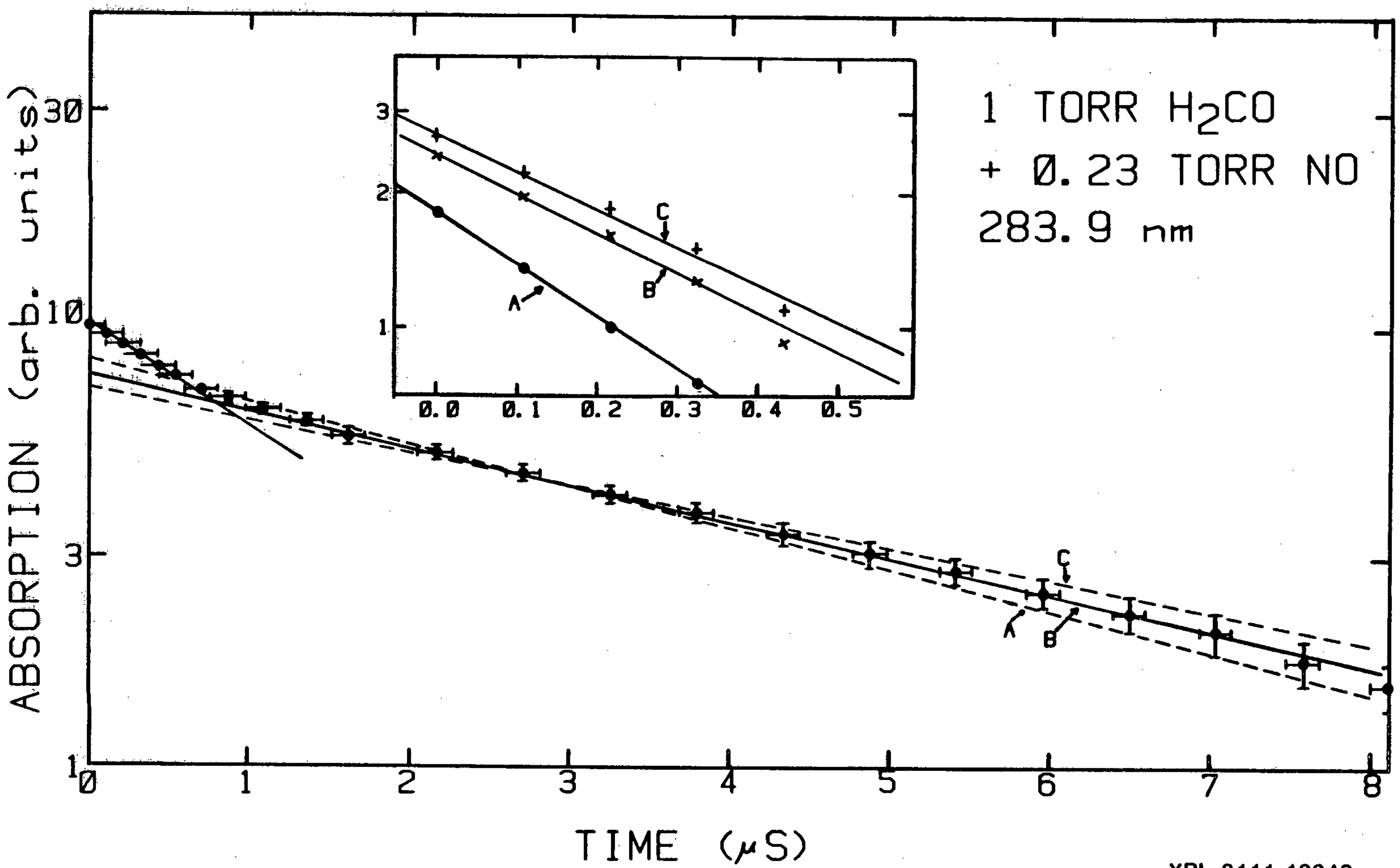

XBL 8111-12342

Fig. III-19.

calculated timescale for HCO + NO given in Table III-8, nothing else is close. The reaction of HCO with NO is much faster than either radical recombination reaction; 95% of the HCO gives CO via this reaction. HCO from the reaction of H + H_2CO is formed on a longer timescale and does not contribute to this signal. Thus, the ratio of the amplitudes of the slow and fast rises gives the radical/molecule branching ratio, ϕ_R/ϕ_M.

The relative amplitudes and appearance rates for measurements using different CO laser lines are given in Table III-9. Since the total quantum yield for dissociation is one, the observed values for ϕ_R/ϕ_M of 2.4 - 3.2 imply that $\phi_R = 0.71 - 0.76$ at this wavelength.

This analysis assumes that the behavior of a limited number of vibrational states is representative of the whole. The observed amplitude ratios for v = 0,1 and 2 are the same within the (large) uncertainty limits, which implies that the vibrational distribution for CO formed via the HCO + NO reaction does not differ greatly from that for CO formed in the molecular dissociation. The exothermicity of the HCO + NO reaction is sufficient to produce CO in $v \leq 5$. For 294 nm photolysis of H_2CO (as well as at longer wavelengths), Houston[1] observed less than 0.5% of the CO in v = 5 or higher, so this assumption is not too unreasonable.

A comparison of absolute signal levels for CO(v=0, J=12) produced at 354.7 and 283.9 nm implies at $\phi_M(283.9 \text{ nm}) = 0.44 \pm 40\%$, which is consistent with the value of $\phi_R/\phi_M \cong 3$ obtained above. The uncertainty given reflects the scatter in the data only. The true uncertainty is

Table III-9. CO appearance rates for photolysis of 1.00 Torr H_2CO in the presence of 0.23 Torr NO (283.9 nm).[a]

Laser Line	τ_f^{-1}[b] (μs^{-1})	τ_s^{-1}[c] (μs^{-1})	A_s/A_f[d]
$P_{1-0}(12)$	2.0	0.19	3.2
$P_{2-1}(9)$	1.6	0.27	2.4
	1.8	0.22	2.4
$P_{2-1}(10)$	1.4	0.23	2.8[e]
	2.2	0.34	3.2[f]
$P_{3-2}(8)$	1.7	0.26	3.0[g]

a) The fast rise corresponds to CO from $H_2CO \rightarrow H_2 + CO$. For 1 Torr of pure H_2CO, the appearance rate is ~2 μs^{-1}. The slow rise is CO from $HCO + NO \rightarrow CO + HNO$. The calculated rate for this reaction is ~0.1 μs^{-1} (see Table III-8).

b) Fast rise, uncertainty ±30%.

c) Slow rise, uncertainty ±20%.

d) Ratio of amplitudes of slow and fast rises. Uncertainty +50%, -20%.

e) Uncertainty, +40%, -20%.

f) Uncertainty, +30%, -20%.

g) Uncertainty, +60%, -20%.

probably larger--the data were not taken for this purpose so the corrections for laser powers, H_2CO pressures and relative absorption cross sections could not be done very carefully.

D. DISCUSSION

1. Appearance Rates

As shown in Fig. III-17, the CO appearance rates measured in this experiment show little or no variation with photolysis laser wavelength. The present results at 283.9, 298.5, 317 and 354.7 nm, as well as the previous 337[1] and 354.7[2] nm risetimes, are the same within the uncertainty of the data (~20%). The slow production of CO observed at shorter wavelengths in the present experiment is in agreement with Houston's[1] upper limit of 0.3 μs^{-1} for 0.15 Torr of H_2CO at 305.5 nm, but disagrees with Zughul's[2] appearance rate of 16 ± 7 μs^{-1} $Torr^{-1}$ at 299 nm.

The homogeneity of the observed appearance rates is inconsistent with the model in which collisional quenching to I competes with fast collisionless decay (see Chapter I). The S_1 formaldehyde lifetimes, τ_{f1}, decrease rapidly with increasing energy; at 354.7 nm τ_{f1} ranges from 110 ns at 0.2 Torr to 70 ns at 2.5 Torr[10] while at 284 nm τ_{f1} ~ 14 ps.[14] Interactions between S_1, S_0^*, the molecular product continuum, T_1 and HCOH should be larger at higher energies, leading to faster transition rates and faster CO appearance rates. Collisionless dissociation should therefore successfully compete with quenching at the higher energies, giving prompt formation of CO.

It is possible that the appearance rates measured by the CO laser absorption method do not represent the nascent production of CO. The molecular beam photofragmentation experiments described in Chapter II indicate that collisionless dissociation occurs with high product translational energies. A very simple impulse approximation model suggests J ~ 23 as the most probable rotational state for CO. In the CO probe laser, only transitions with J ~ 10 lase (see Table III-1) for the low vibrational states of interest (v = 0-2). Product CO formed in higher J states would have to rotationally relax before being detected by the CO laser method. Brechignac[15] has measured a rate of 12.5 ± 1.5 μs^{-1} $Torr^{-1}$ for transfer of population out of the CO(J=10) state. It is not unreasonable to attribute the observed 1.7 μs^{-1} $Torr^{-1}$ appearance rate to rotational relaxation from J ~ 23 to J ~ 10, since this should be slower than simple relaxation out of the J = 10 state. Rotational relaxation could be relatively insensitive to the photolysis energy and therefore consistent with the lack of wavelength dependence of the risetimes. This explanation for the delay in the appearance of CO would predict faster risetimes for CO in higher J states. No such trend is discernable in Table III-7, but the range of accessible rotational states is too limited to be useful.

The results of the curve-fitting calculations described in section C-1 also indicate that the simple model of $H_2CO(S_1) \xrightarrow{M} I \xrightarrow{M} H_2 + CO$ may not be appropriate. The CO rise is well modeled by two sequential first order processes, but the first rate is ~5 times slower than the observed S_1 decay rate. It has been suggested[16] that the "long-lived intermediate" is actually several sequential intermediate states. This would be consistent with the curve-fitting result as one of the intermediate transitions could proceed at the slower rate. It is also reasonable to expect that the kinetics of rotational relaxation from

J ~ 23 to J = 10 could be that of sequential first order processes, but it is impossible to predict the kinetics of the rotational relaxation process without some knowledge of the initial CO rotational distribution.

The present CO laser absorption measurements of the appearance rates are in excellent agreement with the ir chemiluminescence appearance rates measured by Zughul.[2] Thus, if the delayed CO appearance in the present experiments is explained as rotational relaxation, this agreement implies that the ir chemiluminescence results also do not represent the true CO production rate. The rotational relaxation interpretation of the experimental evidence has the advantage of eliminating the "mysterious intermediate" and thus significantly simplifying the photophysics, but requires some explanation for the delay in ir fluorescence.

The infrared fluorescence data presently available do not conclusively support either rotational relaxation or the intermediate as the explanation for the delay in CO appearances, although Zughul's data indicates that CO must be formed with J > 25 for rotational relaxation to be the sole cause of the delay. A detailed analysis of the fluorescence data follows. Figure III-20 shows the bandpass (half-maximum transmission points) of various ir filters relative to CO transitions. Zughul used the N4701 filter cooled with liquid nitrogen and the W4741 filter at room temperature for his ir fluorescence measurements of the CO appearance rate. For CO(v=1-0), this filter combination transmits emission from approximately P(6) through R(25). (For 354.7 nm photolysis, 99% of the CO is formed in v = 0 or

Fig. III-2C. Transmission bands of infrared filters compared with CO transitions. Limits given are the half-of-maximum-transmission points. (COLD) indicates transmission band for the filter cooled to ~100K with ℓN_2. For N4701, the (COLD) spectrum was measured at normal incidence; for W4741, the (COLD) spectrum shown was calculated using a 2% blue shift. N474 was used in the present experiments.

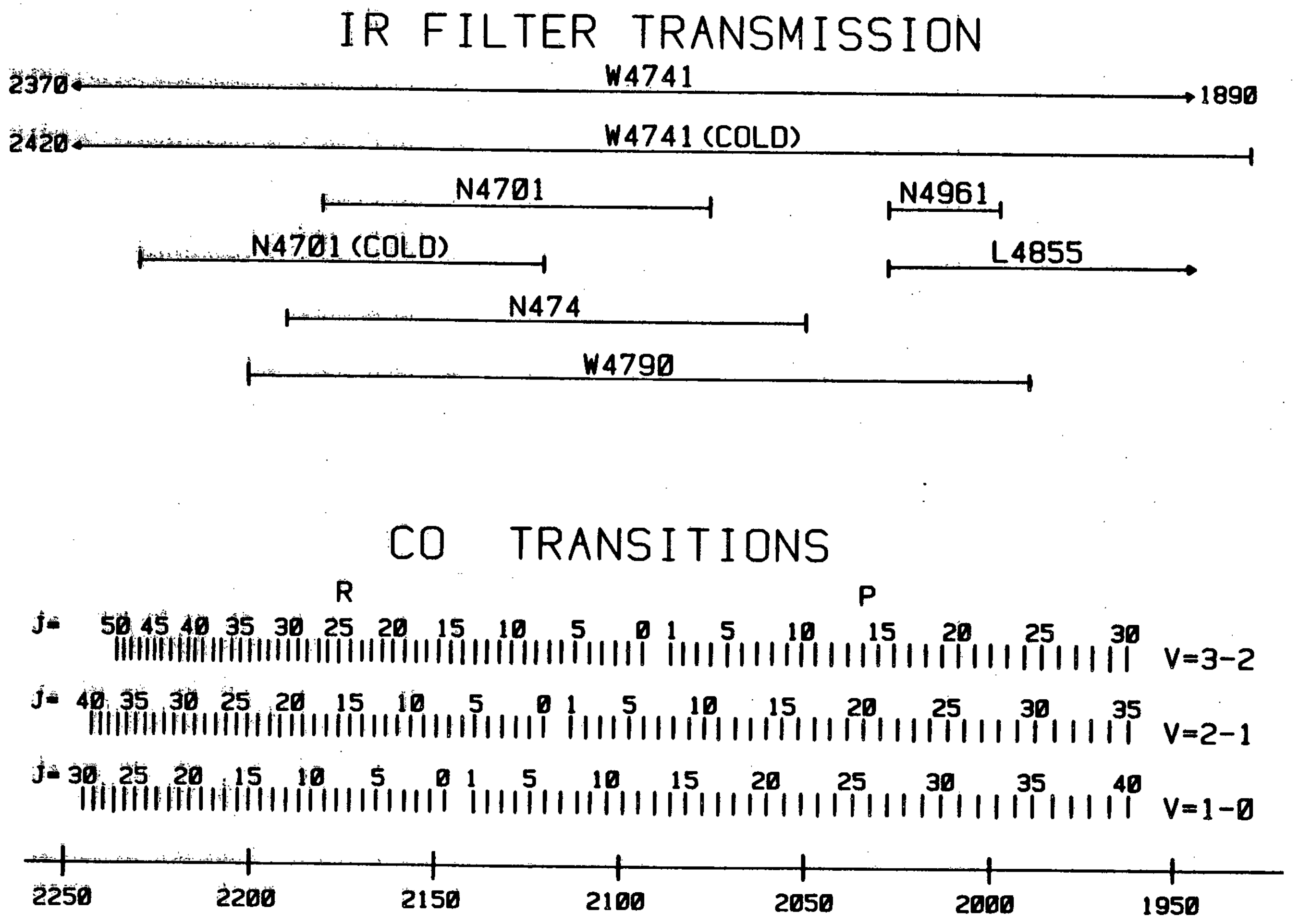

XBL 8111-12343

Fig. III-20.

1.) If CO is formed promptly with $J < \sim 25$, Zughul should have seen a fast rise. If CO is formed promptly, but with $J > 25$, the ir chemiluminescence could be delayed but should have a faster rise than for the CO laser measurements. It is reasonable to expect rotational relaxation to populate $J = 25$ before it populates $J = 10$.

Infrared fluorescence data at other wavelengths, specifically those corresponding to high rotational states of CO, could provide crucial clues. Therefore, some additional ir fluorescence data, consisting of 16 traces obtained by Weisshaar (Chapter VII of Ref. 16), merit discussion even though the sparsity of the data render the discussion highly speculative and inconclusive. The following measurements of ir fluorescence in the CO region were made after 354.7 nm photolysis of 2-5 Torr of H_2CO. (Where it appears, A_f/A_s refers to the ratio of the amplitude of the faster decaying feature to that of the slower.)

1) Using the W4741 filter (cold) and the N4701 filter (room temperature), a signal similar to Zughul's (hereafter referred to as "the slow signal") was observed, which vanished when a CO gas filter cell (4 cm, ~500 Torr CO) was used.

2) Using only the W4741 filter (cold), an additional feature, a spike with a detector limited rise and a decay of $\sim 0.7\ \mu s^{-1}\ Torr^{-1}$ (hereafter referred to as "spike") was observed with an amplitude approximately half that of the slow signal, i.e. $A_f/A_s = 0.5$. Adding the CO gas filter cell to W4741 (cold) attenuated the slow signal so that $A_f/A_s = 2$.

3) Using W4741 (cold) with W4790, the slow signal and a hint of a spike were observed.

4) Using the long-pass filter L4855, a spike with a 100-200 ns decay time at 4.6 Torr (hereafter referred to as "fast spike") and a "tail" with ~1 ms decay were observed with $A_f/A_s \sim 0.5$. When W4741 (cold) and L4855 were combined, the tail was attenuated, giving $A_f/A_s = 3\text{-}4$.

5) N4961 was also tried, but the signal was too weak to be useful.

The slow signal seen in 1) corresponds to that seen by Zughul and can be assigned to emission from CO($v=1$, $J \leq 15$). This feature was also observed in 2) and 3). In these cases, emission from CO($v=1$, $J>15$) probably contributes to the signal, since use of the gas filter cell in 2) only partially attenuated the slow signal and calculations show that 50% of the emission from CO($J=30$) would have been transmitted by the gas filter cell. Thus, the remaining slow signal in 2) could be emission from high J states of CO($v=1$), although no clear corresponding signal was seen in 4). As Weisshaar suggests, the spike seen in 2) is probably emission from a species other than CO. Since it was not absorbed by the gas filter cell, it is not CO($v=1$, $J<30$). The amplitude of the spike is half that of the slow signal which, in view of the measured CO vibrational distribution, precludes emission from CO($v>1$) as the source. This feature was not seen by Zughul, or in 1), 3) or 4), which indicates that the emission must be in the 2420-2230 cm^{-1} region. Emission from CO($v=1$, $J \geq 30$) cannot comprise the spike--the fluorescence from all J states was viewed in 2) so the decay of the spike cannot be attributed to rotational relaxation. In addition, if emission from high J states had formed a spike in the R branch, an analogous feature should have been seen in the P branch. Although the spike is probably not CO emission, its presence could interfere with detection of emission from CO in high J states. It is possible that the fast spike in 4) is P branch emission from CO(v=1, J=35-40). The filters used in 4) do not transmit emission from all lower J states so the decay of the fast spike could be rotational relaxation. The corresponding feature in the R branch could be hidden by the spike which is attributed to some other species. It is also possible that this fast spike is merely scattered light, imperfectly subtracted out, or emission from another species, or even emission from the mysterious intermediate. The slow tail observed in 4) is probably not CO(v=1) since most of the emission is below 1930 cm^{-1}. Weisshaar suggests that the 1 ms decay is characteristic of a V-T equilibration or diffusion. It is possible that the residual slow signal in 4) (between 2030 and 1930 cm^{-1}) actually corresponds to the slow signal in 2) and is emission from CO(v=1, J~30), but it is impossible to tell since the signal-to-noise is ~1 for this feature.

The ir chemiluminescence data are inconclusive. Zughul's data indicate that if rotational relaxation is the cause of the delay in the CO appearance, the CO should be formed with $J > 25$. Weisshaar saw emission features that could be emission from CO(v=1, $J \geq 30$), but these measurements were taken with relatively high H_2CO pressures (2-5 Torr) because of low signal levels, and hence do not give risetime information.

It is possible that both rotational relaxation and a long-lived intermediate are important in CO appearance rates. This scenario is consistent with all the data: rotational relaxation explains the wavelength independent risetimes from the CO laser measurements while the intermediate explains the ir fluorescence data. The tentative but seemingly contradictory results of Houston and Zughul at 305.5 and 299 nm can both be correct, as well as the competition model for collisionless and collisional dissociation. However, this scheme requires that the collision-induced decay rate for the intermediate at 354.7 nm fortuitously match the rotational relaxation rate, and the identity of the intermediate remains a mystery.

Alternatively, the results of the CO laser experiments may represent the true CO production rate. In this case, the fast risetimes observed at 299 nm by Zughul are incorrect, but these results are rather uncertain anyway. But it is difficult to explain why the collision-induced decay of a collisionally formed intermediate should not vary with energy, or how collision formation of I can occur within the 14 ps lifetime of $H_2CO(S_1)$ at 284 nm.[14]

With the present information, it is impossible to say whether the CO laser absorption measurements represent rotational relaxation or the nascent product of CO. More work is needed to decide this question, and then to identify the intermediate, if its exists. Infrared fluorescence measurements covering different wavelength regions would be useful if the signal level could be improved by the 1-2 orders of magnitude needed for reliable appearance rate measurements at low formaldehyde pressures. Careful attention would have to be paid to filter bandpasses to avoid interference from species other than CO. Alternatively, appearance rates for CO in high J states could be measured using a tunable diode laser as the probe; vuv or 2-photon laser-induced fluorescence detection of CO is also a possibility.

2. Vibrational Distribution

The CO vibrational distribution of (91.1 ± 4.0)%, (8.2 ± 0.7)% and (0.7 ± 0.3)% for v = 0, 1 and 2 (354.7 nm) obtained in this experiment is in agreement with the results of Houston and Moore.[1] At their longest photolysis wavelength (347.2 nm), they found 90.0% of the CO in v = 0 and 10.0% in v = 1. The present result at 317.0 nm of (76.9 ± 10.9)%, (19.3 ± 2.7)% and (3.8 ± 0.7)% in v = 0, 1 and 2 is also in agreement with the 73.1%, 21.3%, and 4.9% found by Houston for 317 nm. Although the collisional and collisionless dissociation mechanisms may differ, the low CO vibrational excitation observed in the appearance rate measurements is consistent with the high product translational energy found in the molecular beam experiment. Fananas and Cabello[17] have carried out a surprisal analysis for the CO produced in H_2CO photolysis and find that the experimental vibrational energy distribution is considerably cooler than the statistical model predicts.

3. Radical/Molecule Branching Ratio

The molecular beam photofragmentation experiment showed that at 283.9 nm, collisionless dissociation to radicals dominates dissociation to molecular products by at least one order of magnitude. Although the 280 - 300 nm range has not been studied as intensively as the longer wavelengths, this result is not in agreement with previous quantum yield measurements. Clark, Moore and Nogar[18] found ϕ_R leveling off at ~0.5 for 300 - 320 nm. Horowitz and Calvert[19] found $\phi_R \sim 0.7$ between 289.0 and 317.5 nm. Moortgat[20] obtained $\phi_R = 0.48$ at 276.7 nm, 0.65 at 284.1 nm, and 0.80 at 295.0 nm. Tang, Fairchild and Lee[21] found values for ϕ_R of 0.57 at 294.0 nm, 0.45 at 295.4 nm, and 0.89 at 298.5 nm.

The present measurement gives a value of ϕ_R/ϕ_M of ~3 at 283.9 nm, in contrast to the collisionless $\phi_R/\phi_M \geqq 10$. This discrepancy may be indicative of a true difference in mechanism under collisionless conditions. Given the variation in reported values for ϕ_R, however, errors in the interpretation of the radical scavenger experiments, past and present, cannot be ruled out.

E. SUMMARY

The results of the experiments described in this chapter cannot be unambiguously interpreted at the present time. The CO appearance rates measured by the method of time-resolved absorption of a CO laser could represent either rotational relaxation or the production of CO from a long-lived intermediate; previous ir fluorescence measurements of the CO appearance rate cannot confirm or eliminate either possibility. This raises some doubt as to the existance of an intermediate. The difference between the radical/molecule branching ratio measured under collisionless and collisional conditions at 283.9 nm suggests that there may be real difference in dissociation mechanism; the shape of the observed CO rise suggests that if an intermediate is involved, it may actually be several states.

The mechanism of H_2CO photopredissociation is now fairly well understood in the absence of collisions, but it is clear that further experimental work is needed before collisional effects are equally well understood.

REFERENCES

1. P. L. Houston and C. B. Moore, J. Chem. Phys. 65, 757 (1976).
2. Muhammed B. Zughul, Ph.D. Thesis, University of California, Berkeley, 1978.
3. N. Djeu, Appl. Phys. Lett. 23, 309 (1973).
4. Robert Gerlach and Nabil M. Amer, LBL report #7854, Lawrence Berkeley Laboratory, Berkeley, 1978.
5. J. Finzi, Ph.D. Thesis, University of California, Berkeley, 1972.
6. Linda Young, Ph.D. Thesis, University of California, Berkeley, 1981.
7. R. Spence and W. Wild, J. Chem. Soc. 1935, 338.
8. Edward S. Yeung, Ph.D. Thesis, University of California, Berkeley, 1972.
9. E. F. Hughes, J. Chem. Phys. 35, 1531 (1961).
10. J. C. Weisshaar, A. P. Baronavski, A. Cabello and C. B. Moore, J. Chem. Phys. 69, 4720 (1978).
11. J. P. Reilly, J. H. Clark, C. B. Moore and G. C. Pimentel, J. Chem. Phys. 69, 4381 (1978).
12. A. O. Langford and C. B. Moore, J. Phys. Chem., to be published.
13. J. C. Stephenson, J. Chem. Phys. 59, 1523 (1973).
14. A. P. Baronavski, A. Hartford, Jr. and C. B. Moore, J. Mol. Spectrosc. 60, 111 (1976).
15. Ph. Brechignac, Opt. Comm. 25, 53 (1978).
16. James C. Weisshaar, Ph.D. Thesis, University of California, Berkeley, 1979.

17. J. A. Duenas Fananas and A. Cabello, Nuovo Cimento Soc. Ital. Fis. B 61B, 347 (1981).

18. J. H. Clark, C. B. Moore and N. S. Nogar, J. Chem. Phys. 68, 1264 (1978).

19. A. Horowitz and J. G. Calvert, Int. J. Chem. Kinet. 10, 805 (1978).

20. G. K. Moortgat and P. Warneck, J. Chem. Phys. 70, 3639 (1979).

21. K. Y. Tang, P. W. Fairchild and E. K. C. Lee, J. Phys. Chem. 83, 569 (1979).

CHAPTER IV. ENRICHMENT OF CARBON-14 BY SELECTIVE LASER PHOTOLYSIS OF FORMALDEHYDE

A. INTRODUCTION

Formaldehyde has spectral qualities that make it a convenient molecule for isotope separation. It absorbs in a region accessible to tunable lasers and has well-resolved rovibrational lines[1] that allow different isotopic species to be clearly distinguished. Formaldehyde also has a quantum yield for dissociation to stable products close to one,[2] which allows efficient use of photons.

Significant enrichment of C, H, and O isotopes by photodissociation of formaldehyde has previously been achieved. Clark et al.,[3] enriched carbon-12 by a factor of 80 by photolyzing $^{12}CH_2O$ from a mixture with $^{13}CH_2O$ using a tunable dye laser with a 0.3 cm^{-1} bandwidth. Marling[4] used ion lasers of very limited tunability to enrich D, ^{13}C, ^{17}O, and ^{18}O. He obtained enrichments in the range of 10 to 50, plus a much higher value of 180 for the special case of D_2. More recently, Mannik et al.,[5] achieved an enrichment of 254 for deuterium from CHDO.

In this chapter, a study of carbon-14 enrichment by the selective photolysis of formaldehyde is described. Most of the formaldehyde absorptions in the region between 290 and 345 nm were examined in order to find wavelengths where the ratio of absorption coefficients for $^{14}CH_2O$ and $^{12}CH_2O$ is large. Photolyses were done at a few of these wavelengths and yielded μg amounts of products enriched up to 150-fold in ^{14}C. The method developed could be used to concentrate the carbon-14 occurring in environmental and archaeological samples at very low natural abundance ($<10^{-12}$). Enrichment of samples should have a significant impact on radiocarbon dating because current methods of abundance measurement, both the traditional counter methods and the new accelerator methods, are presently limited by background and counting rate considerations. An enrichment of 150 increases the ^{14}C concentration in an archaeological sample to that of a sample 41,000 years younger, so such enrichment allows much older samples to be dated.[6,7] The method of enrichment and the general results are also relevant to the enrichment of other isotopes found in CH_2O, but carbon-14 is particularly attractive at this time because the amount of formaldehyde that must be photolyzed to be useful is in the mg range. Such amounts can be processed in reasonable times with existing lasers, and need not await the development of more efficient, higher power lasers to be economically worthwhile.

B. EXPERIMENTAL

Many of the details of sample preparation and other procedures have been described elsewhere.[2] Therefore, such procedures will only be outlined and relevant changes described. $^{12}CH_2O$ was prepared by pyrolysis of paraformaldehyde (Matheson, Coleman, and Bell) at ~110°C according to the method of Spence and Wild.[8] The monomer was purified by vacuum distillation from 174 K (methanol slush) to 77 K and stored at 77 K to prevent polymerization. ^{14}C-paraformaldehyde obtained from Amersham-Searle had an activity of 740 μCi/mg (37% $^{14}CH_2O$) and was depolymerized at ~180°C. NO (Matheson) was purified by passing it over silica gel held at dry ice temperature,[9] and was clear blue when liquified. Isobutene (Matheson) was purified by freeze-pump-thaw cycles and by keeping the middle third of a vacuum distillation from butanol slush (184 K) to liquid nitrogen.

1. Spectroscopy

Simultaneous high resolution spectra were measured for $^{14}CH_2O$ and $^{12}CH_2O$ (and in one case for $^{13}CH_2O$), in both absorption and fluorescence. The fluorescence excitation spectra were easier to obtain, especially at longer wavelengths where the fluorescence quantum yield (always << 1) is larger.[10] However, the fluorescence quantum yield is strongly dependent on rovibronic state,[11] so absolute absorption cross sections are more useful for laser isotope separation. Therefore, only the experimental apparatus for the latter, shown in Fig. IV-1, is described here.

Fig. IV-1. Experimental arrangement for measuring simultaneous absorption spectra of $^{14}CH_2O$ and $^{12}CH_2O$.

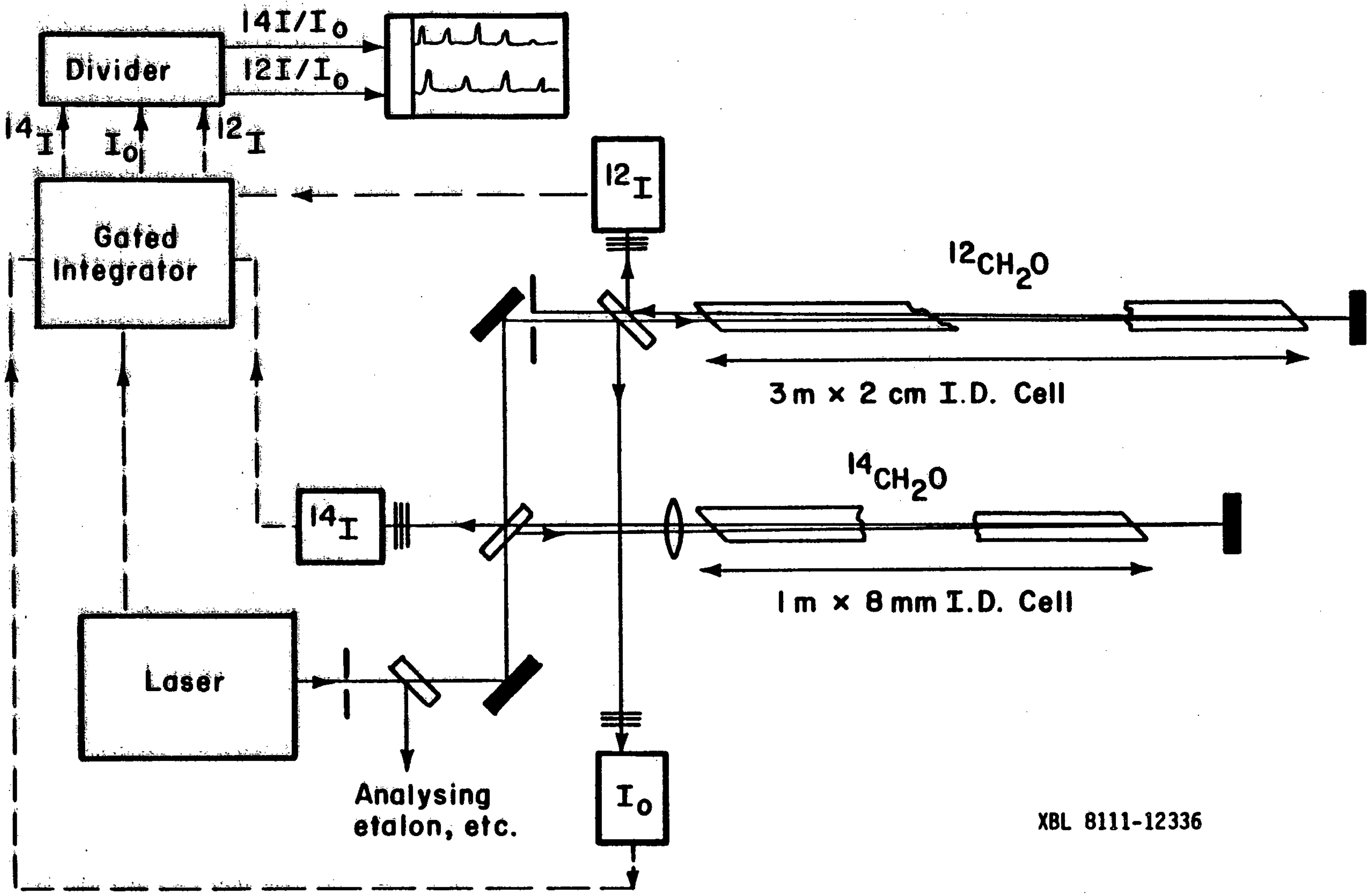

XBL 8111-12336

Fig. IV-1.

The cells used were made of quartz and had Brewster angle windows. The $^{12}CH_2O$ cell was generally filled with 2 to 4 Torr of formaldehyde, although 10 Torr were occasionally used. The use of two passes of the laser beam allowed absorption cross sections as low as 2×10^{-22} cm^{-2} to be measured. The size and design of the $^{14}CH_2O$ cell was constrained by safety considerations, specifically the need to keep a limited amount (≤ 400 μCi) of radioactive gas in a breakable quartz cell. The cell was too narrow to allow use of more than two passes, and was filled to ~2 Torr. To minimize the handling of highly radioactive gas, the $^{14}CH_2O$ was kept sealed in the cell. It is possible to keep such pressures of formaldehyde gas in a well flamed quartz cell for several months without serious loss to polymerization. The $^{14}CH_2O$ concentration in this cell was calculated, when necessary, from the known $^{14}CH_2O$ to $^{12}CH_2O$ ratio and the $^{12}CH_2O$ concentration, which was obtained from a comparison of the absorption of the gas in the cell (on a strong $^{12}CH_2O$ absorption line) to that of a known amount of $^{12}CH_2O$.

The Doppler width of a CH_2O absorption line is 0.06 cm^{-1} (2 GHz). To resolve most of the spectral structure, a laser bandwidth on the order of 0.1 cm^{-1} (3.3 GHz) is needed. For these experiments, two different lasers served as a source of tunable ultraviolet light. One, a Hänsch-type nitrogen pumped dye laser, was only used for study of the 290 nm absorption band. This laser has been described by Weisshaar et al.,[12] and was used with Rh 590, a single amplifier stage, and an ADP frequency doubling crystal. The bandwidth of this laser was typically 0.1 to 0.12 cm^{-1} (FWHM), as measured from the width of the narrower lines of the CH_2O spectrum, after deconvoluting the Doppler linewidth. The second laser, a Chromatix CMX-4 flashlamp pumped dye laser, had higher average power and was used for spectroscopic study of all bands as well as for the enrichment work. This laser had intracavity frequency doubling and an intracavity extra-high finesse etalon (F = 20) which generally gave a bandwidth of 0.14 - 0.18 cm^{-1}. A commercial scanning unit tuned the birefringent filter, doubling crystals, and etalon simultaneously to allow continuous scanning. The laser output was monitored with an external etalon to ensure that only one etalon mode was lasing. Wavelengths were measured with a monochromator calibrated to ±0.03 nm. The laser performance varied with the dye (Rhodamine 575, 590, and 640, or Kiton Red) and dye solvent in use, and was especially sensitive to the tilt of the etalon. The bandwidth, output power, and frequency stability of the laser were therefore somewhat dependent on the operating wavelength. When measuring very small absorptions, the spectrum of the laser output is important since any power at frequencies several bandwidths from line center will be absorbed by lines other than that of interest. The laser spectrum was checked to about 1% of the line center intensity, but the lowest $^{12}CH_2O$ cross sections observed may still be instrument limited.

The electronics of Ref. 2 were used for the light intensity measurements. Using a 5 sec time constant for the integrator and a laser scanning rate of 0.01 cm^{-1} sec^{-1}, an absorption of 5% could be measured with a signal-to-noise ratio of 2 - 10. A large part of the uncertainty in the measured absorptions stems from small variations in the laser beam direction during a scan that result in baseline drift. The position of the baseline then had to be estimated from the appearance of the spectrum, a fairly uncertain process, or located by freezing out the formaldehyde.

The wavelength and absorption cross section for the lines chosen for enrichment were remeasured with special care. σ ($^{14}CH_2O$) was obtained from the absorption of a directly measured pressure of $^{14}CH_2O$, and σ ($^{12}CH_2O$) was checked by repeated freezedown of the formaldehyde. The line positions were determined to ±0.15 cm^{-1} by referring to published $^{12}CH_2O$ absorption spectra.[13,14]

2. Enrichments

The apparatus used for enrichment experiments is similar to that used for the spectroscopy. About 7 Torr of formaldehyde with a ^{14}C concentration of approximately 10^{-4} were photolyzed by two passes of the laser beam in the 3 m long cell. During a photolysis the laser frequency was monitored by observing the laser induced fluorescence from a separate cell filled with ~1 Torr of (37%) $^{14}CH_2O$. When the laser began to drift off the desired line, the photolysis cell was blocked, and the laser manually tuned back to the proper frequency. This had to be done every 15 - 20 minutes. The intensity transmitted through the photolysis cell was also monitored. Due to the low concentration of $^{14}CH_2O$ in the sample, virtually all of the light absorbed is absorbed by $^{12}CH_2O$. Therefore this signal, when normalized by the incident intensity, gives a measure of the absorption cross section for $^{12}CH_2O$ during the photolysis and an additional check of the laser behavior.

The experiments using radical scavengers were done with two 3 meter long photolysis cells, one filled with pure formaldehyde, the other containing formaldehyde plus the scavengers. The laser beam was divided into approximately equal parts and the cells illuminated simultaneously to ensure that any variation in specific activity was indeed due to the presence of the scavengers and not variation in laser behavior.

The laser power was generally on the order of 0.1 mW and samples were photolyzed for 1.5 - 2 hours (~4 hours for the double cell experiments). The laser was run at low power to avoid lasing on a second etalon mode. In these experiments, samples were photolyzed just enough to give measurable amounts of product--no attempt was made to extract a major portion of the ^{14}C in any particular sample. Generally ~3% of the $^{14}CH_2$ was photolyzed, yielding ~0.1 μmole of product.

After a photolysis, the formaldehyde was frozen into a sidearm with liquid nitrogen. The products (H_2 and CO) were collected in a glass transfer loop with liquid helium, then injected into a Varian 3600 gas chromatograph equipped with a thermal conductivity detector and helium carrier gas (40 ml/min). The column (0.25 in OD x 15 ft of MS5A, 50/60 mesh) was held at 40°C for 20 min, then temperature programmed at 10°/min to 70°. For samples containing NO, the analysis was done isothermally at 40°C with a 7 foot column and 60 ml/min of helium to decrease interference between the NO and CO signals. The amount of CO present was determined by the peak area. Since the GC is about 10 - 15 times less sensitive to H_2 than CO when using helium as the carrier gas, the H_2 was barely detectable. The GC was calibrated by injecting known amounts of

CO and was found to be linear in this region. The GC effluent was then mixed with air in a two-to-one ratio and flowed into a Johnston Laboratories Triton 1055C radiation monitor. This instrument measures the conductivity induced by beta activity in a 1 liter chamber, and the composition of the gas mixture in the chamber had to be controlled to obtain reproducible activity measurements. The radiation monitor was calibrated with dilue $^{14}CO_2$ and was found to be linear. The reproducibility of specific activity measurements is estimated at ±10%, based on the analysis of a divided sample.

The enrichment factor was obtained by taking the ratio of the specific activity of the laser photolyzed sample to that of a sample photolyzed for 2 min by a medium pressure mercury lamp. In the latter, ~10% of the formaldehyde was photolyzed, and the samples analyzed in the same manner as the laser photolyzed samples. The products of these short photolyses were found to be slightly (~10%) enriched in ^{14}C, as judged by comparison to the products of 90% complete photolyses, and the enrichment factors have been adjusted accordingly.

C. RESULTS AND DISCUSSION

1. Spectroscopy

Two conditions must be met if photolysis at a given wavelength is to be useful for isotopic enrichment. The cross-section for absorption by $^{14}CH_2O$ must be much greater than that for $^{12}CH_2O$ (i.e. the spectral selectivity must be large), and $\sigma(^{14}CH_2O)$ should be as large as possible for the most efficient use of photons. Table IV-1 lists the wavelengths found where the selectivity was greater than ~50, and $\sigma(^{14}CH_2O)$ was on the order of 10^{-19} cm^2. Except for the 305 and 355 nm bands, which were not carefully studied, these are the only lines among the ~10^4 lines in the formaldehyde absorption spectrum suitable for ^{14}C enrichment. The uncertainties given were estimated from the degree of consistency of repeated experiments, including variation in formaldehyde pressure and laser performance. Values for the cross sections were often based on an estimated baseline position and have a correspondingly large uncertainty.

Figure IV-2 shows the calculated ^{14}C isotope shifts[15] for the vibrational band origins in the formaldehyde S_1 absorption. Because of the bandhead structure, blue-shifted bands should have a higher probability of yielding good selectivities, but only two bands are blue shifted, and only to a small extent. For red-shifted bands, the isotopic shift is larger at shorter wavelengths, and one would expect such regions to be better for enrichment. The results of our spectroscopic studies, however, do not completely agree with these preliminary expectations. The number of anti-coincidences is fairly high for the 290 nm region, but is quite

Table IV-1. Formaldehyde absorption lines suitable for Carbon-14 enrichment.[a]

λ, (nm)	$\sigma(^{14}CH_2O)$, (10^{-19} cm^2)	$\sigma(^{12}CH_2O)$, (10^{-21} cm^2)	$S = \frac{\sigma(^{14}CH_2O)}{\sigma(^{12}CH_2O)}$
289.79[b]	2.5 ± 20%	5 ± 40%	50 ± 50%
289.91[b]	2.5 ± 20%	4 ± 25%[c]	60 ± 35%
290.10[b]	2.5 ± 20%	4 ± 50%	60 ± 60%
290.16[b]	2.1 ± 20%	5 ± 20%[c]	45 ± 35%
295.78	1.2 ± 25%	8 ± 25%	25 ± 50%
297.37	0.8 ± 25%	1 ± 50%[c]	80 ± 60%
299.70	1 ± 20%	3 ± 30%[d]	35 ± 30%
299.75	1.4 ± 20%	2.5 ± 50%[d]	50 ± 60%
300.18	1.1 ± 20%	2 ± 50%	50 ± 60%
300.17	1.5 ± 20%	2 ± 50%[c]	75 ± 60%
300.23	1.1 ± 20%	2 ± 50%[d]	50 ± 60%
318.59	1.5 ± 20%	2.5 ± 25%	60 ± 30%
319.48	1.0 ± 20%	2 ± 50%	50 ± 60%
326.94	3.6 ± 20%	0.8 ± 30%	450 ± 40%
327.03	3.0 ± 20%	1 ± 50%	400 ± 60%
327.40	1.5 ± 20%	1 ± 30%	175 ± 40%
327.42	2.5 ± 20%	1 ± 50%	250 ± 60%
327.65	1.5 ± 20%	1 ± 50%	150 ± 60%
327.89	2.1 ± 20%	1 ± 50%	200 ± 60%
328.23	1.2 ± 20%	1 ± 50%	100 ± 60%

Table IV-1. Continued.

329.97	2.5 ± 20%	1 ± 50%	250 ± 60%
330.10	1.9 ± 20%	1 ± 50%	200 ± 60%
331.19	0.8 ± 20%	0.8 ± 50%	100 ± 60%
381.26	1.3 ± 20%	0.8 ± 50%	150 ± 60%
331.42	1.8 ± 20%	0.6 ± 50%	300 ± 60%
339.56	1.6 ± 20%	2 ± 50%	90 ± 60%
339.58	3.2 ± 25%	2.2 ± 20%	150 ± 35%
339.61	1.3 ± 20%	1.5 ± 50%	100 ± 60%
339.65	1.5 ± 20%	1.5 ± 50%	100 ± 60%
340.11	0.9 ± 20%	0.5 ± 40%	180 ± 50%
340.48	1.1 ± 20%	0.6 ± 30%	180 ± 40%
340.61	1.1 ± 20%	0.4 ± 50%	250 ± 60%
340.62	1.7 ± 20%	0.8 ± 30%	200 ± 35%
342.84	1.1 ± 20%	0.55 ± 40%	200 ± 50%
343.43	0.65 ± 20%	0.3 ± 60%	200 ± 70%
343.45	1.0 ± 20%	0.4 ± 30%	250 ± 40%

---

a) Except as noted, the flashlamp pumped dye laser was used, and $\sigma(^{12}CH_2O)$ was measured using 2 - 4 Torr of formaldehyde and a 600 cm pathlength.

b) N_2 laser pumped dye laser used.

c) A factor of 2 lower at −80°C.

d) A factor of 3 lower at −80°C.

Fig. IV-2. Low resolution absorption spectrum of $^{12}CH_2O$ with the calculated shifts of the band origins for $^{14}CH_2O$ displayed. Shaded portions of the top band indicate spectral regions not searched for enrichment lines.

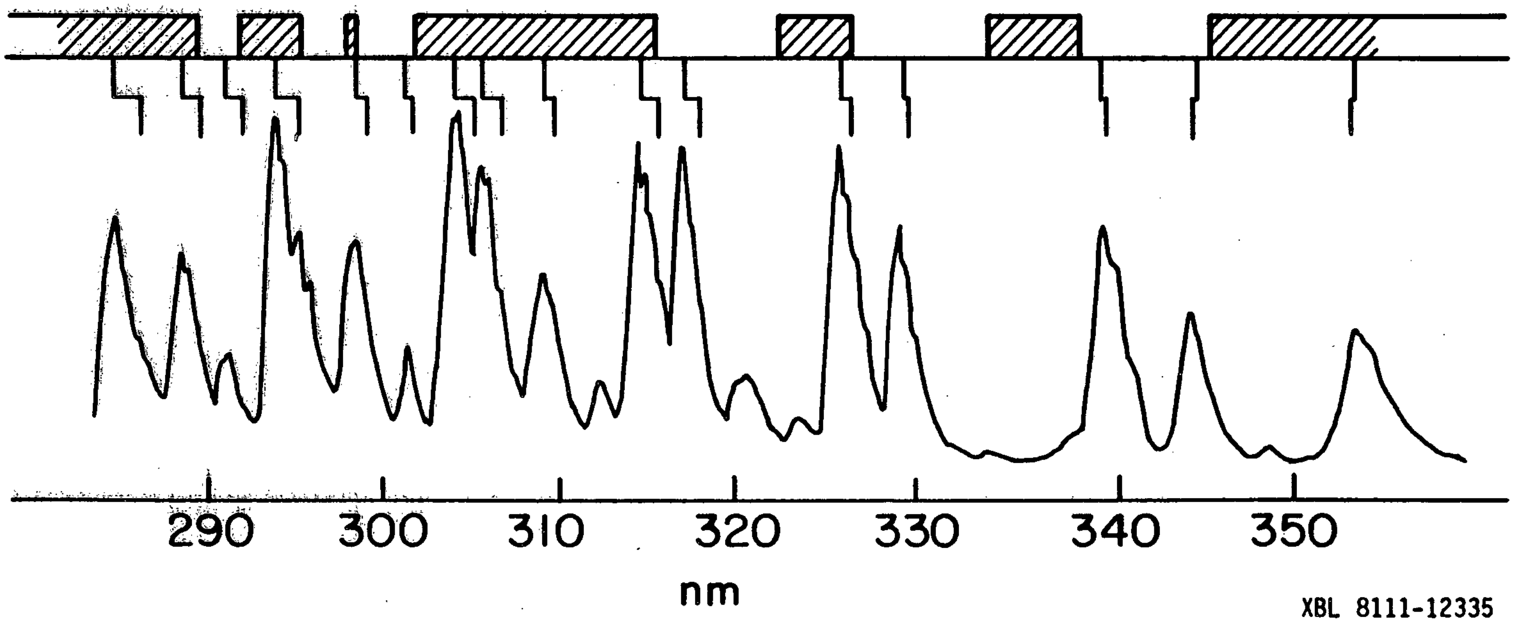

XBL 8111-12335

Fig. IV-2.

low for the 297, 300 and 320 nm bands, becoming large again for the 330 and 340 nm bands. This may be due to the increasing complexity of the spectrum as combination and overtone absorptions appear.

There also appears to be an unresolved absorption underlying the discrete spectrum, which can be seen when the formaldehyde is frozen out of the cell to find the baseline. This residual absorption is stronger at shorter wavelengths--it is significantly smaller at 330 and 340 nm than at 290 nm. Since this feature appears in fluorescence excitation spectra with approximately the same quantum yield as the resolved absorptions, it is unlikely that it involves excitation to a continuum. A reasonable explanation is that this absorption consists of a large number of weak overlapping lines. Since many of these weaker lines would be high rotational states, absorption spectra at -80°C were measured for the 290, 297, and 300 nm regions. The low temperature spectra resemble the room temperature spectra--no important new anti-coincidences were produced. The unresolved absorption was reduced by a factor of 2 or 3, but since the regions explored are well above the vibrational band origin, the overall absorption was reduced by 30 - 40%.

In the 330 and 340 nm regions, the anti-coincidences generally involve smaller $^{12}CH_2O$ cross sections than those at higher energy, and the very lowest cross sections measured seem to be dependent on the laser cavity alignment. In one case, the cross section fell from 1.2×10^{-21} to 0.3×10^{-21} cm^2 upon adjustment of the laser. Since there are strong $^{12}CH_2O$ absorptions near these anti-coincidences, this behavior suggests that the linewidth and spectral purity of the laser have become limiting factors.

Figure IV-3 shows two of the more interesting anti-coincidences. The line at 326.94 nm seemed very promising so it was chosen for further experiments. Careful cross section measurements yielded $\sigma(^{14}CH_2O) = (3.0 \times 0.6) \times 10^{-19}$ cm^2, where the error given reflects the reproducibility of the measurements. Besides being sensitive to laser performance, $\sigma(^{12}CH_2O)$ was found to be depend on pressure over the range 1 - 20 Torr

$$\sigma(^{12}CH_2O) = 1.12 \times 10^{-21} (1 + 0.11 P) \text{ cm}^2$$

where P is the pressure in Torr and the uncertainty is ±10%. Since the lines is located in a narrow valley between two strong absorptions, pressure broadening increases the cross section.

2. Enrichments

Table IV-2 gives the enrichment results at 326.94 nm. Two photolyses done at 331.42 nm gave enrichment factors of only 49 and 59, so that line was not pursued further. The values of $\sigma(^{12}CH_2O)$ given are estimates based on measurements of the absorption as the formaldehyde was being loaded into the cell. The variation of $\sigma(^{12}CH_2O)$, and hence in the selectivity and enrichment, reflects the variation in laser linewidth and spectral purity from run to run.

In pure formaldehyde with a low ^{14}C concentration, the radicals formed in (2) react as follows:

Fig. IV-3. High resolution spectra of $^{12}CH_2O$ and $^{14}CH_2O$ (shaded) showing lines suitable for enrichment. (a) is near 326.94 nm and (b) is near 331.42 nm. The $^{12}CH_2O$ spectrum was taken with 4 Torr and a 600 cm pathlength, the $^{14}CH_2O$ spectrum with ~1 Torr of 37% $^{14}CH_2O$ and 200 cm pathlength.

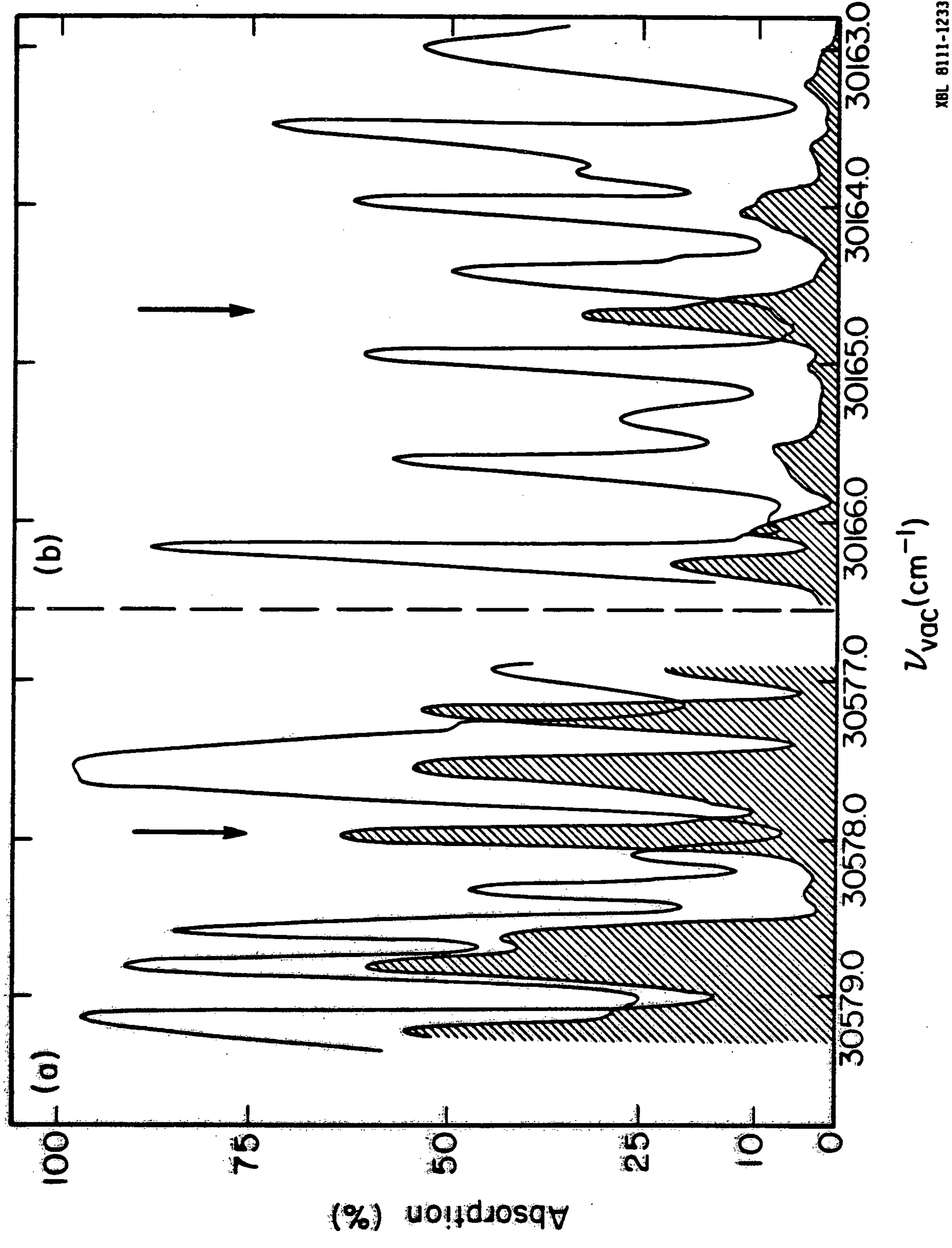

XBL 8111-12337

Fig. IV-3.

Table IV-2. Enrichment experiments at 326.93 nm

E^a	$\sigma(^{12}CH_2O)$,^{b} (10^{-21} cm^2)	S^c	E/S	$E/E_s{}^d$
123	1.76	170	0.72	-
162	1.36	221	0.73	-
91	-	-	-	-
108	2.07	145	0.74	-
129	1.77	169	0.76	-
107	1.94	155	0.69	
150^e			0.97	0.71
98	2.04	147	0.67	0.77
125^f			0.85	

a) Enrichment factor, uncertainty ±15%.

b) Uncertainty, ±10%.

c) Selectivity, $S = \sigma(^{14}CH_2O)/\sigma(^{12}CH_2O)$, $\sigma(^{14}CH_2O) = (3.0 \pm 0.6) \times 10^{-19}$ cm^2.

d) The last two experiments were double cell experiments using radical scavengers.

e) 2 Torr isobutene and 0.4 Torr NO.

f) 4.7 Torr isobutene and 0.4 Torr NO.

$$H + {}^{12}CH_2O \rightarrow H_2 + H^{12}CO$$

$$2\,H^{12}CO \rightarrow {}^{12}CH_2O + {}^{12}CO$$

$$H^{12}CO + H^{14}CO \rightarrow \frac{1}{2}\left[{}^{12}CH_2O + {}^{14}CH_2O + {}^{12}CO + {}^{14}CO\right].$$

In the presence of the scavengers, HCO reacts with NO

$$HCO + NO \rightarrow HNO + CO \qquad (3)$$

while isobutene is a good H atom scavenger

$$H + C_4H_8 \rightarrow C_4H_9. \qquad (4)$$

Further reactions of the species formed in (3) and (4) are not expected to involve CH_2O or CO. The radical chemistry of the CH_2O/NO and CH_2O/isobutene systems has been discussed elsewhere.[2,16-21]

At 326 nm, $\phi_1 = 0.6$ and $\phi_2 = 0.4$,[2] so this simple reaction scheme yields E/S = 0.8 for the pure CH_2O case and E/S = 1.0 with scavengers. The data give E/S (pure CH_2O) $\cong 0.72 \pm 0.05$ and E/S (scavengers) $\cong 0.91 \pm 0.06$. Although the experimental uncertainties (Table IV-2) are rather large, these results suggest that energy transfer, or some other mechanism for loss of isotopic selectivity, may be important. Marling[4] observed a similar loss of selectivity in his experiments. While enriching ^{18}O and ^{13}C near 332 nm, he found a 24% probability of isotopic scrambling, approximately half of which can be accounted for by radical reactions. Photolysing CHDO at 325 nm gave 40% isotopic scrambling, again only partially accounted for by radical scrambling, while CHDO at 338 nm and CD_2O at 332 and 338 nm gave less than 10% scrambling. Although

$$CH_2O(S_1) + CD_2O(S_0) \rightarrow CH_2O(S_0) + CD_2O(S_1)$$

is slow at 370 nm (~2% of gas kinetic),[22] it is not unreasonable to expect that 1) the transfer rate would increase with energy, and 2) transfer to another protonated formaldehyde would be faster than transfer to a deuterated species.[23] Energy transfer could also occur from the intermediate (see Chapter III), if it exists.

Although radical scavengers appear to be effective in reducing isotopic scrambling, the enrichment procedure would be simpler without them. The longer wavelength bands (340 and 350 nm), therefore, may deserve further consideration. The unresolved background absorption is smaller at longer wavelengths, and energy transfer might be less important. However, these wavelengths have a somewhat smaller quantum yield for product formation and are outside the optimum range for frequency-doubled dye lasers.

D. APPLICATION OF ENRICHMENT TO RADIOCARBON DATING

Laser enrichment, when combined with direct detection, should have its most significant impact in the dating of very old samples.[6,7,24] The range of a ^{14}C detection system is ultimately limited by either too low a signal counting rate, too high a background, or both. Groups working with direct detection methods have reported background ^{14}C counting rates equal to[25] or greater than[26] the counting rates of 40,000 to 70,000 year old samples, which were caused by contamination of the accelerator. This problem should be reduced or eliminated in machines dedicated to ^{14}C measurement, so the counting rate could prove to be the limiting factor. The overall detection efficiency of a dedicated tandem Van de Graaf accelerator is expected to be ~2%, at best.[27] Using a 50 μA C^- beam, a 10^5 year old sample would yield one count every 6.6 hours. This would require a run of many days to accumulate a statistically reasonable number of counts, which is not really practical. Enrichment by a factor of 150 would raise the count rate by the same factor to 23 counts/hour, allowing a considerable savings in accelerator time. If 400 counts are desired for an age determination, 2×10^4 ^{14}C atoms are required, and would be provided by 60 mg of 10^5 year old carbon. However, since overall enrichment decreases as the ^{14}C is depleted, it is more practical to photolyse 20 – 50% of the ^{14}C from a correspondingly larger initial sample. At 10 Torr, extracting 50% of the ^{14}C from 120 mg of initial carbon requires 90/L mW hr of laser energy, where L is the pathlength in meters. A 100 m pathlength (e.g. 5 m x 20 passes) is reasonable. In practice these energy figures may need to be increased by a factor of 2 or 3 to allow for losses, monitoring requirements, and the simultaneous photolysis of a standard.

From experiments, it is clear that the laser used for enrichment should have a bandwidth less than the Doppler width of formaldehyde, must run reliably, and have a spectrally pure output. There are several types of lasers that may be suitable. A commercially available ring dye laser has been frequency doubled to give more than 50 mW at 300 nm (the peak of the Rh 6G tuning curve) with a linewidth ≤ 50 MHz, and a commercial option for frequency doubling is available. Commercial YAG-pumped dye lasers provide ~100 mW at 280 nm, but have a uv linewidth of ~0.12 cm^{-1}, a bit wide. Output powers will be lower at other wavelengths. It should be noted that the strong Rhodamine dyes lase at longer wavelengths in the ring dye laser. This is an advantage because the longer wavelengths are of more interest for enrichment. In the 340 - 350 nm region, where the corresponding visible dyes are poor, p-terphenyl, or other dyes that lase directly in the uv, may be pumped with an excimer or quadrupled YAG laser. This type of laser system eliminates the frequency doubling step, but is not as well developed as the commercial systems. It should be possible to enrich several grams of formaldehyde per hour.

In spite of the fairly low efficiency of the lasers, (10^{-5} to 10^{-6}), the cost of the power to run them should be negligible. The capital cost of the laser (about $60,000 for the commercial systems), would, in any case, be much less than the cost of a dedicated accelerator. It is difficult to estimate the cost of sample treatment and chemical processing, but it could represent a significant portion of the total enrichment cost.

The combination of laser isotopic enrichment and accelerator dating should make it possible to measure C-14 abundances corresponding to ages greater than 100,000 years. However, the range of radiocarbon dating may actually prove to be limited by problems of sample integrity. For a 100,000 year old sample, contamination by 6 ppm of modern carbon would double the counting rate. The smaller sample requirement of accelerator dating should make it easier to obtain intact samples, but will also magnify the deleterious effect of any given contamination. The increased manipulation of a sample associated with enrichment may also increase the possibility of laboratory contamination. Groups in Groningen[28] and Seattle[29] using gaseous diffusion methods for ^{14}C enrichment have encountered contamination problems with 75,000 year old samples. Their experiences will serve as a guide to dealing with such problems.

This work at 326.94 nm shows that significant enrichments of carbon-14 by photolysis of formaldehyde can be achieved, even under non-optimal conditions. It is reasonable to expect that use of a more suitable laser will be accompanied by significant improvements in selectivity and enrichment.

REFERENCES

1. D. C. Moule and A. D. Walsh, Chem. Rev. 75, 67 (1975).
2. J. H. Clark, C. B. Moore and N. S. Nogar, J. Chem. Phys. 68, 1264 (1978).
3. J. H. Clark, Y. Haas, P. L. Houston and C. B. Moore, Chem. Phys. Lett. 35, 82 (1975).
4. J. B. Marling, J. Chem. Phys. 66, 4200 (1977).
5. L. Mannik, G. M. Keyser and K. B. Woodall, Chem. Phys. Lett. 65, 231 (1979).
6. R. E. M. Hedges and C. B. Moore, Nature 276 , 255 (1978).
7. E. T. Hall, R. E. M. Hedges, N. R. White, H. R. McK. Hyder and D. Sinclair, in Proceedings of the First Conference on Radiocarbon Dating with Accelerators, ed. by H. E. Gove (Univ. of Rochester Press, Rochester, New York, 1978) p.257.
8. R. Spence and W. Wild, J. Chem. Soc. 338 (1935).
9. E. F. Hughes, J. Chem. Phys. 35, 1531 (1961).
10. R. G. Miller and E. K. C. Lee, J. Chem. Phys. 68, 4448 (1978).
11. J. C. Weisshaar and C. B. Moore, J. Chem. Phys. 72, 5135 (1979), and J. Chem. Phys. 2875 (1980).
12. J. C. Weisshaar, A. P. Baronavski, A. Cabello and C. B. Moore, J. Chem. Phys. 69, 4720 (1978).
13. G. H. Dieke and G. B. Kistiakowsky, Phys. Rev. 45, 4 (1934).
14. V. Sethuraman, V. A. Job and K. K. Innes, J. Mol. Spectrosc. 33, 189 (1976).
15. E. S. Yeung, and C. B. Moore, Appl. Phys. Lett. 21, 109 (1972).

16. A. Horowitz and J. G. Calvert, Int. J. Chem. Kinet. 10, 713 (1978).

17. A. Horowitz and J. G. Calvert, Int. J. Chem. Kinet. 10, 805 (1978).

18. B. M. Morrison, Jr. and J. Heicklen, J. Photochem. 11, 183 (1979).

19. G. K. Moortgat and P. Warneck, J. Chem. Phys. 70, 3639 (1979).

20. R. S. Lewis, and E. K. C. Lee, J. Phys. Chem. 82, 249 (1978).

21. K. Y. Tang, P. W. Fairchild and E. K. C. Lee, J. Phys. Chem. 83, 569 (1979).

22. J. C. Weisshaar, D. J. Bamford, Eliot Specht and C. B. Moore, J. Chem. Phys. 74, 226 (1981).

23. A. Frad and A. Tramer, Chem. Phys. Lett. 23, 297 (1973). In glyoxal, the $h_2 \rightarrow h_2$ electronic energy transfer rate is reported to be 10 times faster than the $h_2 \rightarrow d_2$ rate.

24. A. E. Litherland, in Proceedings of the First Conference on Radiocarbon Dating with Accelerators, ed. by H. E. Gove (Univ. of Rochester Press, Rochester, New York, 1978) p.70.

25. C. L. Bennett, R. P. Beukens, M. R. Clover, D. Elmore, H. E. Gove L. Kilius, A. E. Litherland and K. H. Purser, Science 201, 345 (1978).

26. R. A. Muller, E. J. Stephenson and T. S. Mast, Science 201, 347 (1979).

27. R. E. M. Hedges, N. R. White, J. O. Want and E. T. Hall, in Proceedings of the 10th International Conference on Radiocarbon Dating, 1979 (to be published in Radiocarbon).

28. P. M. Grootes, Science 200, 11 (1978).

29. M. Stuiver, C. J. Heusser and I. C. Yang, Science 200, 16 (1978).

TECHNICAL INFORMATION DEPARTMENT
LAWRENCE BERKELEY LABORATORY
UNIVERSITY OF CALIFORNIA
BERKELEY, CALIFORNIA 94720